Cell

Genome-scale perturb-seq in primary human CD4$^+$ T cells maps context-specific regulators of T cell programs and human immune traits

Graphical abstract

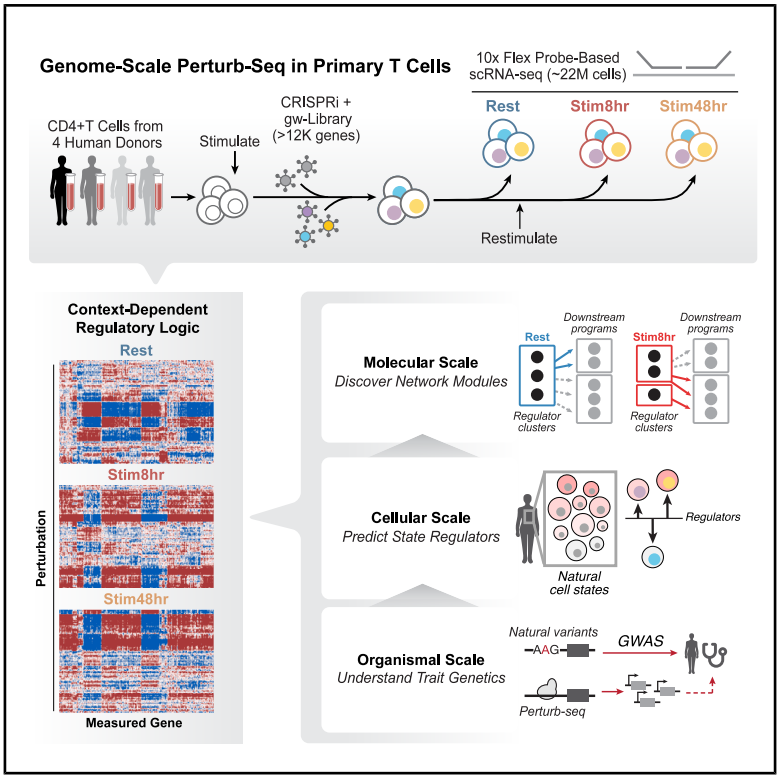

Highlights

- Genome-scale perturb-seq maps gene regulation in ~22 million primary human CD4$^+$ T cells
- Many gene regulatory effects are specific to distinct rest and stimulation time points
- Perturb-seq maps nominate regulators of gene signatures observed in human cohort atlases
- Perturb-seq links regulatory pathways to human traits and disease susceptibility

Authors

Ronghui Zhu, Emma Dann, Jun Yan, ..., Ansuman T. Satpathy, Jonathan K. Pritchard, Alexander Marson

Correspondence

ronghui.zhu@gladstone.ucsf.edu (R.Z.), emmadann@stanford.edu (E.D.), pritch@stanford.edu (J.K.P.), alex.marson@gladstone.ucsf.edu (A.M.)

In brief

A dynamic atlas of gene regulation was generated by perturbing every expressed gene across 22 million primary human CD4$^+$ T cells under resting conditions and following re-stimulation. The resulting map reveals context-specific regulators of immune programs and links regulatory pathways to naturally occurring T cell states and autoimmune disease risk.

Zhu et al., 2026, Cell *189*, 1–25
October 29, 2026 © 2026 The Author(s). Published by Elsevier Inc.
https://doi.org/10.1016/j.cell.2026.08.002

CellPress

Please cite this article in press as: Zhu et al., Genome-scale perturb-seq in primary human CD4+ T cells maps context-specific regulators of T cell programs and human immune traits, Cell (2026), https://doi.org/10.1016/j.cell.2026.08.002

Cell

CellPress
OPEN ACCESS

Article

Genome-scale perturb-seq in primary human CD4+ T cells maps context-specific regulators of T cell programs and human immune traits

Ronghui Zhu,[1,2,18,19,*] Emma Dann,[1,2,18,19,*] Jun Yan,[1] Justine Reyes Retana,[1] Ryunosuke Goto,[3] Reese C. Guitche,[1,4] Lillian Brixi,[2] Mineto Ota,[1,2,5] Austin Hartman,[2,6,7] Theodore L. Roth,[6,7,8,9,10] Ansuman T. Satpathy,[2,6,8,9,10] Jonathan K. Pritchard,[2,11,19,*] and Alexander Marson[1,10,12,13,14,15,16,17,19,20,*]

[1]Gladstone-UCSF Institute of Genomic Immunology, San Francisco, CA, USA
[2]Department of Genetics, Stanford University, Stanford, CA, USA
[3]Department of Biomedical Data Science, Stanford University, Stanford, CA, USA
[4]University of San Francisco, San Francisco, CA, USA
[5]Department of Allergy and Rheumatology, Graduate School of Medicine, The University of Tokyo, Tokyo, Japan
[6]Department of Pathology, Stanford University, Stanford, CA, USA
[7]Arc Institute, Palo Alto, CA, USA
[8]Program in Immunology, Stanford University, Stanford, CA, USA
[9]Stanford Cancer Institute, Stanford University, Stanford, CA, USA
[10]Weill Foundation West Coast Cancer Hub, Stanford, CA, USA
[11]Department of Biology, Stanford University, Stanford, CA, USA
[12]Department of Medicine, University of California, San Francisco, San Francisco, CA, USA
[13]University of California, San Francisco Helen Diller Family Comprehensive Cancer Center, University of California, San Francisco, San Francisco, CA, USA
[14]Parker Institute for Cancer Immunotherapy, San Francisco, CA, USA
[15]Innovative Genomics Institute, University of California, Berkeley, Berkeley, CA, USA
[16]Department of Microbiology and Immunology, University of California, San Francisco, San Francisco, CA, USA
[17]Institute for Human Genetics, University of California, San Francisco, San Francisco, CA, USA
[18]These authors contributed equally
[19]Senior author
[20]Lead contact
*Correspondence: ronghui.zhu@gladstone.ucsf.edu (R.Z.), emmadann@stanford.edu (E.D.), pritch@stanford.edu (J.K.P.), alex.marson@gladstone.ucsf.edu (A.M.)
https://doi.org/10.1016/j.cell.2026.08.002

SUMMARY

Gene regulatory networks encode the fundamental logic of cellular functions, but systematic network mapping remains challenging, especially in cell states relevant to human biology and disease. Here, we perturbed all expressed genes across 22 million primary human CD4+ T cells from four donors and developed a probe-based perturb-seq platform to measure the transcriptome effects in cells at rest and after stimulation. These data allowed us to map genes regulating immune pathways, including previously uncharacterized regulators of cytokine production. Importantly, active regulators and the gene programs they control changed dramatically across stimulation conditions. Perturbation signatures enabled us to model T cell states observed in population-scale transcriptomic atlases, nominating regulators of T cell polarization and of age-related phenotypes. Finally, we leveraged perturb-seq to implicate context-specific gene regulatory pathways in autoimmune disease risk. Our study provides a foundational resource and new approaches to decode T cell function and human immune traits.

INTRODUCTION

Gene regulatory networks (GRNs) constitute the fundamental logic by which cells organize biological functions. Mapping these networks uncovers circuit design principles,[1] guides precise cellular engineering,[2] and mechanistically links genetic variations to complex human traits.[3] While advances in single-cell transcriptomics have allowed for detailed observation of cellular states, inferring causal regulatory relationships from observational data remains challenging.[4]

Large-scale CRISPR screens have ushered in a new era of functional genetics, where the consequences of perturbing

This is an open access article under the CC BY-NC license (http://creativecommons.org/licenses/by-nc/4.0/).

Please cite this article in press as: Zhu et al., Genome-scale perturb-seq in primary human CD4+ T cells maps context-specific regulators of T cell programs and human immune traits, Cell (2026), https://doi.org/10.1016/j.cell.2026.08.002

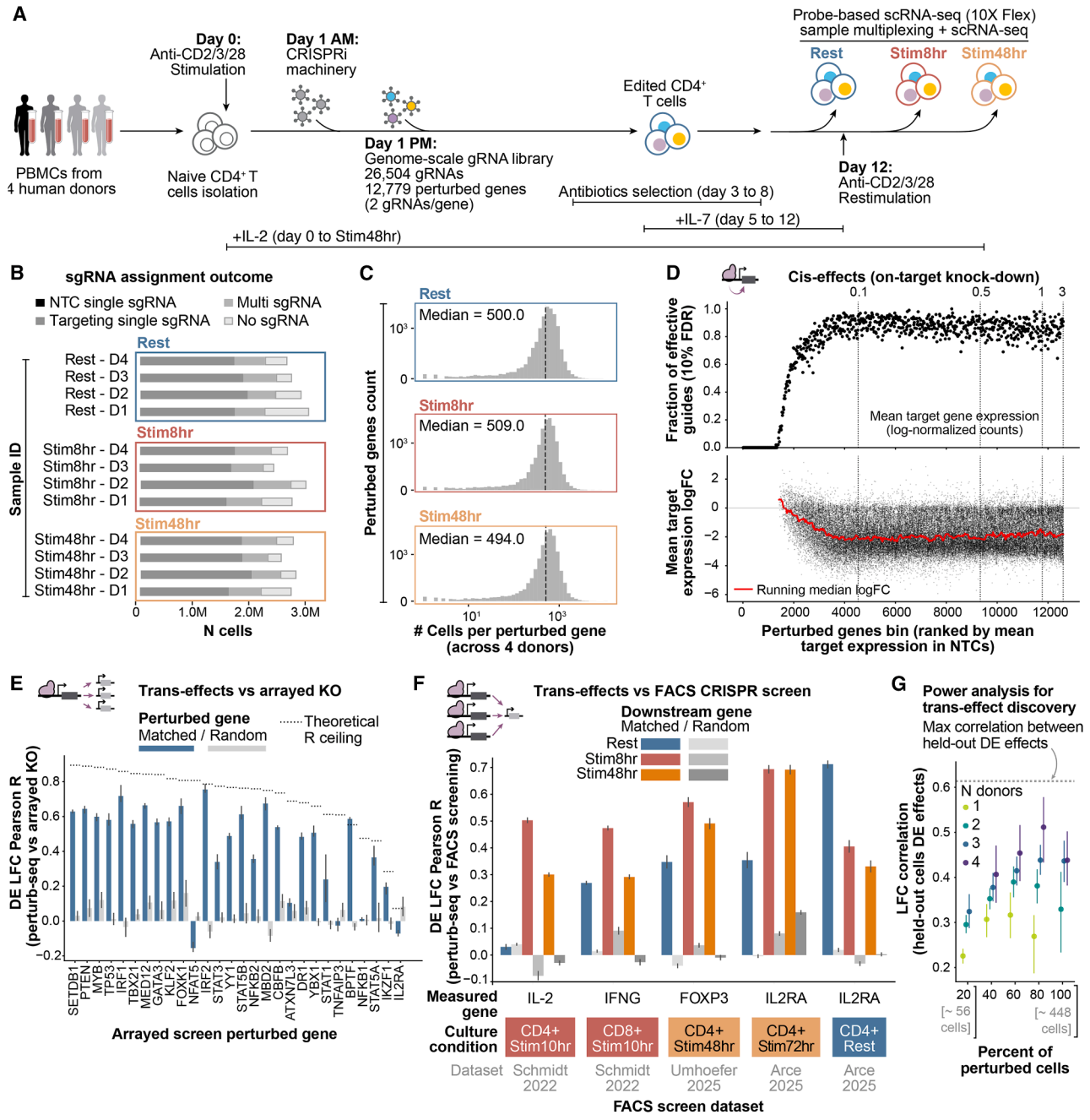

Figure 1. Genome-scale perturb-seq experimental design and quality control

(A) Experimental design of genome-scale perturb-seq in CD4+ T cells from multiple human donors across conditions (see STAR Methods).

(B) Number of cells (*x* axis) for each biological sample (*y* axis, condition-donor) with transcriptome passing quality control. Bars are colored by the outcome of guide RNA assignment (NTCs: non-targeting controls).

(C) Distribution of the number of cells harboring each gene perturbation (*x* axis, log10 scale) across culture conditions (rows). The dotted line denotes the median.

(D) Mean on-target knockdown effect across cells: (top) fraction of guides inducing significant on-target knockdown (*y* axis) versus baseline expression of perturbed genes (*x* axis). Each point represents a bin of 100 guides grouped by similar expression levels. Dotted vertical lines denote mean expression (log-normalized counts) per bin; (bottom) for the same bins, log-fold change in mean expression of target gene across cells (guide versus NTC). Each point denotes a guide in one of the 3 culture conditions. We exclude from this plot guide-condition pairs where (a) the mean target gene log-normalized expression is <0.001 in the NTCs (n = 10,282) and (b) the mean expression across cells with the targeting guide is exactly 0 (n = 8,959). The red line denotes the running median across bins.

(E) Comparison of *trans*-effects between perturb-seq and arrayed knockout (KO) RNA-seq[5,14]: for each perturbed gene (*x* axis), Pearson correlation of gene expression log2 fold changes (LFCs) across all measured genes (*y* axis) is shown. Blue bars: comparison of the same gene perturbed in both platforms; gray bars:

(legend continued on next page)

Please cite this article in press as: Zhu et al., Genome-scale perturb-seq in primary human CD4+ T cells maps context-specific regulators of T cell programs and human immune traits, Cell (2026), https://doi.org/10.1016/j.cell.2026.08.002

each gene can be tested systematically. We and others have coupled CRISPR screens with fluorescence-activated cell sorting (FACS)-based selection strategies to enable comprehensive mapping of upstream regulators of key genes.[5,6] This approach provides a foothold to discover gene regulators but is laborious, is limited to studying one target at a time, and does not immediately reveal the downstream transcriptional programs controlled by each regulator. More recently, perturb-seq (perturbation combined with single-cell RNA sequencing [scRNA-seq]) has emerged as a powerful method to overcome these limitations. By coupling genetic perturbations with high-dimensional transcriptomic readouts, perturb-seq allows for systematic measurement of regulatory relationships and the unbiased discovery of gene functions.[7–9] Published genome-scale perturb-seq studies have been limited to immortalized cell lines,[9,10] which fail to capture cell-type-specific and stimulus-dependent biology. Perturb-seq in primary human cells has been largely restricted to targeted libraries or arrayed formats that bias discovery toward known regulators.

Here, we developed a scalable, probe-based perturb-seq platform to extend perturbation measurements to genome scale in primary human cells with high-resolution measurements of the transcriptional consequences of each perturbation. We focused on CD4+ T cells given their central role in orchestrating adaptive immunity and their relevance in many autoimmune diseases.[11] In response to stimulation via their T cell receptor (TCR), co-stimulation (e.g., via CD28), and additional extracellular signals, CD4+ T cells polarize into distinct effector states defined by transcription factors, surface receptors, and cytokine expression signatures. Well-characterized polarized cell states, including Th1 and Th2 CD4+ T cells, drive distinct modes of immune responses and contribute to different autoimmune or inflammatory conditions.[12] Despite decades of work on CD4+ T cell differentiation, we still lack a comprehensive functional map of the dynamic GRNs that shape the state of CD4+ T cells as they respond to stimulation.

We employed pooled genome-scale CRISPR interference (CRISPRi) to knock down each expressed gene across ~22 million primary human CD4+ T cells. By profiling these cells at rest and after re-stimulation, we provide a dynamic atlas of each perturbation's effects on human T cell state. We demonstrate the utility of this resource through three complementary applications: (1) systematic discovery of context-dependent regulators, (2) nomination of genes regulating natural cell states via perturbation signatures, and (3) mechanistic interpretation of gene-trait associations to define the functional pathways driving disease susceptibility. This study offers new approaches to integrate genome-scale perturb-seq studies of human primary cells with human cell atlases and human genetics and provides a foundational resource for human immunology.

RESULTS

A scalable platform for perturb-seq in primary CD4+ T cells

To map functional GRNs systematically in human primary T cells, we compiled a genome-scale library targeting a union of all expressed genes in human CD4+ T cells and all transcription factors (12,779 genes in total; STAR Methods). Using an optimized high-titer lentiviral production protocol we developed previously,[6] we achieved transduction efficiencies of CRISPRi machinery up to 90% (Figure S1). Primary naive CD4+ T cells isolated from four human donors were stimulated, transduced with CRISPRi machinery and the genome-scale library, and expanded *ex vivo* (Figure 1A; Table S1; STAR Methods). Cells were then allowed to rest without CD3/CD28 stimulation before re-stimulation. To capture the dynamic regulatory circuits during T cell activation,[13] we collected perturbed cells in three different experimental conditions—rested (Rest), 8 h after re-stimulation (Stim8hr), and 48 h after re-stimulation (Stim48hr).

To profile tens of millions of cells for this genome-scale, multi-donor, and multi-time-point study, we leveraged recent advances in probe-based scRNA-seq technology (10x Flex) and its adoption in perturb-seq.[16] This technology provides sample collection flexibility by allowing for cell fixation, offers superior sensitivity for low-abundance transcripts,[17] and enables "superloading" to profile tens of millions of cells across <80 lanes—significantly fewer than traditional methods.[10]

In total, we collected 12 pools of CRISPRi-perturbed cells from four healthy human donors across 3 stimulation conditions (Figure S2A). We recovered a consistent number of mRNA UMIs, genes, and guide UMIs per cell across biological replicates and lanes (Figure S2B, mean UMI/cell per condition: Rest = 10,080; Stim8hr = 14,977; Stim48hr = 13,373). After quality control filtering (>500 genes/cell, <5% mitochondrial reads), we recovered 33.4 M cells across conditions with minimal technical batch effects and expected expression patterns for canonical T cell activation markers across stimulation conditions (Figure S3). Of these, 21.99 M cells (65.8%) were assigned a single targeting or non-targeting guide, 4.69 M (14.0%) had no guide confidently captured, and 6.70 M (20.0%) had multiple guides assigned (Figure 1B). Cells with multiple guides assigned had systematically higher numbers of UMIs per cell, indicating many of these are likely doublets (Figure S2C). Conversely, cells with no assigned guide showed systematically lower expression of the puromycin resistance transgene associated with the

comparison on different perturbed genes. Error bars: 95% confidence interval (CI) from bootstrapping. Dotted line: theoretical maximum correlation given LFC noise.

(F) Comparison of *trans*-effects between perturb-seq and published CRISPRi FACS-based screens.[6,13,15] For each measured gene (*x* axis), Pearson correlation of expression LFCs across all perturbed genes (*y* axis) is shown. Colored bars: same gene measured in both platforms; gray-scale bars: expression-matched different genes. Error bars: 95% CI from bootstrapping. Stimulation conditions of FACS screens are indicated below *x* axis.

(G) Pearson correlation between LFCs from downsampled and held-out validation data (5 lanes, all donors) for genes significant at 10% FDR. *x* axis: fraction of perturbed cells (20%–100%, ~55–450 cells). Colors: number of donors (1–4). Error bars: variability across independent downsampling splits and perturbed genes. Aggregated results across 12 perturbed genes are shown (see Figure S13 for per-gene results). Gray dotted line: maximum correlation between perturbation effects in independent held-out splits.

See also Figures S2–S4, S10, S12, and S13 and Tables S1, S4, S5, S6, S7, and S8.

Please cite this article in press as: Zhu et al., Genome-scale perturb-seq in primary human CD4+ T cells maps context-specific regulators of T cell programs and human immune traits, Cell (2026), https://doi.org/10.1016/j.cell.2026.08.002

gRNA-expressing cassette, suggesting incomplete antibiotic selection rather than failure to detect the gRNA probe (Figure S2C). Cells without guides or with multiple guides assigned were excluded from downstream analyses. Of the 26,504 guides in the library, 23,573 (88.9%) were detected in at least 50 cells across samples. We recovered on average 575 cells per perturbed gene in each condition (Figures 1C and S2E). Outlier perturbations with significantly lower numbers of perturbed cells mostly consisted of essential genes, where we expect knockdown to impair cell survival (Figure S2D). Compared with recent genome-scale perturb-seq datasets, the median transcripts per cell per context in our data (~10,000) was comparable to other genetic perturbation datasets in cell lines,[9,10] but we approximately doubled the total cell coverage per perturbation (Figure S2F).

Trans-effects of genetic perturbations

We next assessed the effects of genetic perturbations on transcriptome-wide gene expression, starting from on-target knockdown efficiency. Of the 24,174 guides detected across conditions, target gene expression was significantly reduced for 73% of tested guides compared with non-targeting control (NTC) guides (Figures 1D and S4A; median log-fold change = -2.33). The subset of guides that failed to achieve significant knockdown predominantly targeted genes with very low baseline expression (Figure S4B). Cells with any of 869 guides that were inefficient across conditions were excluded from downstream analyses (for 100 perturbed genes, both guides were consistently ineffective). Quality control metrics for individual guides are provided in Table S5.

We then quantified the effect of each gene perturbation on all measured transcripts using pseudo-bulk differential expression (DE) analysis in each condition. For perturbations with sufficient cell coverage, we tested for DE relative to NTCs, aggregating data from cells from the same condition, donor (biological replicates), and guide RNA (technical replicates) and regressing out donor effects and cell count per perturbation (Figure S5A; STAR Methods). We were able to estimate transcriptome-wide effects of perturbation of 11,527 genes in at least one condition (with 96% of them tested in all conditions). Of these, 7,807 (67%) perturbed genes had significant DE (false discovery rate [FDR] < 10%) effects on at least 3 genes in at least one condition. Across conditions, we discovered 2,035,311 significant regulator-to-gene *trans*-effects. Throughout the manuscript, we use the term "regulator" to indicate a perturbed gene with significant *trans*-effects on at least one measured gene.

We assessed the robustness of these *trans*-effect estimates in several ways. First, we quantified the transcriptome-wide effects of individual guides with guide-level pseudo-bulk DE analysis to compare DE profiles between guides targeting the same gene for perturbed genes with at least 3 significant DE genes in the target-level test. By examining guide pairs with low correlation in their DE effects, we identified 310 guides with likely distal off-target activity (Note S1; Figure S6; Table S6). We excluded these likely off-targets. Nonetheless, perturbation effects were generally consistent between guides targeting the same gene. Most discrepancies were attributable to differences in on-target knockdown efficiency (Figures S7A and S7B) or overall strength of transcriptome effects (Figures S7C and S7D; Note S2). We also estimated the prevalence of proximal off-target effects, which are expected to occur with all guides, by examining transcription start sites near guide targeting sequences. A significant knockdown of a neighboring gene was detected in at least one condition for 10% (1,152/11,527) of the tested perturbed genes (Figure S8). We flagged these as cases where transcriptional responses may reflect knockdown of both the intended target and the proximal gene. Finally, when testing for correlation between *trans*-effect estimates across donors, we observe transcriptome-wide concordance (Figure S9), although we observe cases where *trans*-effects manifest only in a subset of donors (Note S3). We provide summary statistics for DE analyses at the guide and target level, as well as annotations for guide robustness, donor robustness, and likely off-targets (see additional resources).

To assess regulator-to-gene *trans*-effects genome-wide, we first tested whether transcriptome-wide effects for a given perturbed gene replicate across datasets. We compared the DE effect estimated by our perturb-seq screens with DE effects measured in published arrayed knockout screens in CD4+ T cells (using the Rest condition to match the cellular context).[5,14] We found that DE effects were significantly correlated between perturb-seq and independent arrayed screens for matched targets, with correlations significantly higher than for randomly paired perturbations (27 of 32 tested targets showed significant correlation) (Figure 1E). Non-replicating *trans*-effects may reflect noise in DE estimates due to limited cell numbers, small effect size, or genuine differences between knockdown and knockout responses under distinct culture conditions. We next compared genome-wide regulator effects on individual genes with measurements from FACS-based CRISPR-based screens for regulators of four T cell-relevant genes in both resting and re-stimulated conditions. Regulator effects were consistent with FACS-based screen estimates (Figure 1F), with significantly stronger correlations between matched stimulation conditions than between mismatched conditions. Overall biological reproducibility was remarkable given differences in perturbation techniques and phenotypic readouts. These results indicate that our dataset captures condition-specific regulatory effects on target gene programs across T cell activation states.

Overall, the median number of *trans*-effects per perturbation with significant knockdown was 2 genes, while the top 5% of perturbations affect >427 genes (Figures S10A and S10C; mean = 81.61 genes), reflecting both the sparsity of regulatory networks and the presence of master regulators.[18] The mean number of *trans*-effects was only weakly dependent on the strength of on-target knockdown (Figure S10B) and varied drastically among different classes of genes (Figure S10D). The number of detected incoming *trans*-regulatory connections per measured gene was strongly dependent on baseline expression levels, at least partially reflecting power issues in DE analysis (Figure S10E). After accounting for this expression-dependent detection bias, we found that *trans*-regulatory effects were most prevalent 8 h post-stimulation, with immune-relevant gene sets including cytokines and cytokine receptors, exhibiting more incoming regulatory connections than expected (Figure S10F). Comparison of our CD4+ T cell *trans*-effects to published

Please cite this article in press as: Zhu et al., Genome-scale perturb-seq in primary human CD4+ T cells maps context-specific regulators of T cell programs and human immune traits, Cell (2026), https://doi.org/10.1016/j.cell.2026.08.002

CellPress
OPEN ACCESS

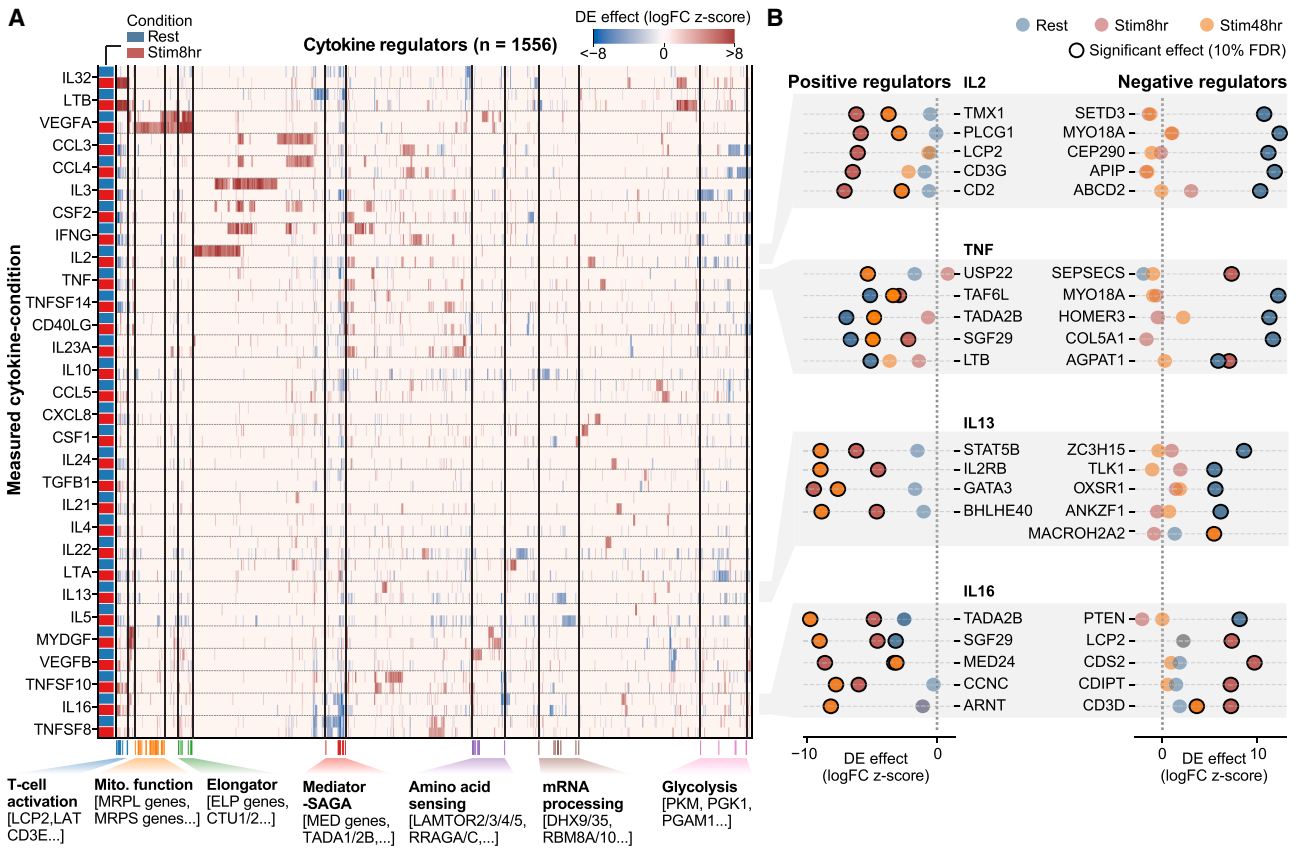

(legend on next page)

Please cite this article in press as: Zhu et al., Genome-scale perturb-seq in primary human CD4+ T cells maps context-specific regulators of T cell programs and human immune traits, Cell (2026), https://doi.org/10.1016/j.cell.2026.08.002

perturb-seq data from K562[9] and Jurkat[19] cells revealed only partial sharing of *trans*-effects across cell types (Figure S11; Note S4).

To our knowledge, no previously available perturb-seq dataset provides the depth, perturbation coverage, and replication structure needed to robustly estimate genome-wide regulator-to-gene effects while accounting for biological and technical variance.[20] To guide the design of future primary-cell screens, we performed a power analysis of how cell number, donor replicates, and read depth affect *trans*-effect estimation accuracy (STAR Methods), measuring correlations between DE estimates in downsampled datasets and either held-out cells (Figures S12A and S12B) or independent arrayed knockout screens (Figures S12C and S12D). Downsampling read depth to ~10% (~1,000 UMIs per cell) substantially reduced *trans*-effect replication (~30% reduction in Pearson R), even with >500 cells per perturbation. At higher read depths, increasing cells per perturbation consistently improved DE estimates, stabilizing at ~200 cells (Figures 1G, S12, and S13). For a fixed number of cells per perturbation, increasing donor replicates further improved robustness (Figures 1G, S12, and S13), likely by better capturing donor-specific response variation. These findings underscore the importance of both cell coverage per perturbation and biological replication in large-scale primary-cell perturb-seq studies.

Identifying regulators of immune cytokines

Genome-wide perturb-seq should enable systematic discovery of all regulators controlling the levels of any given gene. As a first application of the dataset, we tested whether we could correctly identify regulators of cytokine genes. Production of specific sets of cytokines is a major mechanism by which CD4+ T cells orchestrate immune responses. We and others have dedicated considerable efforts to identify genes that regulate production of key cytokines in human T cells to gain insight into immune regulation.[21–23] Our previous CRISPR screening studies have provided comprehensive insights into the regulation of cytokines, including interleukin (IL)-2 and interferon (IFN)-γ,[6] using FACS-based CRISPR screens, but this approach required massive sorting efforts to uncover the regulators of each individual cytokine of interest. Cytokine regulators discovered with our perturb-seq data strongly accord with FACS-based screen results despite differences in the experimental methods and readouts (notably mRNA versus protein levels of cytokines; Figure 1F).

We focused on 30 canonical cytokine genes expressed in our system (Figure S14). These genes encode pro-inflammatory cytokines (IFN-γ and TNF), Th2 cytokines (IL-4/5/13), regulatory cytokines (IL-10 and TGF-β), chemokines (CCL3/4/5 and CXCL8), and others. This analysis identified 1,556 gene perturbations that exerted strong regulatory effects (FDR < 1%) on at least one cytokine in at least one condition (Figures 2A and S15). Regulators controlling broad sets of cytokines included expected TCR signaling components, subunits of the ubiquitous transcriptional coactivator complexes Mediator (*MED12* and *MED24*) and SAGA coactivator complex (*TAF6L*, *TADA1*, *TADA2B*, *SUPT20H*, and *USP22*), as well as genes involved in other functional programs such as mitochondrial function, amino acid sensing, mRNA processing, and glycolysis (Figure 2A). Consistent with our previous findings,[13] knockdown of Mediator and SAGA components appeared to alter T cell rest and activation and caused stimulation-specific effects on genes encoding for multiple cytokines, including *TNF* and *IL16* (Figures 2A and 2B). For stimulation-responsive cytokines like *IL2* and *IL13*, negative regulators (knockdown log2 fold change [LFC] > 0) were detected predominantly in the Rest condition, where cytokines exhibit minimal constitutive expression. By contrast, positive regulators (knockdown LFC < 0) were more readily identified following re-stimulation (e.g., *CD3* and *LCP2* for *IL2*; *GATA3* for *IL13*) (Figures 2A and S15). The *trans*-effects detected by perturb-seq encompass both direct and indirect regulatory relationships. For example, integration with published GATA3 ChIP-seq data showed that some cytokine genes affected by *GATA3* knockdown, such as *IL13*, are directly bound by GATA3 at their promoters, while others are likely regulated indirectly through intermediate effectors (Figures S16A–S16D; Note S5).

We further mapped and validated regulators of two cytokine genes, *IL10* and *IL21*, which play pivotal, yet distinct, roles in immune homeostasis. *IL10* can act as a potent anti-inflammatory cytokine gene and has pleiotropic functions in immune regulation.[24] Defects in IL-10 signaling are genetically linked to early-onset inflammatory bowel disease in both humans and mice.[25,26] Conversely, *IL21* is essential for T cell proliferation and serves as a key mediator of cell-dependent B cell differentiation in germinal centers, with signaling defects often

Figure 2. Mapping regulators of cytokines in primary CD4+ T cells

(A) Heatmap of DE effects (LFC *Z* score) of 1,556 regulators with at least one significant (1% FDR) *trans*-effect on expression of 30 cytokines (*y* axis) in Rest and Stim8hr culture conditions (left color bar). Axes are sorted by hierarchical clustering on Stim8hr DE effects. Colored tick marks below the heatmap highlight selected functionally enriched gene sets among the perturbed regulators.

(B) Scatterplots of top 5 regulators (by *Z* score across conditions) of selected cytokine genes (*IL16*, *TNF*, *IL13*, and *IL2*). For each cytokine, positive regulators (left) and negative regulators (right) are shown. Color: culture condition. Circled points: significant DE effects.

(C) Volcano plots of LFC of *IL10*/*IL21* expression relative to NTCs and −log10 FDR for each regulator that has a minimum cross-donor correlation > 0.35 (Table S7). Significant regulators (FDR < 10%, |LFC| > 1) are colored blue (positive regulators) or red (negative regulators). Regulators validated in (F) are highlighted by white boxes.

(D) Schematic of inferred *IL10*/*IL21* regulatory sub-network inferred from perturb-seq. Connectors denote significant (10% FDR) downregulation (blue arrow) or upregulation (red T-bar) of *IL10*/*IL21* by regulator knockdown.

(E) Experimental workflow schematic for arrayed validation (also see STAR Methods).

(F) (Top) heatmaps summarizing regulator knockdown effects in validation experiments. Regulator names are color-coded the same as (C). * FDR < 10%, ** FDR < 1%, *** FDR < 0.1%. (Bottom) Representative flow cytometry plots showing intracellular staining of IL-10 (left) and IL-21 (right) for NTCs and selected regulator knockdowns. Numbers in the gates indicate the percentage of cytokine-positive cells.

See also Figures S14–S15, S17–S19 and Tables S9, S10, and S11.

Please cite this article in press as: Zhu et al., Genome-scale perturb-seq in primary human CD4+ T cells maps context-specific regulators of T cell programs and human immune traits, Cell (2026), https://doi.org/10.1016/j.cell.2026.08.002

CellPress
OPEN ACCESS

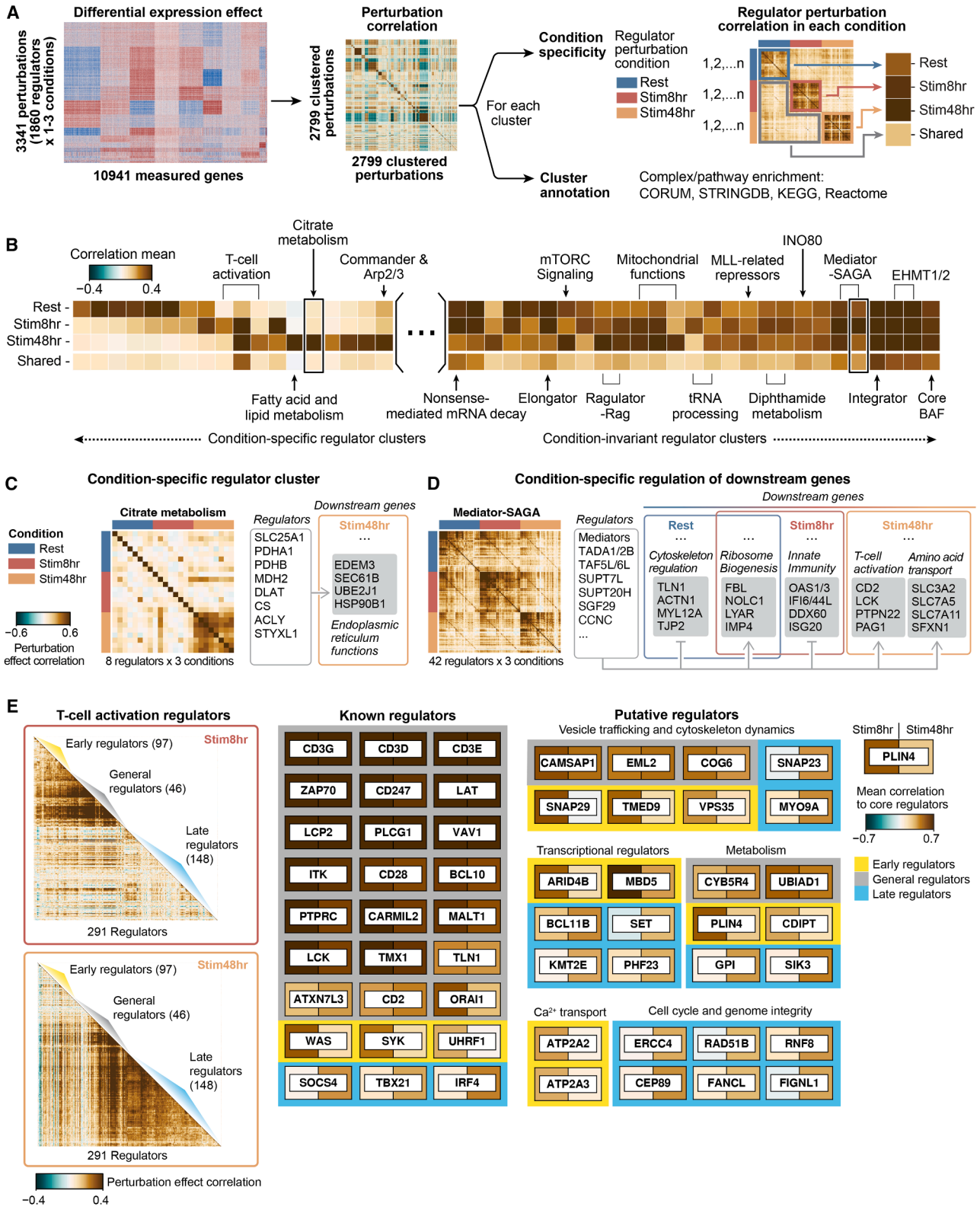

(legend on next page)

manifesting as primary immunodeficiencies.[27–30] Perturb-seq identified a broad network of regulators for both cytokines, recovering both established and putative drivers of cytokine expression (Figure 2C). For example, *MEN1*, a component of the MLL1/2 complex known to repress *IL10* expression,[31] was among the top negative regulators of *IL10*, validating the sensitivity of the perturb-seq. Beyond shared drivers like core genes of the TCR signaling pathway and Mediator complex subunit *MED24*, perturb-seq revealed distinct regulatory architectures for each cytokine (Figure 2D). We observed negative regulation of *IL10* by members of the SAGA complex (*SGF29*, *ATXN7L3*, and *USP22*) and *ELOB*, a regulatory subunit of the Elongin complex. In parallel, perturb-seq identified oxidoreductase *CYB5R4* as a positive regulator of *IL21* and regulators of calcium homeostasis (*ATP2A2* and *ORAI1*) and the Elongator complex (*ELP2* and *ELP3*) as negative regulators of *IL21*. Notably, we found that the transcription factor *NFKB2* and the lysine-specific demethylase *KDM1A* act as divergent regulators—acting as positive regulators for *IL10* but negative regulators for *IL21* (Figures 2C and 2D). Beyond *MEN1* and components of TCR signaling pathway, many of these were not recognized previously to be regulators of *IL10* or *IL21* regulation to our knowledge.

We validated 9 known and candidate regulators nominated by perturb-seq in an arrayed format using two independent guides per target, measuring outcomes via both bulk RNA sequencing (RNA-seq) and intracellular protein staining. Regulatory effects were highly concordant with pooled perturb-seq data and consistent across independent guides (Figures 2E, 2F, S17, and S18). In transcriptional validation, all 12 tested regulatory interactions showed directional effects consistent with the screen, 10 of which were statistically significant (FDR < 10%). This concordance generally extended to the protein level, where flow cytometry confirmed significant shifts in protein production corresponding to the transcriptional changes. A notable exception was observed in the regulation of *IL10* by *NFKB2*, where protein level changes did not mirror the transcriptional phenotype, suggesting additional post-transcriptional mechanisms that regulate cytokine production.[32] Perturbation-driven changes in cellular proliferation were largely independent from shifts in *IL21* expression and are only weakly correlated with shifts in *IL10* expression (Figures S17D and S18C), consistent with specific regulation of cytokine programs rather than expression effects solely through broad impacts on cell growth. Importantly, while our targeted validation focused on *IL10* and *IL21*, these nine regulators exert pleiotropic effects on the expression of many other cytokines as revealed by perturb-seq measurements and arrayed transcriptional profiling, which were largely concordant (Figure S19). Together, these data demonstrate the power of genome-scale perturb-seq to dissect the complex regulatory circuitry of immune cytokines critical for immune homeostasis.

Functional clustering of T cell regulators

We next more comprehensively mapped CD4+ T cell regulatory programs. We clustered perturbations based on their effects on downstream genes, as previous work has shown that genes with similar perturbation profiles frequently have similar functions.[9] We focused on 3,341 strong perturbations (defined as a gene knockdown in a specific stimulation condition) from 1,860 perturbed regulators (STAR Methods; Figure 3A). Unsupervised clustering identified 111 regulator clusters (Table S13). We annotated these regulator clusters using gene set enrichment analysis of public databases combined with manual curation (STAR Methods). We identified clusters governing core cellular processes, including cellular signaling, intracellular trafficking, nonsense-mediated decay, cellular metabolism, genome integrity, and transcriptional regulation (Figures 3B and S20; Table S13). Many clusters could not be readily annotated. Regulators in these clusters tended to be expressed in a tissue-specific manner (Figure S21), which may explain their under-representation in public biological interaction databases.[33]

Given that individual gene perturbations often elicit distinct effects depending on the stimulation context (Figure 2A), we assessed whether these regulator clusters exhibited condition specificity. For each cluster, we computed the intra-condition mean regulator perturbation correlation within each of the three conditions (“Rest,” “Stim8hr,” and “Stim48hr”), as well as inter-condition mean perturbation correlation (“Shared”) (Figure 3A, top right; STAR Methods). We observed two forms of condition-specific clusters.

First, about one-third of regulator clusters had strong intra-condition perturbation effect correlation in only one or two of the three conditions (Figure 3B, left; Table S13). This was not primarily driven by differences in regulator expression or cell numbers across conditions (Figure S22A). These clusters represent regulatory complexes or pathways that only function in

Figure 3. Functional gene programs of CD4+ T cells across conditions

(A) Schematic of clustering analysis on 3,341 strong perturbations (one perturbation: one perturbed gene in one condition). Each cluster was analyzed for condition specificity and annotated by complex/pathway enrichment. The example correlation matrix shown on the right is from cluster 28 (mitochondrial functions).

(B) Condition specificity in a representative set of regulator clusters: heatmap showing mean intra-condition perturbation correlation of cluster regulators in each of the three conditions (“Rest,” “Stim8hr,” and “Stim48hr”) and mean inter-condition perturbation correlation (“Shared”). Biological annotations of a subset of clusters are shown.

(C) An example of condition-specific regulator cluster (cluster 36).

(D) An example regulator cluster showing condition-specific regulation of downstream genes (cluster 10). In both (C) and (D), left heatmaps show the correlation of perturbation effects for the same set of clustered regulators across all conditions. Representative downstream genes grouped by gene ontology analysis are shown on the right (Figure S23). Connectors denote downregulation (arrow) or upregulation (T-bar) of downstream genes by regulator knockdown.

(E) (left) Correlation matrix of T cell activation regulators. The rows and columns are ordered by early, general, and late regulators. (Right) Selected known and putative T cell activation regulators. Tiles are colored by the gene’s mean perturbation correlation with 9 core regulators (*CD3D/E/G*, *CD247*, *ZAP70*, *LAT*, *LCP2*, *PLCG1*, and *VAV1*) in Stim8hr or Stim48hr.

See also Figures S20–S23 and Tables S13, S14, and S15.

Please cite this article in press as: Zhu et al., Genome-scale perturb-seq in primary human CD4+ T cells maps context-specific regulators of T cell programs and human immune traits, Cell (2026), https://doi.org/10.1016/j.cell.2026.08.002

certain stimulation conditions. Regulators of citrate metabolism, for example, exhibited correlated regulator perturbation effects exclusively in the Stim48hr condition (Figure 3C), consistent with their established roles in metabolic regulation during immune activation.[34] Notably, we found many unannotated clusters also exhibited correlated effects in only a subset of conditions (Figure S21).

Second, regulators had correlated effects across multiple conditions but regulated distinct gene sets in different stimulation conditions. This was indicated by lower inter-condition correlations of perturbation effects (Figure 3B, right, the "shared" row). Mediator-SAGA cluster members, for instance, showed high intra-condition correlation across all three conditions, consistent with them acting as a physical complex in all contexts. However, disrupting members of this complex of regulators altered the expression of distinct gene sets depending on the stimulation state of the cell (Figures 3D and S23; Table S14), consistent with our previous findings.[13]

A noteworthy example of condition-specific effects are clusters associated with T cell activation (Figures 3B and 3E). These clusters, active primarily in the Stim8hr and Stim48hr conditions, encompass the majority of canonical activation regulators, including core CD3 receptor complex members (*CD3D/E/G* and *CD247*), stimulatory receptors (*CD2*, *CD28*, and *PTPRC*), adaptor proteins (*LAT* and *LCP2*), and signal transduction enzymes (*ZAP70*, *LCK*, *ITK*, *VAV1*, and *PLCG1*).[35] *TMX1* was also identified as a critical activation regulator, consistent with a recent report[36] demonstrating its requirement for TCR surface expression.

We next asked whether these activation regulators could be distinguished as early- versus late-acting based on their perturbation effects across the two stimulation time points. Regulators mapping to activation clusters at Stim8hr only were classified as "early," at Stim48hr only as "late," and at both time points as "general" (Figure 3E; Table S13). Early regulators included calcium homeostasis factors (e.g., *ATP2A2* and *ATP2A3*), consistent with key roles of calcium signaling following TCR engagement.[37] Late regulators include factors controlling cell cycle and genome integrity (*ERCC4*, *CEP89*, *RNF8*, *RAD51B*, *FANCL*, and *FIGNL1*), highlighting the importance of these processes in supporting rapid cellular expansion. We also identified other putative early, late, or general regulators involved in intracellular vesicle trafficking, cytoskeletal dynamics, central metabolism, cell signaling, and transcriptional regulation (Figure 3E, right). Early and late regulators also controlled distinct downstream programs. 8 h post-stimulation, perturbations of early and general regulators induced changes of early activation markers, including *IL2RA* and *LAG3* (Figures S22B and S22C). By contrast, at 48 h post-stimulation, perturbations of late and general regulators induced changes in metabolic genes, particularly those driving oxidative phosphorylation (Figures S22B and S22C), consistent with metabolic switches accompanying T cell activation.[38] We selected 6 predicted early and late regulators and 3 known core regulators, knocked down each individually in an arrayed format, and measured outcomes via both bulk RNA-seq in Stim8hr and Stim48hr conditions. Perturbations of 5 of 6 early/late regulators selected here (*ATP2A2*, *ATP2A3*, *HEXD*, *MEN1*, and *GPI*) showed condition-specific transcriptional effects consistent with their temporal classification, supporting the robustness of identified temporal regulatory modules (Figure S22D).

In summary, genome-scale perturb-seq in primary human cells performed across multiple stimulation conditions can identify clusters of regulators that act coherently to shape general and, importantly, context-specific gene expression programs.

Predicting regulators of human T cell states: Th1 versus Th2 polarization

We next asked whether we can use our perturb-seq data to interpret external data from human cohorts. Over the past decade, international efforts have generated single-cell atlases of cellular states across human tissues in health and disease. Perturb-seq maps in primary cells offer a unique opportunity to identify regulators driving the transcriptional programs observed in these atlases. If successful, this approach could pinpoint causal factors that establish or maintain tissue cell states, clarify how those states emerge, and guide their programmable control. We therefore tested whether perturb-seq can be leveraged to identify regulators and pathways that contribute to T cell state signatures observed in human tissues.

Given the gene expression profile of a T cell state of interest, from bulk or scRNA-seq experiments, we can compute a "state signature" by contrasting it with a reference T cell population. We hypothesized that the context-specific gene programs controlled by every potential regulator could be used to nominate a set of regulators that, together, move cells toward a desired state. Using DE estimates for each perturbed gene in perturb-seq data, we fit a regression model to reconstruct the state signature as a linear combination of perturbation signatures (Figure 4A; STAR Methods), nominating putative positive and negative regulators of the cell state signature. We can further partition the overall state signature into sets of genes controlled by distinct regulators or pathways.

We first tested this approach to identify regulators of Th1 and Th2 polarized helper CD4+ T cell states, which have well-characterized master regulators and play critical roles in immunity and inflammatory diseases.[39] We derived a Th2/Th1 signature from published bulk RNA-seq data of Th1 and Th2 cells FACS-sorted from human donors (Figure 4B),[40,41] verifying the signature's robustness across independent cohorts (Figure S24A). Significantly DE genes included well-characterized markers, such as *GATA3*, *CCR4*, and *IL13*, upregulated in Th2 cells, and *IFNG*, *EOMES*, and *TBX21*, upregulated in Th1 cells (Figure 4C).

We applied our model to reconstruct the Th2/Th1 signature from perturbation effects in the Stim8hr condition because T cell polarization occurs upon T cell stimulation, and we measured the highest fraction of cells expressing polarization markers in this condition (Figure S3; results in different input conditions are discussed in Note S6). Perturbation responses accurately predicted the sign and magnitude of held-out genes in the Th2/Th1 signature, both in the training cohort (mean cross-validation R = 0.39; Figure 4D) and validation cohort (mean cross-validation R = 0.27; Figure 4E), demonstrating that predicting regulators from one set of genes can predict polarization effects

Please cite this article in press as: Zhu et al., Genome-scale perturb-seq in primary human CD4+ T cells maps context-specific regulators of T cell programs and human immune traits, Cell (2026), https://doi.org/10.1016/j.cell.2026.08.002

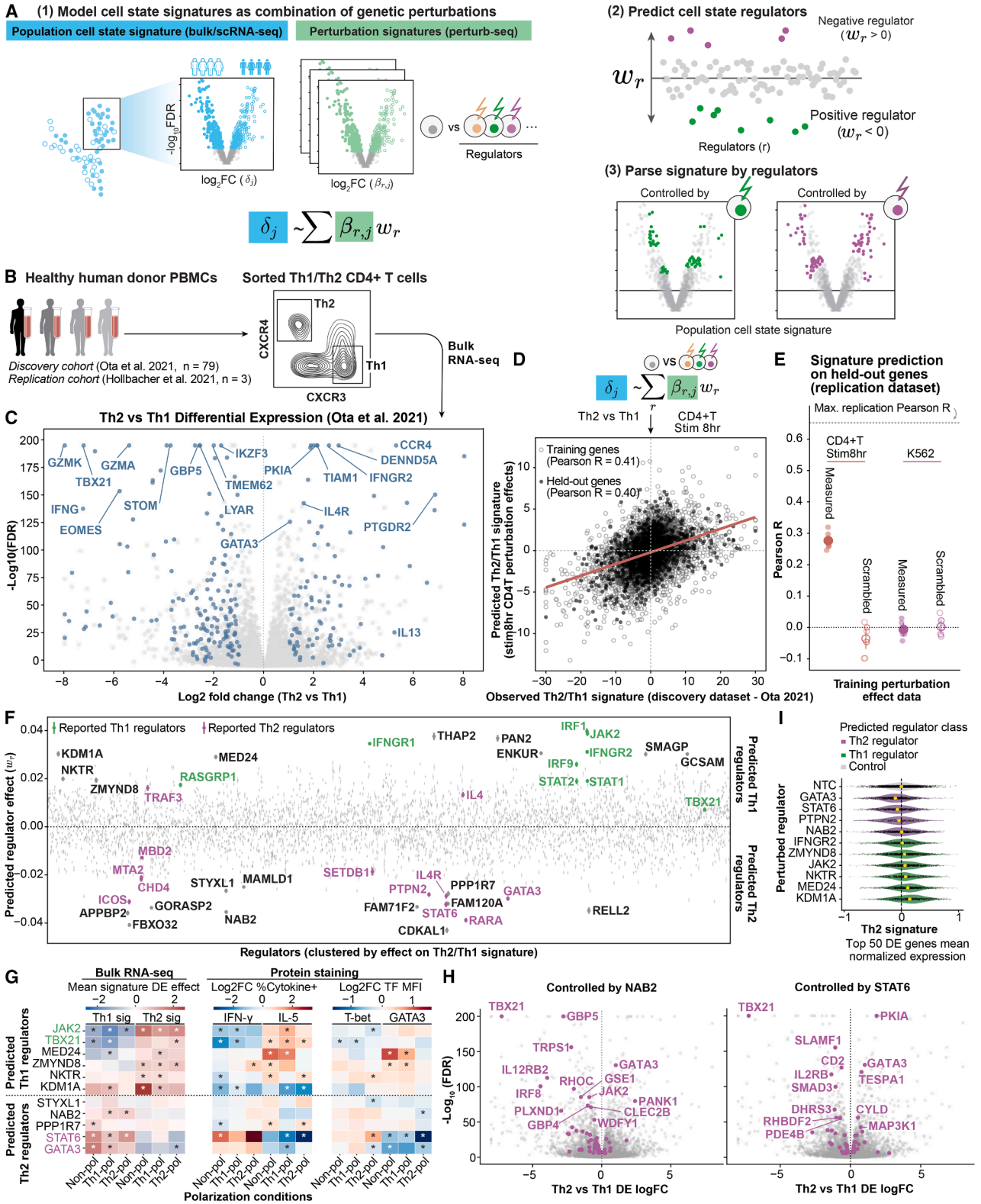

Figure 4. Predicting regulators of CD4+ T cell polarization

(A) Model schematic: cell state signatures from observational (bulk or single-cell) RNA-seq data are modeled as linear combinations of perturbation effects to identify regulators and parse their contributions to gene expression programs.

(legend continued on next page)

Please cite this article in press as: Zhu et al., Genome-scale perturb-seq in primary human CD4+ T cells maps context-specific regulators of T cell programs and human immune traits, Cell (2026), https://doi.org/10.1016/j.cell.2026.08.002

on different genes. Reconstruction from CD4+ T cell perturbations significantly outperformed models trained on K562 cell line data (Figure 4E; Figure S24B), even when restricting the analysis to well-powered perturbed genes in the K562 data (Figure S24C). We fit control models with scrambled perturbation effects for each gene to confirm that performance differences reflected genuine signal rather than baseline expression similarity (Figure 4E). Together, these results indicate that cell-type-specific perturbation responses can reconstruct gene expression signatures of T cell states observed in human populations.

The model successfully nominated Th1/Th2 regulators with the expected directional effects. Top regulators promoting a Th1 state included IFN-γ receptor genes (*IFNGR1* and *IFNGR2*), *JAK2* (a signaling kinase downstream of the IFN-γ receptor),[42] and the IFN-γ-induced transcription factor gene *IRF1*[43] (Figure 4F; Figure S25A). Top Th2 regulators included *IL4R*, *STAT6* (a transcription factor activated by IL-4 signaling), *GATA3* (a master transcription factor induced by *STAT6*), and the retinoic acid receptor (*RARA*), a transcription factor known to regulate Th2 cytokines.[44,45] The regulators identified by this analysis appear to be specific to Th1 and Th2 signatures as opposed to general activation, as different regulators were nominated when we fit an analogous model to predict a general TCR activation signature (Figures S24D and S24E). Genes encoding multiple members of the CHD4/MTA2/NuRD chromatin-remodeling complex were nominated as candidate Th2-promoting regulators; this complex has been shown to interact with GATA3 to control Th2 polarization in mouse models.[46] By contrast, genes encoding components of the EHMT1/2 complex subunits were predicted as Th1 regulators, consistent with their known roles in controlling histone methylation at effector cytokine loci[47,48] (Figure S25B). We found only 2 regulators whose inferred direction was opposite expectations: *TRAF3*, which is reported as a STAT6 regulator skewing cells toward Th2 fate but only in specific contexts,[49] and *IL4*. As with other cytokine perturbations, *IL4* knockdown showed relatively weak transcriptional effects, perhaps due to paracrine signaling between cells in the pooled experimental set-up dampening the perturbation response. The relatively modest score for *TBX21* (encoding for Th1 master regulator T-bet) likely reflects our signature definition: *TBX21* knockdown robustly down-regulated Th1 effectors (*IFNG*, *GNLY*, and *CRTAM*) but did not de-repress Th2 markers, unlike perturbations of *JAK2* or *IRF9*. In addition, *TBX21* loss triggered upregulation of IFNγ-responsive genes (*JAK2*, *STAT1*, and *GBP1/4/5*), which could represent a compensatory feedback mechanism (Note S7). Not all predicted regulators are themselves differentially expressed between Th1 and Th2 cells, indicating that differential activity of a pathway can occur without corresponding changes in regulator transcript levels (Figure S25C).

The model also nominated several putative regulators without established roles in T cell polarization. To validate predictions, we knocked out 18 known and uncharacterized regulators individually in arrayed format—both without polarizing conditions and separately in either Th1 or Th2 polarizing conditions—measuring markers of polarization with bulk RNA-seq and flow cytometry (Figure S26A). After focusing on a set of 13 candidate regulators showing robust perturbation effects across guides and donors in perturb-seq (Table S18; STAR Methods), transcriptome effects in arrayed experiments were largely concordant with perturb-seq, and effects under Th1/Th2 polarizing conditions were consistent with those measured in our non-polarized perturb-seq stimulation (Figures S26B and S26C; Table S19). Of these 13 tested regulators, 12 significantly shifted Th1 and Th2 signature gene expression in the expected direction, including 4 uncharacterized Th1 and 2 uncharacterized Th2 regulators (Figure 4G).

Validated regulators acted through diverse mechanisms and exerted distinct effects on Th1 and Th2 programs

(B) Schematic illustration of public data used to extract Th2/Th1 polarization signatures with bulk-RNA-seq of sorted populations.
(C) Volcano plot of Th2/Th1 signature (discovery cohort). Log-fold change (*x* axis, LFC < 0: high in Th1; LFC > 0: high in Th2) versus −log10 FDR (*y* axis) of DE analysis (FDR values capped at −log10(FDR) = 200; LFC capped between −8 and 8). Robust genes significantly upregulated in both discovery and replication cohorts are highlighted in blue. Top robust DE genes by FDR are annotated.
(D) Reconstruction of polarization signatures from perturbation effects: observed Th2/Th1 signature (*x* axis) versus predicted signature from the model trained on the discovery cohort (*y* axis). Black dots denote genes held out in model fitting.
(E) Evaluation of polarization signature prediction on held-out genes in the replication cohort: mean Pearson correlation coefficients (*y* axis) across splits (5-fold cross-validation with 3 initializations) for model fit on Stim8hr CD4+ T perturbation effects (red, 3,994 regulators) and K562 perturbation effects dataset (blue, 2,190 regulators). Scrambled controls are shown in light colors. Dotted line indicates maximum achievable correlation (inter-cohort agreement). Error bars: 95% CI across cross-validation splits.
(F) Predicted regulator effects (w_r, *y* axis) on polarization signature for all regulators in Stim8hr condition (mean and standard error for w_r on 15 train-test splits). Regulators are ordered by hierarchical clustering on the perturbation effects on Th2/Th1 signature genes. Known Th1 and Th2 regulators highlighted in green and purple, respectively. We annotate in black the top and bottom predicted regulators and regulators selected for follow-up (STAR Methods) without known effects on polarization.
(G) Heatmaps summarizing individual regulator knockdown effects in arrayed CRISPRi validation experiments on robust perturbations (STAR Methods): mean DE effect (logFC *Z* score) on Th2/Th1 signature genes in bulk RNA-seq (left, sig: signature); mean LFC in percentage of IL-5+ and IFN-γ+ cells in flow experiments (center); mean LFC in median fluorescence intensity for GATA3 and T-bet staining (right). Quantifications in non-polarized, Th1- and Th2-polarized conditions are shown (*x* axis). Regulator names are color-coded the same as (F). Validation on known regulators *MTA2* and *PTPN2* was performed only in non-polarizing conditions and is not shown (see Figure S26). * FDR < 10%.
(H) Th2/Th1 signature genes controlled by predicted regulator pathways: volcano plot of DE genes between Th2 and Th1 cells as in (C), highlighting genes significantly regulated by *NAB2* (left) or *STAT6* (right). We highlight signature genes that are significantly differentially expressed (10% FDR) upon knockdown of the regulator and whose direction of change upon perturbation is consistent with both the predicted regulator effect and the cell state signature.
(I) Distributions of Th2 signature gene expression (*x* axis) in single cells with perturbation of validated polarization regulators (*y* axis), ordered by mean signature score across cells (yellow dot). Color: predicted polarization effect (purple: Th2-promoting, green: Th1-promoting, gray: NTCs). Signatures of NTC cells are shown only for cells with a subsample of non-targeting guides.
See also Figures S24–S29 and Tables S16, S17, S18, and S19.

Please cite this article in press as: Zhu et al., Genome-scale perturb-seq in primary human CD4+ T cells maps context-specific regulators of T cell programs and human immune traits, Cell (2026), https://doi.org/10.1016/j.cell.2026.08.002

(Figure S27A). For example, *STAT6* and *NAB2* were both identified as Th2 regulators and had similar average effects on Th1 signature genes but controlled distinct downstream pathways: both modulated *TBX21*, but *STAT6* regulated TGF-β pathway components (*SMAD3*, *SMAD2*, *TGFBR2*, and *LRRC32*; FDR = 0.02), whereas *NAB2* knockdown induced type II IFN response genes (*IRF1/8*, *GBP4/5/2*, *DDX60*, *PRF1*, *IFNGR2*, and *OAS1/3*; FDR = 0.007) (Figure 4H). *NAB2* is a transcriptional repressor that interacts with *CHD4* in the NuRD complex,[50] linking this uncharacterized hit to chromatin-remodeling machinery with previously described roles in Th2 polarization.[46] The Th1 regulators *KDM1A* and *ZMYND8* likewise act as transcriptional repressors: both are chromatin readers that recognize active enhancers and scaffold repressor TF complexes, and their knockdown derepressed T cell activation and metallothionein response signatures. *MED24* is a subunit of the Mediator complex, whose context-specific role in T cell activation we have previously described.[13] *NKTR* encodes a nuclear cyclophilin whose perturb-seq signature was enriched for spliceosomal components, consistent with a proposed role as a spliceophilin.[51]

To assess whether predicted regulators modulate key protein products in addition to transcriptional signatures, we performed arrayed knockdowns and measured protein markers of polarization by flow cytometry (transcription factors T-bet and GATA3 and cytokines IFN-γ and IL-5; Figures S28A and S28B). As expected, knockdown of canonical master regulators (*TBX21*, *JAK2*, and *GATA3*) had strong effects, consistent with these factors being individually required for induction of polarized states (Figures 4G and S28C). Effects of less well-characterized predicted Th1 regulators on protein expression were more subtle but largely consistent with their assignment. *MED24* knockdown produced the strongest effect on GATA3 and IL-5 of any tested regulator, with a weaker T-bet upregulation (Figures 4G and S28C), suggesting a skew toward Th2 polarization alongside a broader effect on activation.[13] *KDM1A* perturbation significantly downregulated both effector cytokines, in contrast to the general upregulation of effector transcript signatures observed by RNA-seq. Predicted Th2 regulators showed weaker effects on marker proteins, with *NAB2* knockdown showing the strongest effects in Th2-polarized conditions. *PPP1R7* perturbation altered marker cytokines in the direction opposite to that expected from its RNA-seq signature. Collectively, these results indicate that not all predicted transcriptional regulators prioritized by genome-scale perturb-seq are individually sufficient to induce a fully polarized state. Complete polarization likely requires the coordinated action of multiple regulators together with external signaling input, and the insufficiency of certain individual perturbations may reflect their position downstream of master regulators within the regulatory hierarchy. This is also reflected in the effect of putative regulators on Th1 or Th2 polarization at the single-cell level in the perturb-seq data (Figures 4H and S27A; STAR Methods). Perturbed CD4+ T cells in non-polarized conditions showed substantial cell state heterogeneity both among control cells and among cells with each perturbation. Even with heterogeneity of initial cell states and potential heterogeneity of knockdown efficiencies (Document S1; Figures S27B and S27C), perturbed cells showed the expected shifts in Th1 and Th2 gene expression compared with NTCs.

Collectively, perturb-seq predictions and arrayed validation experiments show that the nominated regulators contribute to Th1/Th2 polarization through diverse molecular pathways. These analyses illustrate how perturb-seq can identify regulators of cell state signatures and reveal the distinct programs each regulator controls.

Predicting regulators of CD4+ T cell states in population-scale scRNA-seq across age groups

While T cell states like Th1 and Th2 have been extensively characterized through isolation and phenotyping, recent single-cell RNA-seq studies are revealing tissue-specific programs,[52,53] disease-associated states,[54–56] infection responses,[57,58] and population-level variation.[59–61] We therefore tested whether genetic perturbations could recapitulate transcriptional variation in T cells from human cohort studies to identify candidate regulators of observed T cell gene signatures.

As a case study, we analyzed age-associated CD4+ T cell variation, where alterations are thought to contribute to chronic inflammation and multi-organ aging phenotypes.[62] We extracted CD4+ T cell expression profiles from 782 donors in the OneK1K cohort,[59] holding out cells from 199 donors for validation. We tested for age-associated gene expression changes across CD4+ T cell subsets (naive, central memory, and effector memory) (Figure 5A), controlling for subset-specific differences to avoid confounding by changes in cell composition associated with aging (Figure S30A; STAR Methods). The age-associated gene signature replicated in held-out donors and cell-type-specific aging signatures from independent cohorts[63,64] (Figure S30B), showing no significant enrichment for genes associated with cytomegalovirus (CMV)-driven variation, a potential confounder across individuals of different ages[63] (Figure S30C). Age-associated changes include upregulation of pro-inflammatory factors and downregulation of apoptotic pathways (Figure S30D).

We first tested whether genetic perturbation effects could recapitulate the aging signature. Perturbation effects in the Rest condition were predictive of age-associated changes (cross-validation R = 0.366), with significantly better fit than perturbation effects in stimulated CD4+ T conditions or in K562 cells (Figures 5C, S31A, and S31B). This likely reflects the predominance of unstimulated T cells in PBMC samples.

We then examined which regulators are predicted as positive or negative regulators of age-associated changes (Figures 5D and S31C). Among the top aging regulators were components of the mTORC1 signaling pathway, notably TSC complex genes (*TSC1/2*), GATOR complex genes (*DEPDC5* and *NPRL3*), and *RPTOR* (Figure 5D). Hyperactivation of mechanistic target of rapamycin (mTOR) is considered a hallmark of aging: treatment with the mTOR inhibitor rapamycin extends longevity in mammals,[65] and pharmacological mTOR inhibition has been shown to improve immune function in the elderly.[66,67] In T cells, mTOR activates several downstream effector pathways, including immune receptor signaling, metabolic programs, and migratory activity,[68] and aged T cells exhibit increased basal activation of phosphatidylinositol 3-kinase (PI3K)-AKT-mTOR signaling.[62] In line with this evidence, our model prioritized mTORC1 signaling genes as key regulators of age-associated phenotypes. However, the direction of effect of different

Please cite this article in press as: Zhu et al., Genome-scale perturb-seq in primary human CD4+ T cells maps context-specific regulators of T cell programs and human immune traits, Cell (2026), https://doi.org/10.1016/j.cell.2026.08.002

CellPress
OPEN ACCESS

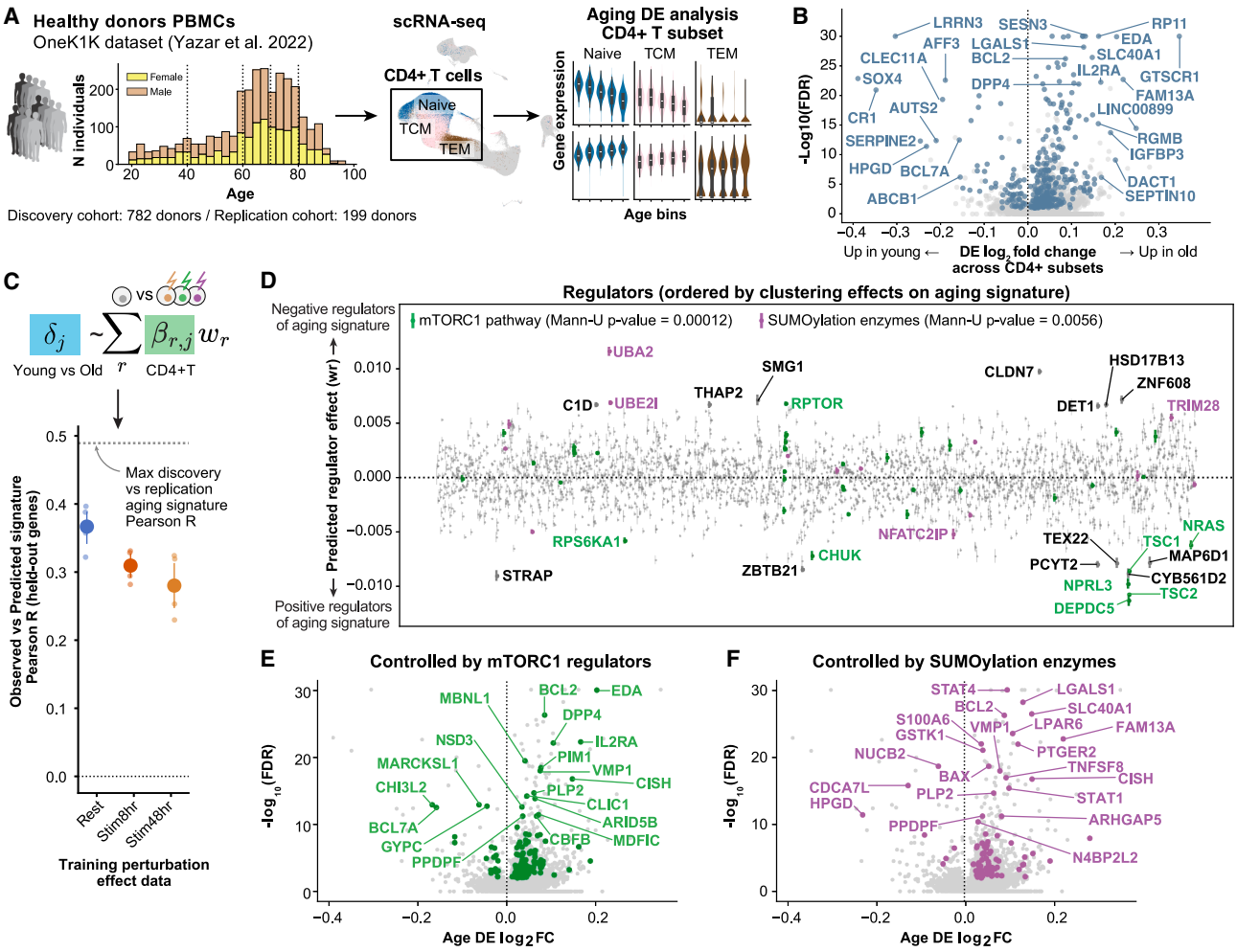

Figure 5. Predicting candidate regulators of CD4+ T cell aging from a population-scale cell atlas

(A) Illustration of analysis of OneK1K cohort scRNA-seq data for aging gene signature. The signature was computed by DE analysis across CD4+ T cell subsets, testing for DE with age across subsets, and accounting for subset differences.

(B) Volcano plot of CD4+ T cell aging signature (discovery cohort). Log-fold change (*x* axis, LFC < 0: high in young; LFC > 0: high in old) versus −log10 FDR (*y* axis) of DE analysis (FDR values capped at −log10(FDR) = 30. Robust genes significantly upregulated in both discovery and replication cohorts are highlighted in blue. Top robust DE genes by LFC are annotated.

(C) Evaluation of aging gene signature prediction on held-out genes: mean Pearson correlation coefficients (*y* axis) across splits (5-fold cross-validation) for model fit on CD4+ T perturbation effects in different conditions. Dotted line indicates maximum correlation between signatures in the discovery and replication cohorts. Error bars: 95% CI across cross-validation splits.

(D) Predicted regulator effects (w_r, *y* axis) on aging gene signature for all regulators in the Rest condition (mean and standard error for w_r on 5 train-test splits). Regulators are ordered by hierarchical clustering on the perturbation effects on aging signature genes. Perturbed regulators involved in the mTORC1 signaling pathway (source: Kyoto Encyclopedia of Genes and Genomes [KEGG]) or protein SUMOylation (source: Gene Ontology) are highlighted.

(E and F) Aging signature genes controlled by predicted regulator pathways (STAR Methods): volcano plot of genes differentially expressed with age as in (B), but highlighting genes significantly regulated by mTORC1 regulators (in E: including *TSC1*, *TSC2*, *DEPDC5*, *NPRL3*, and *RPTOR*) or SUMOylation enzymes (in F: including *UBA1* and *UBE2I*). We highlight signature genes that are significantly differentially expressed (10% FDR) upon knockdown of at least one regulator and whose direction of change upon perturbation is consistent with both the predicted regulator effect and the cell state signature.

See also Figures S30–S32 and Tables S20 and S21.

mTORC1 components on aging is opposite to what we would expect: mTORC1-inhibiting factors are predicted as positive regulators of aging signature (i.e., knockdown of *TSC* and *GATOR* complex genes induces genes that are downregulated in aged CD4+ T cells), while *RPTOR* is predicted as a negative aging regulator, although individual knockdowns have the expected measured transcriptional effects on gold standard signatures of mTORC1 activation (Figure S32A). We hypothesize that this could be due to negative feedback, compensation, or survivor bias in the T cells profiled from aged individuals (Note S7). Despite this complexity, the findings underscore mTOR signaling as a critical node of the observed T cell aging signature.

SUMOylation enzymes were also nominated as regulators of the T cell aging signature: these include *UBA2*, which encodes

the E1 ubiquitin ligase for protein SUMOylation, and *UBE2I*, which encodes the E2 ligase UBC9. SUMOylation is a reversible post-translational modification in which small ubiquitin-like modifier (SUMO) proteins are covalently attached to target proteins, regulating their localization, stability, and activity. This modification has critical effects on transcriptional regulation[69] and has been increasingly recognized as a regulator of aging processes.[70–72] In T cells, UBC9-mediated SUMOylation plays essential roles in peripheral CD4+ T cell proliferation and homeostasis, including SUMOylation of PDPK, which regulates glycolysis-dependent T cell function.[73,74] Perturbing either mTOR signaling components or key SUMOylation genes had marked effects on the age-associated T cell signature, but perturbations in these two pathways affected distinct subsets of the overall signature. mTORC1 regulators control several genes associated with resistance to apoptosis that are overexpressed in aged T cells, including *BCL2*, PIM kinases, *ARID5B*, and *SERPINB6*, as well as genes involved in T cell activation and survival such as *DPP4*,[75] *IL2RB*, *KMT2A*,[14] *KLF3*, and *TCF7* (Figures 5E and S32C). SUMOylation enzymes control expression of STAT genes (*STAT1*, *STAT4*, and *STAT6*), which are known substrates of SUMOylation.[76–78] These enzymes also regulate several cytoskeletal and structural genes, including *TIMP1*, *VIM*, *ITGB1*, and *FLNB* (Figures 5F and S32D). Interestingly, effects of regulators on these processes appear to be specific to the Rest condition and are not detected post-stimulation (Figures S32C and S32D).

Collectively, we demonstrate that genetic perturbations in a limited number of donors can recapitulate transcriptional changes observed in population-scale cohorts. Moreover, while perturbing mTORC1 components and SUMOylation enzymes altered the overall age-associated signature, these regulators do not primarily affect the top DE genes in aging (Figures S31D and S31E), highlighting the value of perturb-seq analysis of signature effects over screening approaches focused on individual markers. In summary, this analysis predicts key pathways shaping population-level changes and partitions signatures based on genes controlled by specific regulatory pathways. We detail recommendations for application and interpretation of perturb-seq analysis of cell state signatures in Note S8.

Interpreting natural genetic variant effects on immune traits with perturb-seq

As a final application, we used the *ex vivo* perturb-seq data to identify the regulatory pathways through which natural genetic variants influence complex immune traits. Interpreting genetic associations with complex traits remains challenging, in part because many genes detected in genome-wide association studies (GWASs) act on a trait primarily through *trans*-regulation of other genes.[79,80] Perturb-seq can help decipher these regulatory relationships and identify the key transcriptional programs impacting phenotypic variation. Indeed, recent studies show that CRISPR perturbations of selected genes can identify transcriptional programs enriched for GWAS hits.[3,5,14,81,82] Since CD4+ T cells are central to many immune-mediated diseases and complex traits,[83,84] we hypothesized that our perturbation data could provide a powerful interpretive tool for immune traits.

We tested this using human lymphocyte counts measured in the UK Biobank[85] as a model T cell-relevant trait. Following recent work from our group,[3] we focused on the phenotypic effects of rare coding loss-of-function (LoF) variants, which can directly quantify the magnitude and direction by which single gene dosage affects organism-level traits.[85] We reasoned that if a gene is a "core gene" for lymphocyte count (i.e., exerting a more direct causal effect on the trait[79]), then its major regulators, as identified by perturb-seq, should also show genetic signals in the human LoF data. To identify putative core genes, we tested for each gene *j* whether the knockdown effects of regulators on *j* were significantly correlated with the LoF effects of those regulators on lymphocyte count in the UK Biobank. We refer to the correlation between LoF effects and knockdown effects as the regulator-burden correlation (Figure 6A).

Analysis of regulator-burden correlations in stimulated T cells indicated an excess of significant correlations at both time points. By contrast, we did not find higher-than-expected correlations in rested T cells, K562 cells, or a screen of essential genes in Jurkat cells (an immortalized T cell line) (Figure 6B), suggesting that these other cell states and types are poor proxies for lymphocyte count regulation. The difference in enrichment between Jurkats versus primary T cells could also be explained by the larger number of genetic perturbations measured in our data (Figure S33A). However, the different correlations in genome-scale perturb-seq in stimulated T cells compared with those in rested T cells or K562 cells indicate that both the number of knockdowns and the specific cellular context matter for recapitulating gene effects on complex traits.

We next characterized the putative core genes with high regulator-burden correlations at the stimulation time points. Among the top putative core genes in the Stim8hr condition was *ADAM19*, a metalloprotease involved in cell-cell communication. *ADAM19* expression is significantly regulated by high-burden genes in the Stim8hr condition (including *KLF2*, *NDFIP2*, *NSD1*, *PLCG1*, and *ERGIC1*). These genes do not significantly regulate ADAM19 at the later time point (Figure S33C). In Stim48hr condition, core genes included multiple subunits of the IL-18 receptor (*IL18R1* and *IL18RAP*), which induces proliferation of lymphocytes, including NK cells and activated T cells[86] (Figure S33C). Notably, *MYD88*, the signaling adapter downstream of the IL-18 receptor, was one of the strongest positive hits from LoF burden analysis on lymphocyte counts. Although *MYD88* knockdown produced only weak effects in our perturb-seq data (<3 DE genes in any condition, despite significant knockdown), the regulator-burden correlation analysis nonetheless converged on IL-18 signaling as a pathway driving this trait, highlighting the power of this integrative approach.

Core genes identified in the two conditions were significantly correlated (Pearson R = 0.36), but several top putative core genes were condition-specific (Figure S33B). Gene set enrichment analysis on the top genes positively associated with lymphocyte counts showed that in both conditions putative core genes are enriched in T cell activation markers (Figure 6C). However, genes prioritized in different conditions mapped to different biological processes: core genes at 8 h were enriched in actin fiber assembly (including *PXN*, *S100A10*, and *GPR65*) and cell-cell adhesion genes (including *ADAM8*, *ADAM19*, and *DPP4*), whereas those at 48 h post-

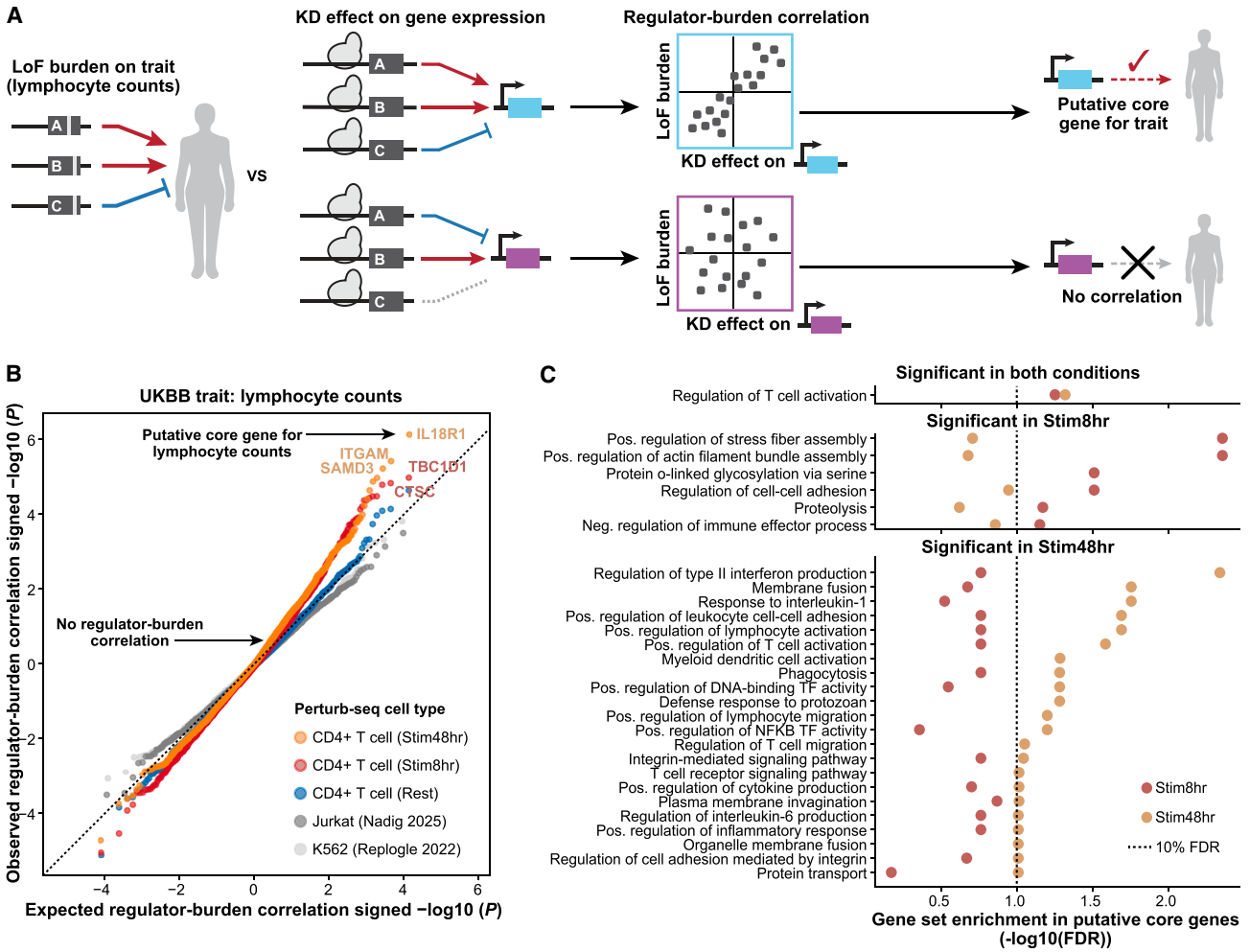

Figure 6. Context-specific regulatory effects in perturb-seq explain genetic association signals on lymphocyte counts

(A) Schematic of regulator-burden correlation analysis: we compare directional gene loss-of-function (LoF) burden estimates on complex traits (based on UK Biobank [UKBB] annotation of human variants and traits) with regulatory effects on each measured gene in perturb-seq. The correlation between the two estimates is used to nominate putative "core" genes affecting the complex trait.

(B) Signed *Q-Q* plot comparing expected versus observed signed *p* values for regulator-burden correlations for LoF burden on lymphocyte counts in the UKBB and regulatory effects estimated from perturb-seq data in different cell types/conditions (color). Sign denotes the direction of correlation. Each dot represents one measured gene. Perturb-seq data from this study is colored, while perturb-seq data on control cell types is in shades of gray.

(C) Gene Ontology enrichment of putative core genes positively associated with lymphocyte counts (top 50 by signed −log10 *p* value reg-burden correlation) in Stim8hr (red) and Stim48hr (orange) conditions. *x* axis: FDR from hypergeometric test. Top: terms enriched in both conditions; middle: Stim8hr only; bottom: Stim48hr only. Missing points indicate no overlap between core genes and gene set.

See also Figures S33 and S34.

stimulation were enriched in lymphocyte activation pathways and regulation of cytokine production. These results indicate that measuring perturbation responses across conditions can detect different aspects of complex trait biology.

Having shown that perturb-seq provides a useful model for studying lymphocyte count, we next characterized genes associated with autoimmune disease risk. Genetic association studies have identified hundreds of loci linked to autoimmune diseases, yet translating these findings into therapeutics requires understanding the causal genes, the cell types in which they exert their effects, and their molecular effects. To address these questions, we tested whether our clusters of perturbed regulators affecting shared downstream gene programs in T cells (Figure 3; Table S13) were enriched for autoimmune disease-associated genes. Although some associations are likely driven by gene functions in other cell types, we aimed to characterize shared regulatory effects and assign putative immunological functions to genes with established genetic associations but unknown roles in T cell biology. We annotated a set of genes associated with 14 autoimmune conditions (hereafter *autoimmune genes*) from Open Targets[87] (Figure S34A), then tested the odds of enrichment of these autoimmune genes in each cluster of regulators and among the top condition-specific genes downstream of these regulators (Figure 7A).

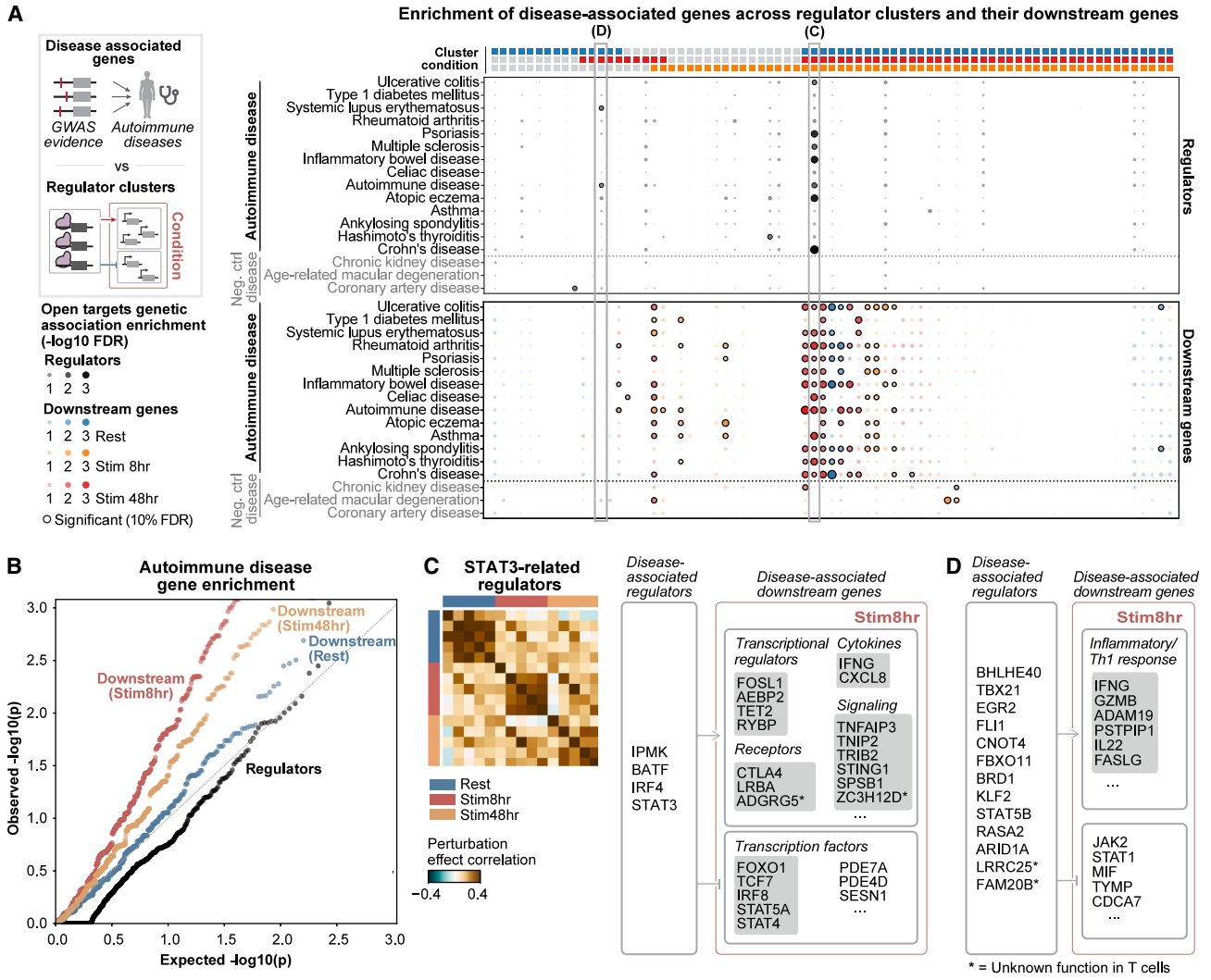

Figure 7. Regulation of autoimmune-associated genes

(A) Enrichment of GWAS-evidence genes (Open Targets) for autoimmune and control diseases (*y* axis) in regulators (top) and downstream genes (bottom) per cluster (*x* axis). Only clusters with at least 5 regulators were tested ($n = 77$). Dot size and color scale are proportional to the −log10(FDR) of the Fisher's exact test for enrichment in GWAS-evidence genes. Dots with a black outline indicate significant enrichment (10% FDR). Clusters are ordered by condition specificity, as annotated in the top bar. Clusters highlighted in follow-up vignettes are outlined with gray boxes.

(B) *Q*-*Q* plot of *p* values for enrichment in disease-associated genes across clusters in regulator genes (black) or downstream genes across conditions (colored).

(C and D) Illustrations of clustered regulators and downstream genes with genetic evidence for autoimmune conditions from Open Targets: (C) regulatory relationships in cluster 80 (STAT3-related regulators). Heatmap shows the correlation between perturbation effects of the 5 clustered regulators across conditions (as in Figure 3), and (D) illustrates regulatory relationships in cluster 79.

See also Figures S35–S36 and Table S22.

We found significant enrichment of autoimmune genes in 33 of 77 tested clusters, among either regulators or condition-specific downstream genes. By contrast, enrichment was significantly weaker for genes associated with three non-immune diseases where CD4+ T cell contribution is expected to be minimal (Figures 7A and S34B). Among condition-specific regulator clusters, autoimmune genes showed significant overlap among clusters that show correlated regulator effects in Stim8hr and/or Stim48hr conditions but not in clusters whose regulators only show correlated effects in the Rest condition (Figures 7A and S35). Similarly, within clusters of regulators with correlated effects across conditions but distinct sets of downstream target genes in different conditions, we observed notable enrichment of autoimmune genes among downstream targets regulated in stimulated cells (Figures 7B and S35).

One such example is a STAT3-related regulatory network. We identified a cluster of regulators enriched for autoimmune disease-associated genes encoding a core network of transcription factors involved in Th1/Th17 cell specification—*STAT3*, *IRF4*, *BATF*,[88] and *IPMK*, which encodes inositol polyphosphate

Please cite this article in press as: Zhu et al., Genome-scale perturb-seq in primary human CD4+ T cells maps context-specific regulators of T cell programs and human immune traits, Cell (2026), https://doi.org/10.1016/j.cell.2026.08.002

multikinase and was recently shown to control STAT3 phosphorylation via Akt/mTOR signaling in mice[89] (Figure 7C). Perturbations of these regulators had coordinated effects across conditions, but the set of co-regulated downstream genes changed, with autoimmune gene enrichment observed only among targets in the Stim8hr condition (Figures 7B and S35). This STAT3-related network positively regulated autoimmune disease-associated genes encoding pro-inflammatory cytokines (*IFNG* and *CXCL8*), signaling proteins (*TNFAIP3*, *TNIP2*, *STING1*, and *SPSB1*), transcriptional regulators (*FOSL1*, Polycomb components), and immune receptors (*CTLA4* and *LRBA*). The network negatively regulated the transcription factor *STAT4* and the phosphodiesterases *PDE4A* and *PDE7A* (which regulate intracellular cyclic AMP [cAMP] levels),[90] as well as other transcription factors linked to T cell regulation and memory (*FOXO1*, *TCF7*, *IRF8*, and *STAT5A*). Several of these downstream genes showed minimal transcriptome-wide effects when individually perturbed (Figure S36A), possibly due to low baseline expression or synergistic mechanisms, as for the PDE4/7 phosphodiesterases.[90] Among genes co-regulated by the STAT3 network in stimulated cells, we identified genes with autoimmune risk associations but limited functional characterization in T cells (Figure S36B). These included the putative tumor suppressor *ZC3H12D*, primarily studied in innate immunity,[91] and the GPCR family receptor *ADGRG5*, which may also function in cAMP signaling.[92]

Prioritizing candidate genes and discovering their mechanisms of action in relevant cell types remain significant bottlenecks in leveraging human genetics data for biological discovery. To this end, we examined if correlated gene perturbation effects could link new disease-risk genes to recognizable pathways in human T cells. For example, we identified a Stim8hr-specific cluster of regulators enriched for autoimmune disease-associated genes (FDR < 0.1), controlling expression of Th1 effector genes (*IFNG* and FASLG[93]) and other genes involved in T cell activation and function (Figure 7C). This cluster included known regulators of Th1 polarization (*TBX21*, *BHLHE40*, *EGR2*, and *FLI1*), MHC-II regulators (*CNOT4* and *FBXO11*), and regulators of anti-tumor T cell functions (*RASA2*[94] and *ARID1A*[95]). Notably, two autoimmune disease-associated genes with limited functional characterization in T cells clustered with these characterized regulators: *LRRC25* and *FAM20B*. *LRRC25* encodes a membrane protein involved in type 1 IFN signaling,[96] primarily described as a myeloid-specific receptor.[97] *FAM20B* encodes a kinase involved in proteoglycan metabolism[98] and is annotated as a likely causal gene for allergy and systemic lupus erythematosus in Open Targets but remains largely unstudied in the immune system. *FAM20B* knockdown induced a substantial transcriptome-wide effect in the Stim8hr condition (Figure S36C) that correlated with the effects of knocking down known Th1 regulators (Figure S36D). This transcriptome-wide effect was consistent between guides (Pearson R = 0.81) and across donors (mean correlation = 0.50). Our data nominate *LRRC25* and *FAM20B* as unappreciated regulators of T cell activation and Th1 polarization pathways, illustrating how guilt-by-perturbational association can nominate immunological roles for disease-implicated genes with previously unknown function in T cells. In summary, joint analysis of perturb-seq responses and human population genetic studies provides new insights into the functional roles of gene products harboring disease-associated variants and the regulatory relationships between them.

DISCUSSION

High-content CRISPR-based perturbation screens promise to map genetic circuits at scale. However, no public study had previously combined genome-scale perturbation libraries across multiple primary-cell contexts with deep transcriptional readouts, thus limiting our ability to robustly measure dynamic regulatory maps. We now leverage a CRISPR toolkit developed for primary T cells[5,6,13] and advances in scRNA-seq[17] to generate genome-scale perturb-seq maps of primary human T cells across multiple stimulation time points. The cell coverage, single-cell transcript recovery, and biological replication in our dataset enable reliable quantitative estimates of each perturbation's effect on individual genes throughout the transcriptome (Figure 1). Previous perturb-seq studies have been limited largely to analyzing aggregated gene signature effects of each perturbation due to low cell coverage and sequencing depth[9,81,99,100] (Figure S11). While gene program signatures can provide a useful abstraction,[3] here, quantification of gene-level effects enabled us to discover cytokine regulators not previously reported (Figure 2) and query regulators of specific disease-associated genes (Figure 7). Moreover, gene-level summary statistics are readily comparable across datasets, facilitating meta-analysis of perturbation studies and integration with human cohort data (Figures 4 and 5). Performing biological replicates of each perturbation in hundreds of cells from multiple human donors was a critical factor enabling this level of resolution in measurements of perturbation effects.

These data bring us closer to the systematic identification of circuit motifs—such as feed-forward loops and autoregulation—serving as the fundamental building blocks of cellular computation.[101] While such motifs have been extensively characterized in prokaryotes and yeast,[102,103] revealing the circuit design principles of mammalian cells has remained challenging due to the lack of high-resolution, genome-scale functional maps. Future measurements incorporating dosage-controlled perturbations[104] and dynamic readouts[105] could better capture non-linear regulatory relationships and deconvolve direct regulatory interactions from indirect ones (Note S5). Eventually, we envision these efforts could converge into dynamic and quantitative models that predict GRNs controlling complex cellular computations.

We found striking evidence of context-specific gene regulation relevant to human disease (Figure 2). For example, perturbations in stimulated cells reveal the effects of canonical Th1/Th2 regulators (Figure 4), while responses in rested cells capture aging-associated transcriptional signatures (Figure 5). When examining regulatory effects of genes with high LoF burden on lymphocyte counts, both stimulation time points help to explain the signal through distinct downstream genes (Figure 6). Our observations demonstrate the value of measuring gene perturbation effects in diverse primary cells captured in multiple cellular contexts. We anticipate future studies will capture perturbation effects in primary T cells exposed to distinct modes

Please cite this article in press as: Zhu et al., Genome-scale perturb-seq in primary human CD4+ T cells maps context-specific regulators of T cell programs and human immune traits, Cell (2026), https://doi.org/10.1016/j.cell.2026.08.002

of cytokine, TCR, costimulatory, and metabolic signals *in vitro* and eventually *in vivo*.[16]

We demonstrate new opportunities to integrate systematic gene perturbation studies in human primary cells with human genetic studies and atlases of human cells measured in healthy and diseased tissues. Experimentally derived GRNs provide a framework to interpret the molecular effects of human genetic variants associated with diverse traits and diseases. In addition, we demonstrate that the regulators and gene programs mapped in our perturb-seq data provide insights into key pathways shaping cell states observed in human samples. Previous studies derived perturbation-based gene signatures and searched for *in vivo* cells expressing these signatures.[106–108] Others have proposed methods to identify which experimental perturbations best match the transcriptional profile of a query cell, with metric learning on large cell atlases[109] or, more recently, using a regression approach termed "RNA fingerprinting" that is conceptually similar to the approach we propose here.[110] Our framework differs in two key assumptions: first, that signatures of natural cell states arise from the combined effects of multiple regulators rather than a single best-matching perturbation, and second, that both positive and negative regulators contribute to observed expression changes. This enables us to partition cell state signatures into genes controlled by each predicted regulator or pathway. Modeling DE statistics controls for systematic differences between tissue and *ex vivo* cells, making this framework broadly applicable across conditions and cell states. While we employ a relatively simple model here, we view this as a proof-of-concept and a baseline for more sophisticated approaches, for example, models that directly incorporate context-dependent perturbation effects (Note S8). Ultimately, we envision perturb-seq in primary cells as a critical bridge that will allow us to understand how genetic variation governing health and disease shapes molecular programs that operate in the cells comprising human tissues.[111]

We anticipate that our dataset will be particularly valuable for the development of predictive models of molecular responses to genetic perturbations, viewed as central to building AI virtual cells.[112] Biological replicates provide a framework for testing out-of-sample predictions and calibrating reproducibility expectations in human biology. Furthermore, our genome-wide measurements across multiple cell states provide a foundation for predicting perturbation effects across cellular contexts, a difficult but essential task for prediction models .[113–118] Additionally, screens in primary cells facilitate integration with multi-cell-type observational data, which could further guide generalization across contexts. However, our findings on context-specific responses also suggest that models may face substantial hurdles in predicting the effects of perturbations in contexts that were not directly tested. Accurate cross-context prediction may require large-scale data acquired from substantially more cellular contexts than are currently available.

Our study establishes a systematic mapping framework for GRNs and genotype-phenotype relationships in primary human cells. Here, we analyze gene knockdown effects with CRISPRi, but the approach is readily adaptable to additional genetic perturbation modalities[6,119–122] and delivery methods to edit more difficult-to-transfect primary cell types.[123,124] Technologies are also facilitating more comprehensive perturbation effects readouts: increasing the scale and reducing the per-cell cost of single-cell library preparation[125–127] and sequencing,[128] coupling additional cellular measurements to each perturbation,[16,129–131] and reading out effects in their native contexts.[16]

Over the past two decades, human population genetics has associated genetic variation with human traits. More recently, single-cell genomic technologies have mapped diverse cell states in human health and disease. Now, perturb-seq in human primary cells has the potential to map how genetic variation controls cell states, offering new hope that we can systematically link genome sequences to cell programs to human health outcomes. Our analyses showcase how this genome-scale perturb-seq map assembled in human primary CD4+ T cells across stimulation time points and multiple donors can be harnessed for insights into human immunology, immunotherapy design, dynamic gene regulatory control of human cells, and human disease genetics. We make the data publicly available to facilitate these efforts and accelerate community-driven discovery.

Limitations of the study

Despite performing large-scale perturb-seq with 2 gRNAs per target across multiple human blood donors, future work with additional guides per target gene would help resolve potential off-target guide effects in instances where guides targeting the same gene disagree. Similarly, further work will be needed to differentiate donor-specific biology from experimental batch effects. Additionally, because CRISPRi achieves partial repression rather than complete gene knockout, our approach may miss phenotypes for genes whose biochemical activity saturates at low protein abundance. Reliance on probe-based scRNA-seq is a powerful approach but limits measurements of certain coding and non-coding RNAs, allelic variants, and isoform- or UTR-level regulatory dynamics. Our analysis uses pseudobulk aggregation to compare mean expression profiles across cells with the same perturbation. This enhances statistical robustness but potentially masks heterogeneity of response to perturbation across cells, which could be resolved by future distribution-aware analyses. Our study focuses on a non-polarized stimulation condition. Consequently, the regulatory rewiring driven by polarizing cytokines—central to CD4+ T cell plasticity—remains unmapped. Furthermore, as our experiments were performed using blood-derived T cells cultured *ex vivo*, tissue-specific regulatory effects that occur in distinct anatomical microenvironments are likely missed. Future work extending this framework to include diverse *in vitro* polarization contexts and complex *in vivo* signals is essential to generate a comprehensive model of context-dependent immune regulation. Although perturb-seq elucidates causal gene regulatory relationships, future experimental and computational efforts will be required to link the transcription effects of each perturbation to specific immune cell functions in order to harness these data for immunology and immunotherapy development.

RESOURCE AVAILABILITY

Lead contact

Further information and requests for resources and reagents should be directed to and will be fulfilled by the lead contact, Alexander Marson (alex.marson@gladstone.ucsf.edu).

Please cite this article in press as: Zhu et al., Genome-scale perturb-seq in primary human CD4+ T cells maps context-specific regulators of T cell programs and human immune traits, Cell (2026), https://doi.org/10.1016/j.cell.2026.08.002

CellPress
OPEN ACCESS

Materials availability

The constructs and genome-scale CRISPRi library used in this study are available on Addgenes or upon request. Other resources generated in this study are available upon request as of the date of publication.

Data and code availability

- As listed in the key resources table, cell-level count matrices, pseudobulk-level count matrices, and DE estimates are available at https://virtualcellmodels.cziscience.com/dataset/genome-scale-tcell-perturb-seq. Raw sequencing data and cellranger outputs are available through SRA/GEO (SRA: SRP643211 and GEO: GSE314342). Supplemental tables and additional metadata are available via our code repository (https://github.com/emdann/GWT_perturbseq_analysis_2025). All processing and analysis code is available at https://github.com/emdann/GWT_perturbseq_analysis_2025.
- The model to predict regulators of observed cell states is implemented as a stand-alone Python class (https://github.com/emdann/pert2state_model). Any additional information required to reanalyze the data reported in this paper is available from the lead contact upon request.
- All raw sequencing data generated in this study—genome-scale perturb-seq and the three arrayed validation bulk RNA-seq experiments (*IL10/IL21* regulators, T cell activation regulator clusters, Th1/Th2 regulators)—together with cellranger outputs and count matrices, have been deposited at SRA and GEO and are publicly available as of the date of publication under accession numbers SRA: SRP643211 and GEO: GSE314342.
- Cell-level count matrices, pseudobulk-level count matrices, and DESeq2 DE estimates for the genome-scale perturb-seq screen are available at the CZI Virtual Cell Models platform: https://virtualcellmodels.cziscience.com/dataset/genome-scale-tcell-perturb-seq. Processed data from the arrayed validation experiments are provided as supplemental tables with this paper: DESeq2 DE estimates for the IL10/IL21 regulator experiment (Tables S9 and S10), for the T cell activation regulator cluster experiment (Table S15), and for the Th1/Th2 regulator experiment (Table S19); processed flow cytometry data for the *IL10/IL21* regulator experiment (Table S11) and the Th1/Th2 regulator experiment (Table S18); and cell expansion data for the *IL10/IL21* regulator experiment (Table S12).
- We additionally analyze publicly available datasets generated by others, all of which are listed in the key resources table.
- Genome-wide perturb-seq in K562 cells (Replogle et al.[9]) and essential-gene perturb-seq in Jurkat cells (Nadig et al.[19]), both count matrices and cell metadata, obtained via scPerturb132: https://zenodo.org/records/7041849.
- Arrayed knockout bulk RNA-seq screens used for *trans*-effect validation (DESeq2 statistics and count matrices; Weinstock et al.,[14] Freimer et al.[5]), GEO: GSE171737.
- Published CRISPRi FACS-based screens (MAGeCK statistics; Schmidt et al.,[6], Arce et al.,[13] Umhoefer et al.[15]), GEO: GSE171674, GSE271090, and GSE286473.
- Th1/Th2 sorted-cell bulk RNA-seq, discovery cohort (Ota et al.[40]), NBDC: E-GEAD-397, and replication cohort (Höllbacher et al.[41]), GEO: GSE149090.
- OneK1K cohort scRNA-seq, used for the aging analysis (Yazar et al.[59]): https://cellxgene.cziscience.com/collections/dde06e0f-ab3b-46be-96a2-a8082383c4a1.
- Published age-associated DE estimates in CD4+ T cells, used for benchmarking (Wells et al.,[63] Terekhova et al.[64]), obtained from the supplementary tables of the respective publications.
- UK Biobank LoF burden test summary statistics (Ota et al.[3]): 10.5281/zenodo.14751877.
- Additional metadata supporting the analyses reported in this paper are available via our code repository (https://github.com/emdann/GWT_perturbseq_analysis_2025).
- All data processing and analysis code is publicly available at https://github.com/emdann/GWT_perturbseq_analysis_2025. The model to predict regulators of observed cell states is implemented as a stand-alone Python class and is publicly available at https://github.com/emdann/pert2state_model.
- Any additional information required to reanalyze the data reported in this paper is available from the lead contact upon request.

ACKNOWLEDGMENTS

We thank T. Gjorgjieva, T. Zeng, S. Alatkar, J. Spence, R. Lopez, S. Dodgson, Z. Steinhart, M. Arce, N. Leung, B. Shy, and all members of the Marson lab and Pritchard lab for helpful discussions on the project and for feedback on the manuscript. We additionally thank Z. Steinhart for generously sharing the EF1a-Zim-3-dCas9-P2A-BSD construct. We thank early inputs on 10x Flex from G. Xing, R. Stickels, and T. Abay. This project has been made possible in part by grant number CZIF2025-011112 from the Chan Zuckerberg Initiative Foundation DAF, an advised fund of Silicon Valley Community Foundation. We thank B. Bova and J. Cool from CZI for their support, as well as other grantees of the Billion Cell Project initiative for useful discussions. We thank I. Gabdank, J. Chien, J. Zamanian, and all of the Lattice team for supporting data and metadata curation and sharing. In partnership with CZI, 10x Genomics, Ultima Genomics, and Psomagen provided reagents and expertise on scRNA-seq. We also thank P. Lund and P. Smibert from 10x Genomics for early technical support on CRISPR protocols with 10x Flex and J. Kim, J. Yeoh, and D. Cooper for overall 10x-related support. We thank T. Clark and the team at Ultima Genomics and J. Stone and the team at Psomagen for providing technical support on sequencing. We thank T. Tolpa for support on figure design. We thank the James B. Pendleton Charitable Trust for common equipment support. R.Z. is the Connie and Bob Lurie fellow of the Damon Runyon Cancer Research Foundation (DRG-2509-23). E.D. is supported by a Helen Hay Whitney Foundation fellowship and by an EMBO non-stipendiary postdoctoral fellowship. A.M. received funding from the Simons Foundation, the Parker Institute for Cancer Immunotherapy, the Weill Cancer Hub West, K. Jordan, the Biswas Family Foundation, and the CRISPR Cures for Cancer Initiative. This work was supported by the US National Institutes of Health (grants R01HG008140, R01HG014005, P01AI138962, R01DK129364, R01CA276368, and P01AI155393). We thank the anonymous reviewers for their thoughtful comments, which substantially improved this manuscript.

AUTHOR CONTRIBUTIONS

R.Z., E.D., A.M., and J.K.P. conceived and designed the study. R.Z., J.Y., and J.R.R. performed the perturb-seq experiments. E.D. and R.Z. performed all the data analyses. R.Z., J.R.R., and R.C.G. performed validation experiments. M.O. contributed to the design and interpretation of the analyses and provided intellectual contributions to all aspects of the study. R.G. contributed to the data analysis on LoF burden statistics. L.K.P. contributed to the data analysis on aging T cells in OneK1K. A.H., T.L.R., and A.T.S. contributed to the analysis on the guide off-target effects. R.Z., E.D., A.M., and J.K.P. wrote the manuscript, with critical input from all authors. J.K.P. and A.M. supervised the study and acquired funding.

DECLARATION OF INTERESTS

A.M. is a cofounder of Site Tx, Arsenal Biosciences, and Survey Genomics; serves on the board of directors for Site Tx and Survey Genomics; is a member of the scientific advisory board for Network Bio, Site Tx, Arsenal Biosciences, Cellanome, Survey Genomics, NewLimit, Amgen, and Tenaya; owns stock in Network Bio, Arsenal Biosciences, Site Tx, Cellanome, NewLimit, Survey Genomics, Tenaya, and Lightcast; and has received fees from Network Bio, Site Tx, Arsenal Biosciences, Cellanome, Spotlight Therapeutics, NewLimit, AbbVie, Gilead, Pfizer, 23andMe, PACT Pharma, Juno Therapeutics, Tenaya, Lightcast, Trizell, Vertex, Merck, Amgen, Genentech, GLG, ClearView Healthcare, AlphaSights, and Rupert Case Management. A.M. is an investor in and informal advisor to Offline Ventures and a client of EPIQ. The Marson laboratory has received research support from Biohub/Chan Zuckerberg Initiative, the Parker Institute for Cancer Immunotherapy, the Emerson Collective, the Arc Institute, Juno Therapeutics, Epinomics, Sanofi, GlaxoSmithKline, Gilead,

and Anthem and reagents from 10x, Ultima, GenScript, Illumina, and Cellanome. A.T.S. is a founder of Immunai, Cartography Biosciences, Santa Ana Bio, and Arpelos Biosciences and an advisor to 10x Genomics and Wing Venture Capital.

DECLARATION OF GENERATIVE AI AND AI-ASSISTED TECHNOLOGIES IN THE WRITING PROCESS

During the preparation of this work, the authors used Claude and Gemini to improve the readability and language of the manuscript. The authors reviewed and edited the content as needed and take full responsibility for the content of the published article.

STAR★METHODS

Detailed methods are provided in the online version of this paper and include the following:

- KEY RESOURCES TABLE
- EXPERIMENTAL MODEL AND STUDY PARTICIPANT DETAILS
  - Isolation and culture of naive human CD4+ T cells
- METHOD DETAILS
  - Genome-scale gRNA library design and library cloning
  - Plasmids
  - Lentivirus production
  - Functional titering of lentivirus
  - Genome-scale perturb-seq
  - Single-cell library construction
  - Sequencing
  - Arrayed validation of *IL10*/*IL21* regulation
  - Arrayed validation of TCR functional clusters
  - Arrayed validation of predicted Th1/Th2 regulators
  - Perturb-seq data preprocessing and quality control
  - Analysis of trans effects
  - Analysis of arrayed validation of *IL10*/*IL21* regulation
  - Functional clustering of perturbations
  - Cell state signature analysis
- QUANTIFICATION AND STATISTICAL ANALYSIS
- ADDITIONAL RESOURCES

SUPPLEMENTAL INFORMATION

Supplemental information can be found online at https://doi.org/10.1016/j.cell.2026.08.002.

Received: January 20, 2026
Revised: May 31, 2026
Accepted: August 3, 2026

REFERENCES

1. Karlebach, G., and Shamir, R. (2008). Modelling and analysis of gene regulatory networks. Nat. Rev. Mol. Cell Biol. *9*, 770–780. https://doi.org/10.1038/nrm2503.
2. Rackham, O.J.L., Firas, J., Fang, H., Oates, M.E., Holmes, M.L., Knaupp, A.S., FANTOM Consortium, Suzuki, H., Nefzger, C.M., Daub, C.O., and et al.. (2016). A predictive computational framework for direct reprogramming between human cell types. Nat. Genet. *48*, 331–335. https://doi.org/10.1038/ng.3487.
3. Ota, M., Spence, J.P., Zeng, T., Dann, E., Milind, N., Marson, A., and Pritchard, J.K. (2025). Causal modelling of gene effects from regulators to programs to traits. Nature *650*, 399–408. https://doi.org/10.1038/s41586-025-09866-3.
4. Badia-i-Mompel, P., Casals-Franch, R., Wessels, L., Müller-Dott, S., Trimbour, R., Yang, Y., Ramirez Flores, R.O., and Saez-Rodriguez, J. (2024). Comparison and evaluation of methods to infer gene regulatory networks from multimodal single-cell data. Preprint at bioRxiv. https://doi.org/10.1101/2024.12.20.629764.
5. Freimer, J.W., Shaked, O., Naqvi, S., Sinnott-Armstrong, N., Kathiria, A., Garrido, C.M., Chen, A.F., Cortez, J.T., Greenleaf, W.J., Pritchard, J.K., et al. (2022). Systematic discovery and perturbation of regulatory genes in human T cells reveals the architecture of immune networks. Nat. Genet. *54*, 1133–1144. https://doi.org/10.1038/s41588-022-01106-y.
6. Schmidt, R., Steinhart, Z., Layeghi, M., Freimer, J.W., Bueno, R., Nguyen, V.Q., Blaeschke, F., Ye, C.J., and Marson, A. (2022). CRISPR activation and interference screens decode stimulation responses in primary human T cells. Science *375*, eabj4008. https://doi.org/10.1126/science.abj4008.
7. Dixit, A., Parnas, O., Li, B., Chen, J., Fulco, C.P., Jerby-Arnon, L., Marjanovic, N.D., Dionne, D., Burks, T., Raychowdhury, R., et al. (2016). Perturb-seq: dissecting molecular circuits with scalable single-cell RNA profiling of pooled genetic screens. Cell *167*, 1853–1866.e17. https://doi.org/10.1016/j.cell.2016.11.038.
8. Adamson, B., Norman, T.M., Jost, M., Cho, M.Y., Nuñez, J.K., Chen, Y., Villalta, J.E., Gilbert, L.A., Horlbeck, M.A., Hein, M.Y., et al. (2016). A multiplexed single-cell CRISPR screening platform enables systematic dissection of the unfolded protein response. Cell *167*, 1867–1882.e21. https://doi.org/10.1016/j.cell.2016.11.048.
9. Replogle, J.M., Saunders, R.A., Pogson, A.N., Hussmann, J.A., Lenail, A., Guna, A., Mascibroda, L., Wagner, E.J., Adelman, K., Lithwick-Yanai, G., et al. (2022). Mapping information-rich genotype-phenotype landscapes with genome-scale Perturb-seq. Cell *185*, 2559–2575.e28. https://doi.org/10.1016/j.cell.2022.05.013.
10. Huang, A.C., Hsieh, T.-H.S., Zhu, J., Michuda, J., Teng, A., Kim, S., Rumsey, E.M., Lam, S.K., Anigbogu, I., Wright, P., et al. (2025). X-atlas/Orion: genome-wide Perturb-seq datasets via a scalable Fix-Cryopreserve platform for training dose-dependent biological foundation models. Preprint at bioRxiv. https://doi.org/10.1101/2025.06.11.659105.
11. Zhu, J., and Paul, W.E. (2008). CD4 T cells: fates, functions, and faults. Blood *112*, 1557–1569. https://doi.org/10.1182/blood-2008-05-078154.
12. Hirahara, K., and Nakayama, T. (2016). CD4+ T-cell subsets in inflammatory diseases: beyond the Th1/Th2 paradigm. Int. Immunol. *28*, 163–171. https://doi.org/10.1093/intimm/dxw006.
13. Arce, M.M., Umhoefer, J.M., Arang, N., Kasinathan, S., Freimer, J.W., Steinhart, Z., Shen, H., Pham, M.T.N., Ota, M., Wadhera, A., et al. (2024). Central control of dynamic gene circuits governs T cell rest and activation. Nature *637*, 930–939. https://doi.org/10.1038/s41586-024-08314-y.
14. Weinstock, J.S., Arce, M.M., Freimer, J.W., Ota, M., Marson, A., Battle, A., and Pritchard, J.K. (2024). Gene regulatory network inference from CRISPR perturbations in primary CD4+ T cells elucidates the genomic basis of immune disease. Cell Genom. *4*, 100671. https://doi.org/10.1016/j.xgen.2024.100671.
15. Umhoefer, J.M., Arce, M.M., Kasinathan, S., Whalen, S., Dajani, R., Subramanya, S., Goudy, L., Belk, J.A., Zhou, R., Pham, M.T.N., et al. (2025). FOXP3 expression depends on cell-type-specific cis-regulatory elements and transcription factor circuitry. Immunity *59*, 129–144.e13. https://doi.org/10.1016/j.immuni.2025.10.020.
16. Saunders, R.A., Allen, W.E., Pan, X., Sandhu, J., Lu, J., Lau, T.K., Smolyar, K., Sullivan, Z.A., Dulac, C., Weissman, J.S., et al. (2025). Perturb-Multimodal: a platform for pooled genetic screens with imaging and sequencing in intact mammalian tissue. Cell *188*, 4790–4809.e22. https://doi.org/10.1016/j.cell.2025.05.022.
17. De Simone, M., Hoover, J., Lau, J., Bennett, H.M., Wu, B., Chen, C., Menon, H., Au-Yeung, A., Lear, S., Vaidya, S., et al. (2025). A comprehensive analysis framework for evaluating commercial single-cell RNA sequencing technologies. Nucleic Acids Res. *53*, gkae1186. https://doi.org/10.1093/nar/gkae1186.
18. Aguirre, M., Spence, J.P., Sella, G., and Pritchard, J.K. (2025). Gene regulatory network structure informs the distribution of perturbation effects.

Please cite this article in press as: Zhu et al., Genome-scale perturb-seq in primary human CD4+ T cells maps context-specific regulators of T cell programs and human immune traits, Cell (2026), https://doi.org/10.1016/j.cell.2026.08.002

PLoS Comput. Biol. *21*, e1013387. https://doi.org/10.1371/journal.pcbi.1013387.

19. Nadig, A., Replogle, J.M., Pogson, A.N., Murthy, M., McCarroll, S.A., Weissman, J.S., Robinson, E.B., and O'Connor, L.J. (2025). Transcriptome-wide analysis of differential expression in perturbation atlases. Nat. Genet. *57*, 1228–1237. https://doi.org/10.1038/s41588-025-02169-3.

20. Squair, J.W., Gautier, M., Kathe, C., Anderson, M.A., James, N.D., Hutson, T.H., Hudelle, R., Qaiser, T., Matson, K.J.E., Barraud, Q., et al. (2021). Confronting false discoveries in single-cell differential expression. Nat. Commun. *12*, 5692. https://doi.org/10.1038/s41467-021-25960-2.

21. McCutcheon, S.R., Swartz, A.M., Brown, M.C., Barrera, A., McRoberts Amador, C., Siklenka, K., Humayun, L., ter Weele, M.A., Isaacs, J.M., Reddy, T.E., et al. (2023). Transcriptional and epigenetic regulators of human CD8+ T cell function identified through orthogonal CRISPR screens. Nat. Genet. *55*, 2211–2223. https://doi.org/10.1038/s41588-023-01554-0.

22. Henriksson, J., Chen, X., Gomes, T., Ullah, U., Meyer, K.B., Miragaia, R., Duddy, G., Pramanik, J., Yusa, K., Lahesmaa, R., et al. (2019). Genome-wide CRISPR screens in T helper cells reveal pervasive crosstalk between activation and differentiation. Cell *176*, 882–896.e18. https://doi.org/10.1016/j.cell.2018.11.044.

23. Shifrut, E., Carnevale, J., Tobin, V., Roth, T.L., Woo, J.M., Bui, C.T., Li, P.J., Diolaiti, M.E., Ashworth, A., and Marson, A. (2018). Genome-wide CRISPR screens in primary human T cells reveal key regulators of immune function. Cell *175*, 1958–1971.e15. https://doi.org/10.1016/j.cell.2018.10.024.

24. Neumann, C., Scheffold, A., and Rutz, S. (2019). Functions and regulation of T cell-derived interleukin-10. Semin. Immunol. *44*, 101344. https://doi.org/10.1016/j.smim.2019.101344.

25. Kühn, R., Löhler, J., Rennick, D., Rajewsky, K., and Müller, W. (1993). Interleukin-10-deficient mice develop chronic enterocolitis. Cell *75*, 263–274. https://doi.org/10.1016/0092-8674(93)80068-P.

26. Glocker, E.-O., Kotlarz, D., Boztug, K., Gertz, E.M., Schäffer, A.A., Noyan, F., Perro, M., Diestelhorst, J., Allroth, A., Murugan, D., et al. (2009). Inflammatory bowel disease and mutations affecting the interleukin-10 receptor. N. Engl. J. Med. *361*, 2033–2045. https://doi.org/10.1056/NEJMoa0907206.

27. Kotlarz, D., Ziętara, N., Uzel, G., Weidemann, T., Braun, C.J., Diestelhorst, J., Krawitz, P.M., Robinson, P.N., Hecht, J., Puchałka, J., et al. (2013). Loss-of-function mutations in the IL-21 receptor gene cause a primary immunodeficiency syndrome. J. Exp. Med. *210*, 433–443. https://doi.org/10.1084/jem.20111229.

28. Linterman, M.A., Beaton, L., Yu, D., Ramiscal, R.R., Srivastava, M., Hogan, J.J., Verma, N.K., Smyth, M.J., Rigby, R.J., and Vinuesa, C.G. (2010). IL-21 acts directly on B cells to regulate Bcl-6 expression and germinal center responses. J. Exp. Med. *207*, 353–363. https://doi.org/10.1084/jem.20091738.

29. Zotos, D., Coquet, J.M., Zhang, Y., Light, A., D'Costa, K., Kallies, A., Corcoran, L.M., Godfrey, D.I., Toellner, K.-M., Smyth, M.J., et al. (2010). IL-21 regulates germinal center B cell differentiation and proliferation through a B cell-intrinsic mechanism. J. Exp. Med. *207*, 365–378. https://doi.org/10.1084/jem.20091777.

30. Parrish-Novak, J., Foster, D.C., Holly, R.D., and Clegg, C.H. (2002). Interleukin-21 and the IL-21 receptor: novel effectors of NK and T cell responses. J. Leukoc. Biol. *72*, 856–863. https://doi.org/10.1189/jlb.72.5.856.

31. Suzuki, J., Yamada, T., Inoue, K., Nabe, S., Kuwahara, M., Takemori, N., Takemori, A., Matsuda, S., Kanoh, M., Imai, Y., et al. (2018). The tumor suppressor menin prevents effector CD8 T-cell dysfunction by targeting mTORC1-dependent metabolic activation. Nat. Commun. *9*, 3296. https://doi.org/10.1038/s41467-018-05854-6.

32. Saraiva, M., and O'Garra, A. (2010). The regulation of IL-10 production by immune cells. Nat. Rev. Immunol. *10*, 170–181. https://doi.org/10.1038/nri2711.

33. Van de Graaf, M.W., Eggertsen, T.G., Zeigler, A.C., Tan, P.M., and Saucerman, J.J. (2024). Benchmarking of protein interaction databases for integration with manually reconstructed signalling network models. J. Physiol. *602*, 4529–4542. https://doi.org/10.1113/JP284616.

34. Shyer, J.A., Flavell, R.A., and Bailis, W. (2020). Metabolic signaling in T cells. Cell Res. *30*, 649–659. https://doi.org/10.1038/s41422-020-0379-5.

35. Gaud, G., Lesourne, R., and Love, P.E. (2018). Regulatory mechanisms in T cell receptor signalling. Nat. Rev. Immunol. *18*, 485–497. https://doi.org/10.1038/s41577-018-0020-8.

36. Chai, T., Loh, K.M., and Weissman, I.L. (2024). TMX1, a disulfide oxidoreductase, is necessary for T cell function through regulation of CD3ζ. Preprint at bioRxiv. https://doi.org/10.1101/2024.09.22.614388.

37. Jakobs, J., Bertram, J., and Rink, L. (2024). Ca2+ signals are essential for T-cell proliferation, while Zn2+ signals are necessary for T helper cell 1 differentiation. Cell Death Discov. *10*, 336. https://doi.org/10.1038/s41420-024-02104-1.

38. Sena, L.A., Li, S., Jairaman, A., Prakriya, M., Ezponda, T., Hildeman, D.A., Wang, C.-R., Schumacker, P.T., Licht, J.D., Perlman, H., et al. (2013). Mitochondria are required for antigen-specific T cell activation through reactive oxygen species signaling. Immunity *38*, 225–236. https://doi.org/10.1016/j.immuni.2012.10.020.

39. Künzli, M., and Masopust, D. (2023). CD4+ T cell memory. Nat. Immunol. *24*, 903–914. https://doi.org/10.1038/s41590-023-01510-4.

40. Ota, M., Nagafuchi, Y., Hatano, H., Ishigaki, K., Terao, C., Takeshima, Y., Yanaoka, H., Kobayashi, S., Okubo, M., Shirai, H., et al. (2021). Dynamic landscape of immune cell-specific gene regulation in immune-mediated diseases. Cell *184*, 3006–3021.e17. https://doi.org/10.1016/j.cell.2021.03.056.

41. Höllbacher, B., Duhen, T., Motley, S., Klicznik, M.M., Gratz, I.K., and Campbell, D.J. (2020). Transcriptomic profiling of human effector and regulatory T cell subsets identifies predictive population signatures. ImmunoHorizons *4*, 585–596. https://doi.org/10.4049/immunohorizons.2000037.

42. Seif, F., Khoshmirsafa, M., Aazami, H., Mohsenzadegan, M., Sedighi, G., and Bahar, M. (2017). The role of JAK-STAT signaling pathway and its regulators in the fate of T helper cells. Cell Commun. Signal. *15*, 23. https://doi.org/10.1186/s12964-017-0177-y.

43. Kano, S.-I., Sato, K., Morishita, Y., Vollstedt, S., Kim, S., Bishop, K., Honda, K., Kubo, M., and Taniguchi, T. (2008). The contribution of transcription factor IRF1 to the interferon-gamma–interleukin 12 signaling axis and TH1 versus TH-17 differentiation of CD4+ T cells. Nat. Immunol. *9*, 34–41. https://doi.org/10.1038/ni1538.

44. Zhu, J., Yamane, H., and Paul, W.E. (2010). Differentiation of effector CD4 T cell populations (*). Annu. Rev. Immunol. *28*, 445–489. https://doi.org/10.1146/annurev-immunol-030409-101212.

45. Hall, J.A., Grainger, J.R., Spencer, S.P., and Belkaid, Y. (2011). The role of retinoic acid in tolerance and immunity. Immunity *35*, 13–22. https://doi.org/10.1016/j.immuni.2011.07.002.

46. Dege, C., and Hagman, J. (2014). Mi-2/NuRD chromatin remodeling complexes regulate B and T-lymphocyte development and function. Immunol. Rev. *261*, 126–140. https://doi.org/10.1111/imr.12209.

47. Scheer, S., and Zaph, C. (2017). The lysine methyltransferase G9a in immune cell differentiation and function. Front. Immunol. *8*, 429. https://doi.org/10.3389/fimmu.2017.00429.

48. Fang, T.C., Schaefer, U., Mecklenbrauker, I., Stienen, A., Dewell, S., Chen, M.S., Rioja, I., Parravicini, V., Prinjha, R.K., Chandwani, R., et al. (2012). Histone H3 lysine 9 di-methylation as an epigenetic signature of the interferon response. J. Exp. Med. *209*, 661–669. https://doi.org/10.1084/jem.20112343.

49. Arkee, T., Hornick, E.L., and Bishop, G.A. (2024). TRAF3 regulates STAT6 activation and T-helper cell differentiation by modulating the phosphatase PTP1B. J. Biol. Chem. *300*, 107737. https://doi.org/10.1016/j.jbc.2024.107737.

50. Srinivasan, R., Mager, G.M., Ward, R.M., Mayer, J., and Svaren, J. (2006). NAB2 represses transcription by interacting with the CHD4 subunit of the nucleosome remodeling and deacetylase (NuRD) complex. J. Biol. Chem. *281*, 15129–15137. https://doi.org/10.1074/jbc.M600775200.

51. Thapar, R. (2015). Roles of prolyl isomerases in RNA-mediated gene expression. Biomolecules *5*, 974–999. https://doi.org/10.3390/biom5020974.

52. Domínguez Conde, C., Xu, C., Jarvis, L.B., Rainbow, D.B., Wells, S.B., Gomes, T., Howlett, S.K., Suchanek, O., Polanski, K., King, H.W., et al. (2022). Cross-tissue immune cell analysis reveals tissue-specific features in humans. Science *376*, eabl5197. https://doi.org/10.1126/science.abl5197.

53. Eraslan, G., Drokhlyansky, E., Anand, S., Fiskin, E., Subramanian, A., Slyper, M., Wang, J., Van Wittenberghe, N., Rouhana, J.M., Waldman, J., et al. (2022). Single-nucleus cross-tissue molecular reference maps toward understanding disease gene function. Science *376*, eabl4290. https://doi.org/10.1126/science.abl4290.

54. Zhang, F., Jonsson, A.H., Nathan, A., Millard, N., Curtis, M., Xiao, Q., Gutierrez-Arcelus, M., Apruzzese, W., Watts, G.F.M., Weisenfeld, D., et al. (2023). Deconstruction of rheumatoid arthritis synovium defines inflammatory subtypes. Nature *623*, 616–624. https://doi.org/10.1038/s41586-023-06708-y.

55. Zheng, L., Qin, S., Si, W., Wang, A., Xing, B., Gao, R., Ren, X., Wang, L., Wu, X., Zhang, J., et al. (2021). Pan-cancer single-cell landscape of tumor-infiltrating T cells. Science *374*, abe6474. https://doi.org/10.1126/science.abe6474.

56. Chu, Y., Dai, E., Li, Y., Han, G., Pei, G., Ingram, D.R., Thakkar, K., Qin, J.-J., Dang, M., Le, X., et al. (2023). Pan-cancer T cell atlas links a cellular stress response state to immunotherapy resistance. Nat. Med. *29*, 1550–1562. https://doi.org/10.1038/s41591-023-02371-y.

57. Lindeboom, R.G.H., Worlock, K.B., Dratva, L.M., Yoshida, M., Scobie, D., Wagstaffe, H.R., Richardson, L., Wilbrey-Clark, A., Barnes, J.L., Kretschmer, L., et al. (2024). Human SARS-CoV-2 challenge uncovers local and systemic response dynamics. Nature *631*, 189–198. https://doi.org/10.1038/s41586-024-07575-x.

58. Nathan, A., Beynor, J.I., Baglaenko, Y., Suliman, S., Ishigaki, K., Asgari, S., Huang, C.-C., Luo, Y., Zhang, Z., Lopez, K., et al. (2021). Multimodally profiling memory T cells from a tuberculosis cohort identifies cell state associations with demographics, environment and disease. Nat. Immunol. *22*, 781–793. https://doi.org/10.1038/s41590-021-00933-1.

59. Yazar, S., Alquicira-Hernandez, J., Wing, K., Senabouth, A., Gordon, M.G., Andersen, S., Lu, Q., Rowson, A., Taylor, T.R.P., Clarke, L., et al. (2022). Single-cell eQTL mapping identifies cell type-specific genetic control of autoimmune disease. Science *376*, eabf3041. https://doi.org/10.1126/science.abf3041.

60. Kock, K.H., Tan, L.M., Han, K.Y., Ando, Y., Jevapatarakul, D., Chatterjee, A., Lin, Q.X.X., Buyamin, E.V., Sonthalia, R., Rajagopalan, D., et al. (2025). Asian diversity in human immune cells. Cell *188*, 2288–2306.e24. https://doi.org/10.1016/j.cell.2025.02.017.

61. Cuomo A.S.E., Spenceley E., Tanudisastro H.A., Bowen B., Henry A., Huang H.L., Xue A., Zhou W., Welland M.J., Bryen S.J., et al. Impact of rare and common genetic variation on cell type-specific gene expression in human blood Preprint at. medRxiv. https://doi.org/10.1101/2025.03.20.25324352.

62. Mittelbrunn, M., and Kroemer, G. (2021). Hallmarks of T cell aging. Nat. Immunol. *22*, 687–698. https://doi.org/10.1038/s41590-021-00927-z.

63. Wells, S.B., Rainbow, D.B., Mark, M., Szabo, P.A., Ergen, C., Caron, D.P., Maceiras, A.R., Rahmani, E., Benuck, E., Valiollah Pour Amiri, V., et al. (2025). Multimodal profiling reveals tissue-directed signatures of human immune cells altered with age. Nat. Immunol. *26*, 1612–1625. https://doi.org/10.1038/s41590-025-02241-4.

64. Terekhova, M., Swain, A., Bohacova, P., Aladyeva, E., Arthur, L., Laha, A., Mogilenko, D.A., Burdess, S., Sukhov, V., Kleverov, D., et al. (2023). Single-cell atlas of healthy human blood unveils age-related loss of NKG2C+GZMB−CD8+ memory T cells and accumulation of type 2 memory T cells. Immunity *56*, 2836–2854.e9. https://doi.org/10.1016/j.immuni.2023.10.013.

65. López-Otín, C., Blasco, M.A., Partridge, L., Serrano, M., and Kroemer, G. (2013). The hallmarks of aging. Cell *153*, 1194–1217. https://doi.org/10.1016/j.cell.2013.05.039.

66. Mannick, J.B., Del Giudice, G., Lattanzi, M., Valiante, N.M., Praestgaard, J., Huang, B., Lonetto, M.A., Maecker, H.T., Kovarik, J., Carson, S., et al. (2014). mTOR inhibition improves immune function in the elderly. Sci. Transl. Med. *6*, 268ra179. https://doi.org/10.1126/scitranslmed.3009892.

67. Mannick, J.B., Morris, M., Hockey, H.P., Roma, G., Beibel, M., Kulmatycki, K., Watkins, M., Shavlakadze, T., Zhou, W., Quinn, D., et al. (2018). TORC1 inhibition enhances immune function and reduces infections in the elderly. Sci. Transl. Med. *10*, eaaq1564. https://doi.org/10.1126/scitranslmed.aaq1564.

68. Chi, H. (2012). Regulation and function of mTOR signalling in T cell fate decisions. Nat. Rev. Immunol. *12*, 325–338. https://doi.org/10.1038/nri3198.

69. DelRosso, N., Tycko, J., Suzuki, P., Andrews, C., Aradhana, M., Mukund, A., Liongson, I., Ludwig, C., Spees, K., Fordyce, P., et al. (2023). Large-scale mapping and mutagenesis of human transcriptional effector domains. Nature *616*, 365–372. https://doi.org/10.1038/s41586-023-05906-y.

70. Zhang, L., Li, F., Dimayuga, E., Craddock, J., and Keller, J.N. (2007). Effects of aging and dietary restriction on ubiquitination, sumoylation, and the proteasome in the spleen. FEBS Lett. *581*, 5543–5547. https://doi.org/10.1016/j.febslet.2007.10.054.

71. Princz, A., Pelisch, F., and Tavernarakis, N. (2020). SUMO promotes longevity and maintains mitochondrial homeostasis during ageing in *Caenorhabditis elegans*. Sci. Rep. *10*, 15513. https://doi.org/10.1038/s41598-020-72637-9.

72. Princz, A., and Tavernarakis, N. (2017). The role of SUMOylation in ageing and senescent decline. Mech. Ageing Dev. *162*, 85–90. https://doi.org/10.1016/j.mad.2017.01.002.

73. Xiong, Y., Yi, Y., Wang, Y., Yang, N., Rudd, C.E., and Liu, H. (2019). Ubc9 interacts with and SUMOylates the TCR adaptor SLP-76 for NFAT transcription in T cells. J. Immunol. *203*, 3023–3036. https://doi.org/10.4049/jimmunol.1900556.

74. Tharuka, M.D.N., Courelli, A.S., and Chen, Y. (2025). Immune regulation by the SUMO family. Nat. Rev. Immunol. *25*, 608–620. https://doi.org/10.1038/s41577-025-01155-4.

75. Hollande, C., Boussier, J., Ziai, J., Nozawa, T., Bondet, V., Phung, W., Lu, B., Duffy, D., Paradis, V., Mallet, V., et al. (2019). Inhibition of the dipeptidyl peptidase DPP4 (CD26) reveals IL-33-dependent eosinophil-mediated control of tumor growth. Nat. Immunol. *20*, 257–264. https://doi.org/10.1038/s41590-019-0321-5.

76. Begitt, A., Droescher, M., Knobeloch, K.-P., and Vinkemeier, U. (2011). SUMO conjugation of STAT1 protects cells from hyperresponsiveness to IFNγ. Blood *118*, 1002–1007. https://doi.org/10.1182/blood-2011-04-347930.

77. Grönholm, J., Vanhatupa, S., Ungureanu, D., Väliaho, J., Laitinen, T., Valjakka, J., and Silvennoinen, O. (2012). Structure-function analysis indicates that sumoylation modulates DNA-binding activity of STAT1. BMC Biochem. *13*, 20. https://doi.org/10.1186/1471-2091-13-20.

78. Droescher, M., Begitt, A., Marg, A., Zacharias, M., and Vinkemeier, U. (2011). Cytokine-induced paracrystals prolong the activity of signal transducers and activators of transcription (STAT) and provide a model

Please cite this article in press as: Zhu et al., Genome-scale perturb-seq in primary human CD4+ T cells maps context-specific regulators of T cell programs and human immune traits, Cell (2026), https://doi.org/10.1016/j.cell.2026.08.002

for the regulation of protein solubility by small ubiquitin-like modifier (SUMO). J. Biol. Chem. *286*, 18731–18746. https://doi.org/10.1074/jbc.M111.235978.

79. Liu, X., Li, Y.I., and Pritchard, J.K. (2019). Trans effects on gene expression can drive omnigenic inheritance. Cell *177*, 1022–1034.e6. https://doi.org/10.1016/j.cell.2019.04.014.

80. Boyle, E.A., Li, Y.I., and Pritchard, J.K. (2017). An expanded view of complex traits: from polygenic to omnigenic. Cell *169*, 1177–1186. https://doi.org/10.1016/j.cell.2017.05.038.

81. Schnitzler, G.R., Kang, H., Fang, S., Angom, R.S., Lee-Kim, V.S., Ma, X.R., Zhou, R., Zeng, T., Guo, K., Taylor, M.S., et al. (2024). Convergence of coronary artery disease genes onto endothelial cell programs. Nature *626*, 799–807. https://doi.org/10.1038/s41586-024-07022-x.

82. Geiger-Schuller, K., Eraslan, B., Kuksenko, O., Dey, K.K., Jagadeesh, K.A., Thakore, P.I., Karayel, O., Yung, A.R., Rajagopalan, A., Meireles, A.M., et al. (2023). Systematically characterizing the roles of E3-ligase family members in inflammatory responses with massively parallel Perturb-seq. Preprint at bioRxiv. https://doi.org/10.1101/2023.01.23.525198.

83. Farh, K.K.-H., Marson, A., Zhu, J., Kleinewietfeld, M., Housley, W.J., Beik, S., Shoresh, N., Whitton, H., Ryan, R.J.H., Shishkin, A.A., et al. (2015). Genetic and epigenetic fine mapping of causal autoimmune disease variants. Nature *518*, 337–343. https://doi.org/10.1038/nature13835.

84. Kanai, M., Akiyama, M., Takahashi, A., Matoba, N., Momozawa, Y., Ikeda, M., Iwata, N., Ikegawa, S., Hirata, M., Matsuda, K., et al. (2018). Genetic analysis of quantitative traits in the Japanese population links cell types to complex human diseases. Nat. Genet. *50*, 390–400. https://doi.org/10.1038/s41588-018-0047-6.

85. Backman, J.D., Li, A.H., Marcketta, A., Sun, D., Mbatchou, J., Kessler, M.D., Benner, C., Liu, D., Locke, A.E., Balasubramanian, S., et al. (2021). Exome sequencing and analysis of 454,787 UK Biobank participants. Nature *599*, 628–634. https://doi.org/10.1038/s41586-021-04103-z.

86. Landy, E., Carol, H., Ring, A., and Canna, S. (2024). Biological and clinical roles of IL-18 in inflammatory diseases. Nat. Rev. Rheumatol. *20*, 33–47. https://doi.org/10.1038/s41584-023-01053-w.

87. Buniello, A., Suveges, D., Cruz-Castillo, C., Llinares, M.B., Cornu, H., Lopez, I., Tsukanov, K., Roldán-Romero, J.M., Mehta, C., Fumis, L., et al. (2025). Open Targets Platform: facilitating therapeutic hypotheses building in drug discovery. Nucleic Acids Res. *53*, D1467–D1475. https://doi.org/10.1093/nar/gkae1128.

88. Ciofani, M., Madar, A., Galan, C., Sellars, M., Mace, K., Pauli, F., Agarwal, A., Huang, W., Parkhurst, C.N., Muratet, M., et al. (2012). A validated regulatory network for Th17 cell specification. Cell *151*, 289–303. https://doi.org/10.1016/j.cell.2012.09.016.

89. Yuk, C.M., Hong, S., Kim, D., Kim, M., Jeong, H.-W., Park, S.J., Min, H., Kim, W., Lim, J., Kim, H.D., et al. (2025). Inositol polyphosphate multikinase regulates Th1 and Th17 cell differentiation by controlling Akt-mTOR signaling. Cell Rep. *44*, 115281. https://doi.org/10.1016/j.celrep.2025.115281.

90. Szczypka, M. (2020). Role of phosphodiesterase 7 (PDE7) in T cell activity. Effects of selective PDE7 inhibitors and dual PDE4/7 inhibitors on T cell functions. Int. J. Mol. Sci. *21*, 6118. https://doi.org/10.3390/ijms21176118.

91. Huang, S., Qi, D., Liang, J., Miao, R., Minagawa, K., Quinn, T., Matsui, T., Fan, D., Liu, J., and Fu, M. (2012). The putative tumor suppressor Zc3h12d modulates toll-like receptor signaling in macrophages. Cell. Signal. *24*, 569–576. https://doi.org/10.1016/j.cellsig.2011.10.011.

92. Bernadyn, T.F., Vizurraga, A., Adhikari, R., Kwarcinski, F., and Tall, G.G. (2023). GPR114/ADGRG5 is activated by its tethered peptide agonist because it is a cleaved adhesion GPCR. J. Biol. Chem. *299*, 105223. https://doi.org/10.1016/j.jbc.2023.105223.

93. Cencioni, M.T., Santini, S., Ruocco, G., Borsellino, G., De Bardi, M., Grasso, M.G., Ruggieri, S., Gasperini, C., Centonze, D., Barilá, D., et al. (2015). FAS-ligand regulates differential activation-induced cell death of human T-helper 1 and 17 cells in healthy donors and multiple sclerosis patients. Cell Death Dis. *6*, e1741. https://doi.org/10.1038/cddis.2015.100.

94. Carnevale, J., Shifrut, E., Kale, N., Nyberg, W.A., Blaeschke, F., Chen, Y.Y., Li, Z., Bapat, S.P., Diolaiti, M.E., O'Leary, P., et al. (2022). RASA2 ablation in T cells boosts antigen sensitivity and long-term function. Nature *609*, 174–182. https://doi.org/10.1038/s41586-022-05126-w.

95. Belk, J.A., Yao, W., Ly, N., Freitas, K.A., Chen, Y.-T., Shi, Q., Valencia, A.M., Shifrut, E., Kale, N., Yost, K.E., et al. (2022). Genome-wide CRISPR screens of T cell exhaustion identify chromatin remodeling factors that limit T cell persistence. Cancer Cell *40*, 768–786.e7. https://doi.org/10.1016/j.ccell.2022.06.001.

96. Du, Y., Duan, T., Feng, Y., Liu, Q., Lin, M., Cui, J., and Wang, R.-F. (2018). LRRC25 inhibits type I IFN signaling by targeting ISG15-associated RIG-I for autophagic degradation. EMBO J. *37*, 351–366. https://doi.org/10.15252/embj.201796781.

97. Zhang, G., Yu, H., Liu, J., Dong, G., and Cai, Z. (2025). Myeloid-lineage-specific membrane protein LRRC25 suppresses immunity in solid tumor and is a potential cancer immunotherapy checkpoint target. Cell Rep. *44*, 115631. https://doi.org/10.1016/j.celrep.2025.115631.

98. Koike, T., Izumikawa, T., Tamura, J.-I., and Kitagawa, H. (2009). FAM20B is a kinase that phosphorylates xylose in the glycosaminoglycan-protein linkage region. Biochem. J. *421*, 157–162. https://doi.org/10.1042/BJ20090474.

99. Zhang, J., Ubas, A.A., de Borja, R., Svensson, V., Thomas, N., Thakar, N., Lai, I., Winters, A., Khan, U., Jones, M.G., et al. (2025). Tahoe-100M: a giga-scale single-cell perturbation atlas for context-dependent gene function and cellular modeling. Preprint at bioRxiv. https://doi.org/10.1101/2025.02.20.639398.

100. Nourreddine, S., Doctor, Y., Dailamy, A., Forget, A., Lee, Y.-H., Chinn, B., Khaliq, H., Polacco, B., Muralidharan, M., Pan, E., et al. (2024). A perturbation cell atlas of human induced pluripotent stem cells. Preprint at bioRxiv. https://doi.org/10.1101/2024.11.03.621734.

101. Alon, U. (2007). Network motifs: theory and experimental approaches. Nat. Rev. Genet. *8*, 450–461. https://doi.org/10.1038/nrg2102.

102. Shen-Orr, S.S., Milo, R., Mangan, S., and Alon, U. (2002). Network motifs in the transcriptional regulation network of *Escherichia coli*. Nat. Genet. *31*, 64–68. https://doi.org/10.1038/ng881.

103. Lee, T.I., Rinaldi, N.J., Robert, F., Odom, D.T., Bar-Joseph, Z., Gerber, G.K., Hannett, N.M., Harbison, C.T., Thompson, C.M., Simon, I., et al. (2002). Transcriptional regulatory networks in *Saccharomyces cerevisiae*. Science *298*, 799–804. https://doi.org/10.1126/science.1075090.

104. Naqvi, S., Kim, S., Hoskens, H., Matthews, H.S., Spritz, R.A., Klein, O.D., Hallgrímsson, B., Swigut, T., Claes, P., Pritchard, J.K., et al. (2023). Precise modulation of transcription factor levels identifies features underlying dosage sensitivity. Nat. Genet. *55*, 841–851. https://doi.org/10.1038/s41588-023-01366-2.

105. Xu, Z., Sziraki, A., Lee, J., Zhou, W., and Cao, J. (2024). Dissecting key regulators of transcriptome kinetics through scalable single-cell RNA profiling of pooled CRISPR screens. Nat. Biotechnol. *42*, 1218–1223. https://doi.org/10.1038/s41587-023-01948-9.

106. Southard, K.M., Ardy, R.C., Tang, A., O'Sullivan, D.D., Metzner, E., Guruvayurappan, K., and Norman, T.M. (2025). Comprehensive transcription factor perturbations recapitulate fibroblast transcriptional states. Nat. Genet. *57*, 2323–2334. https://doi.org/10.1038/s41588-025-02284-1.

107. Morris, J.A., Caragine, C., Daniloski, Z., Domingo, J., Barry, T., Lu, L., Davis, K., Ziosi, M., Glinos, D.A., Hao, S., et al. (2023). Discovery of target genes and pathways at GWAS loci by pooled single-cell CRISPR screens. Science *380*, eadh7699. https://doi.org/10.1126/science.adh7699.

108. Jiang, L., Dalgarno, C., Papalexi, E., Mascio, I., Wessels, H.-H., Yun, H., Iremadze, N., Lithwick-Yanai, G., Lipson, D., and Satija, R. (2025). Systematic reconstruction of molecular pathway signatures using scalable single-cell perturbation screens. Nat. Cell Biol. *27*, 505–517. https://doi.org/10.1038/s41556-025-01622-z.

109. Heimberg, G., Kuo, T., DePianto, D.J., Salem, O., Heigl, T., Diamant, N., Scalia, G., Biancalani, T., Turley, S.J., Rock, J.R., et al. (2025). A cell atlas foundation model for scalable search of similar human cells. Nature *638*, 1085–1094. https://doi.org/10.1038/s41586-024-08411-y.

110. Grabski, I.N., Lee, J., Blair, J., Dalgarno, C., Mascio, I., Bradu, A., Knowles, D.A., and Satija, R. (2025). Mapping transcriptional responses to cellular perturbation dictionaries with RNA fingerprinting. Preprint at bioRxiv. https://doi.org/10.1101/2025.09.19.676866.

111. Rood, J.E., Hupalowska, A., and Regev, A. (2024). Toward a foundation model of causal cell and tissue biology with a Perturbation Cell and Tissue Atlas. Cell *187*, 4520–4545. https://doi.org/10.1016/j.cell.2024.07.035.

112. Bunne, C., Roohani, Y., Rosen, Y., Gupta, A., Zhang, X., Roed, M., Alexandrov, T., AlQuraishi, M., Brennan, P., Burkhardt, D.B., et al. (2024). How to build the virtual cell with artificial intelligence: priorities and opportunities. Cell *187*, 7045–7063. https://doi.org/10.1016/j.cell.2024.11.015.

113. Viñas Torné, R., Wiatrak, M., Piran, Z., Fan, S., Jiang, L., Teichmann, S.A., Nitzan, M., and Brbić, M. (2025). Systema: a framework for evaluating genetic perturbation response prediction beyond systematic variation. Nat. Biotechnol. *44*, 1050–1059. https://doi.org/10.1038/s41587-025-02777-8.

114. Mejia, G.M., Miller, H.E., Leblanc, F.J.A., Wang, B., Swain, B., and de Lima Camillo, L.P. (2025). Diversity by design: addressing mode collapse improves scRNA-seq perturbation modeling on well-calibrated metrics. Preprint at arXiv. https://doi.org/10.48550/arXiv.2506.22641.

115. Kernfeld, E., Yang, Y., Weinstock, J.S., Battle, A., and Cahan, P. (2025). A comparison of computational methods for expression forecasting. Genome Biol. *26*, 388. https://doi.org/10.1186/s13059-025-03840-y.

116. Ahlmann-Eltze, C., Huber, W., and Anders, S. (2025). Deep-learning-based gene perturbation effect prediction does not yet outperform simple linear baselines. Nat. Methods *22*, 1657–1661. https://doi.org/10.1038/s41592-025-02772-6.

117. Adduri, A.K., Gautam, D., Bevilacqua, B., Imran, A., Shah, R., Naghipourfar, M., Teyssier, N., Ilango, R., Nagaraj, S., Dong, M., et al. (2025). Predicting cellular responses to perturbation across diverse contexts with State. Preprint at bioRxiv. https://doi.org/10.1101/2025.06.26.661135.

118. Wenkel, F., Tu, W., Masschelein, C., Shirzad, H., Eastwood, C., Whitfield, S.T., Bendidi, I., Russell, C., Hodgson, L., Mesbahi, Y.E., et al. (2025). TxPert: leveraging biochemical relationships for out-of-distribution transcriptomic perturbation prediction. Preprint at arXiv. https://doi.org/10.48550/arXiv.2505.14919.

119. Schmidt, R., Ward, C.C., Dajani, R., Armour-Garb, Z., Ota, M., Allain, V., Hernandez, R., Layeghi, M., Xing, G., Goudy, L., et al. (2024). Base-editing mutagenesis maps alleles to tune human T cell functions. Nature *625*, 805–812. https://doi.org/10.1038/s41586-023-06835-6.

120. Goudy, L., Ha, A., Borah, A.A., Umhoefer, J.M., Chow, L., Tran, C., Winters, A., Talbot, A., Hernandez, R., Li, Z., et al. (2025). Integrated epigenetic and genetic programming of primary human T cells. Nat. Biotechnol. https://doi.org/10.1038/s41587-025-02856-w.

121. Pacalin, N.M., Steinhart, Z., Shi, Q., Belk, J.A., Dorovskyi, D., Kraft, K., Parker, K.R., Shy, B.R., Marson, A., and Chang, H.Y. (2025). Bidirectional epigenetic editing reveals hierarchies in gene regulation. Nat. Biotechnol. *43*, 355–368. https://doi.org/10.1038/s41587-024-02213-3.

122. Hartman, A., Takacsi-Nagy, O., Kernick, C., Theberath, N.E., Lu, J., Wu, L., Mantilla, M., Mittra, S., McClellan, A., Johnson, N., et al. (2025). A unified genetic perturbation language for human cellular programming. Preprint at bioRxiv. https://doi.org/10.1101/2025.11.20.689421.

123. Jung, H., Devant, P., Ching, C., Ota, M., Hamilton, J., Steinhart, Z., Ngo, W., Sandoval, L., Jung, J.H., Xu, D., et al. (2025). Virus-like particles enable targeted gene engineering and pooled CRISPR screening in primary human myeloid cells. Preprint at bioRxiv. https://doi.org/10.64898/2025.12.14.692434.

124. Botchkarev, V.V., Harrington, S., Stoppato, M., Justen, A., Kimber, C., Kapuria, A., Gibson, K.M., Chu, C.-S., Xu, Y., Haugh, K., et al. (2025). In vivo gene editing of human hematopoietic stem and progenitor cells using envelope-engineered virus-like particles. Nat. Biotechnol., 1–13. https://doi.org/10.1038/s41587-025-02915-2.

125. Baronas, D., Norvaisis, S., Zvirblyte, J., Leonaviciene, G., Mikulenaite, V., Goda, K., Kaseta, V., Sablauskas, K., Griskevicius, L., Juzenas, S., et al. (2025). High-throughput single-cell omics using semipermeable capsules. Science *391*, 1138–1145. https://doi.org/10.1126/science.ady7227.

126. Mazelis, I., Sun, H., Kulkarni, A., Torre, T.L., and Klein, A.M. (2025). Multistep genomics on single cells and live cultures in subnanoliter capsules. Science *391*, 1130–1137. https://doi.org/10.1126/science.ady7209.

127. Mullaney, D.B., Sgrizzi, S.R., Mai, D., Campbell, I., Huang, Y., Šinkūnas, A., Kerr, D.L., Browning, V.E., Eisenach, H.E., Sims, J., et al. (2025). Capsule-based single-cell genome sequencing. Preprint at bioRxiv. https://doi.org/10.1101/2025.03.14.643253.

128. Kokoris, M., McRuer, R., Nabavi, M., Jacobs, A., Prindle, M., Cech, C., Berg, K., Lehmann, T., Machacek, C., Tabone, J., et al. (2025). Sequencing by expansion (SBX): a novel, high-throughput single-molecule sequencing technology. Preprint at bioRxiv. https://doi.org/10.1101/2025.02.19.639056.

129. Gu, J., Iyer, A., Wesley, B., Taglialatela, A., Leuzzi, G., Hangai, S., Decker, A., Gu, R., Klickstein, N., Shuai, Y., et al. (2025). Mapping multimodal phenotypes to perturbations in cells and tissue with CRISPRmap. Nat. Biotechnol. *43*, 1101–1115. https://doi.org/10.1038/s41587-024-02386-x.

130. Binan, L., Jiang, A., Danquah, S.A., Valakh, V., Simonton, B., Bezney, J., Manguso, R.T., Yates, K.B., Nehme, R., Cleary, B., et al. (2025). Simultaneous CRISPR screening and spatial transcriptomics reveal intracellular, intercellular, and functional transcriptional circuits. Cell *188*, 2141–2158.e18. https://doi.org/10.1016/j.cell.2025.02.012.

131. Kudo, T., Meireles, A.M., Moncada, R., Chen, Y., Wu, P., Gould, J., Hu, X., Kornfeld, O., Jesudason, R., Foo, C., et al. (2025). Multiplexed, image-based pooled screens in primary cells and tissues with PerturbView. Nat. Biotechnol. *43*, 1091–1100. https://doi.org/10.1038/s41587-024-02391-0.

132. Peidli, S., Green, T.D., Shen, C., Gross, T., Min, J., Garda, S., Yuan, B., Schumacher, L.J., Taylor-King, J.P., Marks, D.S., et al. (2024). scPerturb: harmonized single-cell perturbation data. Nat. Methods *21*, 531–540. https://doi.org/10.1038/s41592-023-02144-y.

133. Braunger, J.M., and Velten, B. (2024). Guide assignment in single-cell CRISPR screens using crispat. Bioinformatics *40*, btae535. https://doi.org/10.1093/bioinformatics/btae535.

134. Wolf, F.A., Angerer, P., and Theis, F.J. (2018). SCANPY: large-scale single-cell gene expression data analysis. Genome Biol. *19*, 15. https://doi.org/10.1186/s13059-017-1382-0.

135. Lopez, R., Regier, J., Cole, M.B., Jordan, M.I., and Yosef, N. (2018). Deep generative modeling for single-cell transcriptomics. Nat. Methods *15*, 1053–1058.

136. McInnes, L., Healy, J., and Astels, S. (2017). hdbscan: Hierarchical density based clustering. J. Open Source Soft. *2*, 205. https://doi.org/10.21105/joss.00205.

137. Virshup, I., Bredikhin, D., Heumos, L., Palla, G., Sturm, G., Gayoso, A., Kats, I., Koutrouli, M., Scverse Community, Berger, B., and et al.. (2023). The scverse project provides a computational ecosystem for single-cell omics data analysis. Nat. Biotechnol. *41*, 604–606. https://doi.org/10.1038/s41587-023-01733-8.

Please cite this article in press as: Zhu et al., Genome-scale perturb-seq in primary human CD4+ T cells maps context-specific regulators of T cell programs and human immune traits, Cell (2026), https://doi.org/10.1016/j.cell.2026.08.002

138. Love, M.I., Huber, W., and Anders, S. (2014). Moderated estimation of fold change and dispersion for RNA-seq data with DESeq2. Genome Biol. *15*, 550. https://doi.org/10.1186/s13059-014-0550-8.

139. Heumos, L., Ji, Y., May, L., Green, T.D., Peidli, S., Zhang, X., Wu, X., Ostner, J., Schumacher, A., Hrovatin, K., et al. (2025). Pertpy: an end-to-end framework for perturbation analysis. Nat. Methods *23*, 350–359. https://doi.org/10.1038/s41592-025-02909-7.

140. Urbut, S.M., Wang, G., Carbonetto, P., and Stephens, M. (2019). Flexible statistical methods for estimating and testing effects in genomic studies with multiple conditions. Nat. Genet. *51*, 187–195. https://doi.org/10.1038/s41588-018-0268-8.

141. Pedregosa, F., Varoquaux, G., Gramfort, A., Michel, V., Thirion, B., Grisel, O., Blondel, M., Müller, A., Nothman, J., Louppe, G., et al. (2011). Scikit-learn: machine learning in Python. J. Mach. Learn. Res. *12*, 2825–2830.

142. Xie, Z., Bailey, A., Kuleshov, M.V., Clarke, D.J.B., Evangelista, J.E., Jenkins, S.L., Lachmann, A., Wojciechowicz, M.L., Kropiwnicki, E., Jagodnik, K.M., et al. (2021). Gene Set Knowledge Discovery with Enrichr. Curr. Protoc. *1*, e90. https://doi.org/10.1002/cpz1.90.

143. Rohatgi, N., Fortin, J.-P., Lau, T., Ying, Y., Zhang, Y., Lee, B.L., Costa, M.R., and Reja, R. (2024). Seed sequences mediate off-target activity in the CRISPR-interference system. Cell Genom. *4*, 100693. https://doi.org/10.1016/j.xgen.2024.100693.

144. Schmiedel, B.J., Singh, D., Madrigal, A., Valdovino-Gonzalez, A.G., White, B.M., Zapardiel-Gonzalo, J., Ha, B., Altay, G., Greenbaum, J.A., McVicker, G., et al. (2018). Impact of Genetic Polymorphisms on Human Immune Cell Gene Expression. Cell *175*, 1701–1715.e16. https://doi.org/10.1016/j.cell.2018.10.022.

145. ENCODE Project Consortium (2012). An integrated encyclopedia of DNA elements in the human genome. Nature *489*, 57–74.

146. Lambert, S.A., Jolma, A., Campitelli, L.F., Das, P.K., Yin, Y., Albu, M., Chen, X., Taipale, J., Hughes, T.R., and Weirauch, M.T. (2018). The human transcription factors. Cell *172*, 650–665. https://doi.org/10.1016/j.cell.2018.01.029.

147. Ruepp, A., Waegele, B., Lechner, M., Brauner, B., Dunger-Kaltenbach, I., Fobo, G., Frishman, G., Montrone, C., and Mewes, H.W. (2010). CORUM: the comprehensive resource of mammalian protein complexes–2009. Nucleic Acids Res. *38*, D497–D501. https://doi.org/10.1093/nar/gkp914.

148. Szklarczyk, D., Kirsch, R., Koutrouli, M., Nastou, K., Mehryary, F., Hachilif, R., Gable, A.L., Fang, T., Doncheva, N.T., Pyysalo, S., et al. (2023). The STRING database in 2023: protein-protein association networks and functional enrichment analyses for any sequenced genome of interest. Nucleic Acids Res. *51*, D638–D646. https://doi.org/10.1093/nar/gkac1000.

149. Kanehisa, M., and Goto, S. (2000). KEGG: kyoto encyclopedia of genes and genomes. Nucleic Acids Res. *28*, 27–30. https://doi.org/10.1093/nar/28.1.27.

150. Milacic, M., Beavers, D., Conley, P., Gong, C., Gillespie, M., Griss, J., Haw, R., Jassal, B., Matthews, L., May, B., et al. (2024). The Reactome Pathway Knowledgebase 2024. Nucleic Acids Res. *52*, D672–D678. https://doi.org/10.1093/nar/gkad1025.

151. Ashburner, M., Ball, C.A., Blake, J.A., Botstein, D., Butler, H., Cherry, J.M., Davis, A.P., Dolinski, K., Dwight, S.S., Eppig, J.T., et al. (2000). Gene ontology: tool for the unification of biology. Nat. Genet. *25*, 25–29. https://doi.org/10.1038/75556.

152. Uhlén, M., Fagerberg, L., Hallström, B.M., Lindskog, C., Oksvold, P., Mardinoglu, A., Sivertsson, Å., Kampf, C., Sjöstedt, E., Asplund, A., et al. (2015). Proteomics. Tissue-based map of the human proteome. Science *347*, 1260419. https://doi.org/10.1126/science.1260419.

153. Tabula Sapiens Consortium, Jones, R.C., Karkanias, J., Krasnow, M.A., Pisco, A.O., Quake, S.R., Salzman, J., Yosef, N., Bulthaup, B., Brown, P., and et al.. (2022). The Tabula Sapiens: a multiple-organ, single-cell transcriptomic atlas of humans. Science *376*, eabl4896. https://doi.org/10.1126/science.abl4896.

154. Horlbeck, M.A., Gilbert, L.A., Villalta, J.E., Adamson, B., Pak, R.A., Chen, Y., Fields, A.P., Park, C.Y., Corn, J.E., Kampmann, M., et al. (2016). Compact and highly active next-generation libraries for CRISPR-mediated gene repression and activation. eLife *5*, e19760. https://doi.org/10.7554/eLife.19760.

155. Sanson, K.R., Hanna, R.E., Hegde, M., Donovan, K.F., Strand, C., Sullender, M.E., Vaimberg, E.W., Goodale, A., Root, D.E., Piccioni, F., et al. (2018). Optimized libraries for CRISPR-Cas9 genetic screens with multiple modalities. Nat. Commun. *9*, 5416. https://doi.org/10.1038/s41467-018-07901-8.

156. Tian, R., Gachechiladze, M.A., Ludwig, C.H., Laurie, M.T., Hong, J.Y., Nathaniel, D., Prabhu, A.V., Fernandopulle, M.S., Patel, R., Abshari, M., et al. (2019). CRISPR interference-based platform for multimodal genetic screens in human iPSC-derived neurons. Neuron *104*, 239–255.e12. https://doi.org/10.1016/j.neuron.2019.07.014.

157. Tian, R., Abarientos, A., Hong, J., Hashemi, S.H., Yan, R., Dräger, N., Leng, K., Nalls, M.A., Singleton, A.B., Xu, K., et al. (2021). Genome-wide CRISPRi/a screens in human neurons link lysosomal failure to ferroptosis. Nat. Neurosci. *24*, 1020–1034. https://doi.org/10.1038/s41593-021-00862-0.

158. Tidball, A.M., Luo, J., Walker, J.C., Takla, T.N., Carvill, G.L., and Parent, J.M. (2023). Genome-wide CRISPRi screen in human iNeurons to identify novel focal cortical dysplasia genes. Preprint at bioRxiv. https://doi.org/10.1101/2023.12.13.571474.

159. Muzellec, B., Teleńczuk, M., Cabeli, V., and Andreux, M. (2023). PyDESeq2: a Python package for bulk RNA-seq differential expression analysis. Bioinformatics *39*, btad547. https://doi.org/10.1093/bioinformatics/btad547.

160. Qi, L.S., Larson, M.H., Gilbert, L.A., Doudna, J.A., Weissman, J.S., Arkin, A.P., and Lim, W.A. (2013). Repurposing CRISPR as an RNA-guided platform for sequence-specific control of gene expression. Cell *152*, 1173–1183. https://doi.org/10.1016/j.cell.2013.02.022.

161. Larson, M.H., Gilbert, L.A., Wang, X., Lim, W.A., Weissman, J.S., and Qi, L.S. (2013). CRISPR interference (CRISPRi) for sequence-specific control of gene expression. Nat. Protoc. *8*, 2180–2196. https://doi.org/10.1038/nprot.2013.132.

162. Hartman, A., Blair, J.D., Nguyen, T.P., Dyson, K., Bradu, A., Takacsi-Nagy, O., Santostefano, K., Boade, T., Bolaños, M., Zhu, R., et al. (2026). Systematic identification of seed-driven off-target effects in Perturb-seq experiments. Preprint at bioRxiv. https://doi.org/10.64898/2026.03.27.714658.

163. Karlsson, M., Zhang, C., Méar, L., Zhong, W., Digre, A., Katona, B., Sjöstedt, E., Butler, L., Odeberg, J., Dusart, P., et al. (2021). A single-cell type transcriptomics map of human tissues. Sci. Adv. *7*, eabh2169. https://doi.org/10.1126/sciadv.abh2169.

164. Yanai, I., Benjamin, H., Shmoish, M., Chalifa-Caspi, V., Shklar, M., Ophir, R., Bar-Even, A., Horn-Saban, S., Safran, M., Domany, E., et al. (2005). Genome-wide midrange transcription profiles reveal expression level relationships in human tissue specification. Bioinformatics *21*, 650–659. https://doi.org/10.1093/bioinformatics/bti042.

165. Zeng, T., Spence, J.P., Mostafavi, H., and Pritchard, J.K. (2024). Bayesian estimation of gene constraint from an evolutionary model with gene features. Nat. Genet. *56*, 1632–1643. https://doi.org/10.1038/s41588-024-01820-9.

166. Spence, J.P., Mostafavi, H., Ota, M., Milind, N., Gjorgjieva, T., Smith, C.J., Simons, Y.B., Sella, G., and Pritchard, J.K. (2025). Specificity, length and luck drive gene rankings in association studies. Nature *649*, 918–925. https://doi.org/10.1038/s41586-025-09703-7.

Please cite this article in press as: Zhu et al., Genome-scale perturb-seq in primary human CD4+ T cells maps context-specific regulators of T cell programs and human immune traits, Cell (2026), https://doi.org/10.1016/j.cell.2026.08.002

STAR★METHODS

KEY RESOURCES TABLE

REAGENT or RESOURCE	SOURCE	IDENTIFIER
Antibodies		
PE anti-human CD45 Antibody	Biolegend	AB_314396
Brilliant Violet 711™ anti-human IFN-γ Antibody	Biolegend	AB_2563506
IL-4 Monoclonal Antibody (8D4-8), APC	eBioscience	AB_469498
IL-5 Monoclonal Antibody (TRFK5), PE	eBioscience	AB_763587
PE/Cyanine7 anti-human IL-13 Antibody	Biolegend	AB_2616746
Brilliant Violet 421™ anti-human IL-10 Antibody	Biolegend	AB_2632952
PerCP/Cyanine5.5 anti-human IL-21 Antibody	Biolegend	AB_2820095
Brilliant Violet 421™ anti-T-bet Antibody	Biolegend	AB_10959653
Gata-3 Monoclonal Antibody (TWAJ), PE	eBioscience	AB_1963600
Bacterial and virus strains		
Endura electrocompetent cells	LGC Biosearch Technologies	60242-2
Biological samples		
Human Peripheral Blood Leukopak, Fresh	STEMCELL Technologies	Catalog no. 70500, Table S23
Chemicals, peptides, and recombinant proteins		
DMEM, high glucose, GlutaMAX™ Supplement, HEPES	Gibco	10564029
Fetal Bovine Serum, Premium Select	R&D systems	S11550
Penicillin-Streptomycin (10,000 U/mL)	Gibco	1514022
Sodium Pyruvate (100 mM)	Gibco	11360070
MEM Non-Essential Amino Acids Solution	Gibco	11140050
TrypLE™ Express Enzyme (1X), no phenol red	Gibco	12604013
Opti-MEM™ I Reduced Serum Medium, GlutaMAX™ Supplement	Gibco	51985034
Lipofectamine 3000 Transfection Reagent	Invitrogen	L3000075
ViralBoost Reagent	Alstem	VB100
Lenti-X Concentrator	Takara Bio	631232
Recombinant Human IL-2 GMP Protein, CF	R&D systems	BT-002-GMP
ImmunoCult human CD3/CD28/ CD2 T cell activator	STEMCELL Technologies	10990
Recombinant Human IL-7 Protein	R&D systems	207-IL
Recombinant Human IL-12 (linked heterodimer) Protein, CF	R&D systems	10018-IL
Recombinant Human IL-4 Protein, 10µg, with Carrier	R&D systems	204-IL
Blasticidin S HCl	Gibco	A1113903
Puromycin Dihydrochloride	Gibco	A1113803
Cell Activation Cocktail (with Brefeldin A)	Biolegend	423304
GolgiPlug Protein Transport Inhibitor (Brefeldin A)	BD Biosciences	555029
DNA/RNA Shield	Zymo Research	R1100-250
KAPA HiFi HotStart ReadyMix	Roche	07958935001
SPRIselect Reagent	Beckman Coulter	B23318

(*Continued on next page*)

Please cite this article in press as: Zhu et al., Genome-scale perturb-seq in primary human CD4+ T cells maps context-specific regulators of T cell programs and human immune traits, Cell (2026), https://doi.org/10.1016/j.cell.2026.08.002

Continued

REAGENT or RESOURCE	SOURCE	IDENTIFIER
Critical commercial assays		
EasySep™ Human Naïve CD4+ T Cell Isolation Kit	STEMCELL Technologies	19555
BD Cytofix/Cytoperm Fixation/ Permeabilization Solution Kit	BD Biosciences	554714
True-Nuclear Transcription Factor Buffer Set	Biolegend	424401
NEB Golden Gate Assembly Kit (BsmBI-HF v2)	New England Biolabs	E1602L
MinElute PCR Purification Kit	Qiagen	28004
ZymoPURE II Plasmid Maxiprep Kit	Zymo Research	D4203
Qubit 1X dsDNA High Sensitivity Assay Kit	Invitrogen	Q33231
GEM-X Flex Sample Preparation v2 Kit	10x Genomics	1000781
GEM-X Flex Gene Expression Human n-plex, 64 samples	10x Genomics	1000829
GEM-X Flex Gene Expression Human, 4 samples	10x Genomics	1000792
Deposited data		
Perturb-seq raw sequencing data and cellranger outputs	This paper	SRA: SRP643211 GEO: GSE314342
Perturb-seq processed data (cell-level count matrices, pseudobulk-level count matrices and DESeq2 differential expression estimates)	This paper	https://virtualcellmodels.cziscience.com/dataset/genome-scale-tcell-perturb-seq
Arrayed validation RNA-seq (IL10/IL21 regulators) – raw sequencing data and count matrices	This paper	SRA: SRP643211 GEO: GSE314342
Arrayed validation RNA-seq (IL10/IL21 regulators) – DESeq2 differential expression estimates	This paper	Table S9 Table S10
Arrayed validation RNA-seq (T cell activation regulator clusters) – raw sequencing data and count matrices	This paper	SRA: SRP643211 GEO: GSE314342
Arrayed validation RNA-seq (T cell activation regulator clusters) – DESeq2 differential expression estimates	This paper	Table S15
Arrayed validation RNA-seq (Th1/Th2 regulators) – raw sequencing data and count matrices	This paper	SRA: SRP643211 GEO: GSE314342
Arrayed validation RNA-seq (Th1/Th2 regulators) – DESeq2 differential expression estimates	This paper	Table S19
Arrayed validation flow cytometry processed data (IL10/IL21 regulators)	This paper	Table S11
Arrayed validation cell expansion data (IL10/IL21 regulators)	This paper	Table S12
Arrayed validation flow cytometry processed data (Th1/Th2 regulators)	This paper	Table S18
K562 genome-wide perturb-seq (count matrices and cell metadata)	Replogle et al.[9]; obtained via scPerturb[132]	https://zenodo.org/records/7041849
Jurkat essential-gene perturb-seq (count matrices and cell metadata)	Nadig et al.[19]; obtained via scPerturb[132]	https://zenodo.org/records/7041849
Arrayed KO bulk RNA-seq screens for trans-effect validation (DESeq2 statistics / count matrices; reanalyzed)	Weinstock et al., Freimer et al.[5,14]	GEO: GSE171737
Published CRISPRi FACS-based screens (MAGeCK statistics; reanalyzed)	Schmidt et al.,[6] Arce et al.,[13] Umhoefer et al.[15]	GEO: GSE171674, GSE271090, GSE286473
Th1/Th2 sorted-cell bulk RNA-seq, Discovery cohort.	Ota et al.[40]	NBDC: E-GEAD-397
Th1/Th2 sorted-cell bulk RNA-seq, Replication cohort	Höllbacher et al.[41]	GEO: GSE149090
OneK1K cohort scRNA-seq (aging analysis)	Yazar et al.[59]	https://cellxgene.cziscience.com/collections/dde06e0f-ab3b-46be-96a2-a8082383c4a1

(*Continued on next page*)

Please cite this article in press as: Zhu et al., Genome-scale perturb-seq in primary human CD4+ T cells maps context-specific regulators of T cell programs and human immune traits, Cell (2026), https://doi.org/10.1016/j.cell.2026.08.002

Continued

REAGENT or RESOURCE	SOURCE	IDENTIFIER
Published age-associated differential expression estimates in CD4+ T cells (benchmarking)	Wells et al.,[63] Terekhova et al.[64]	Publication supplementary tables
UK Biobank loss-of-function burden test summary statistics	Ota et al.[3]	10.5281/zenodo.14751877
Experimental models: Cell lines		
Lenti-X™ 293T	Takara Bio	632180
Oligonucleotides		
Custom gRNA detection spike-in probes, oPool	Integrated DNA Technologies (IDT)	N/A
Custom PuroR detection spike-in probes	Integrated DNA Technologies (IDT)	N/A
Genome-scale gRNA oligonucleotide pool (26504 gRNAs)	Agilent Technologies	N/A
Recombinant DNA		
psPAX2 (lentiviral packaging)	Didier Trono lab	Addgene #12260
pMD2.G (VSV-G envelope)	Didier Trono lab	Addgene #12259
ZIM3KRAB-dCas9-BlastR (pZR316)	Arce et al.[13]	Addgene #252529
lentiGuide-Puro-BlpI (PJY390)	This paper	Addgene #251159
Genome-scale CRISPRi library (htCRISPRi-Puro)	This paper	Addgene #254479
lentiGuide-Puro	Feng Zhang lab	Addgene #52963
pRZ109 (single gRNA expression backbone with GFP)	This paper	Addgene #261828
pRZ111 (single gRNA expression backbone with mCherry)	This paper	Addgene #261832
Software and algorithms		
Code for all processing and analysis in this paper	This paper	https://github.com/emdann/GWT_perturbseq_analysis_2025
Python class to predict regulators of observed cell states (pert2state_model)	This paper	https://github.com/emdann/pert2state_model
CellRanger	10x Genomics	https://www.10xgenomics.com/support/software/cell-ranger
crispat (Poisson-Gaussian mixture model for guide assignment)	Braunger and Velten[133]	https://github.com/velten-group/crispat
scanpy	Wolf et al.,[133] Virshup et al.[134]	https://scanpy.readthedocs.io/
scvi-tools	Lopez et al.[135]	https://scvi-tools.org/
hdbscan (HDBSCAN clustering of perturbation effects)	McInnes et al.[136]	https://hdbscan.readthedocs.io/
DESeq2	Love et al.,[137] via python implementation[138,139]	https://pertpy.readthedocs.io/
mashr (Multivariate Adaptive Shrinkage)	Urbut et al.[140]	https://github.com/stephenslab/mashr
scikit-learn	Pedregosa et al.[141]	https://scikit-learn.org/
GSEApy EnrichR methods	Xie et al.[142]	https://github.com/zqfang/GSEApy
Off-target CRISPRi detection pipeline (adapted)	Hartman et al.[143]	https://github.com/AustinHartman/perturb_seed
FastQC	v0.12.1	https://www.bioinformatics.babraham.ac.uk/projects/fastqc/
Fastp	v0.24.0	https://github.com/OpenGene/fastp
STAR aligner	v2.7.11	https://github.com/alexdobin/STAR
Samtools	v1.22.1	http://www.htslib.org/
UMIcollapse	v1.1.0	https://github.com/Daniel-Liu-c0deb0t/UMICollapse
RSeQC	v5.0.4	https://rseqc.sourceforge.net/

(*Continued on next page*)

Please cite this article in press as: Zhu et al., Genome-scale perturb-seq in primary human CD4+ T cells maps context-specific regulators of T cell programs and human immune traits, Cell (2026), https://doi.org/10.1016/j.cell.2026.08.002

Continued

REAGENT or RESOURCE	SOURCE	IDENTIFIER
Qualimap	v2.3	http://qualimap.conesalab.org/
MultiQC	v1.32	https://multiqc.info/
featureCounts (subread package)	v2.1.1	https://subread.sourceforge.net/
FlowJo	v10.10.1	https://www.flowjo.com/
Other		
Human transcription factor annotations	Lambert et al.[132]	N/A
Database of Immune Cell Expression, Expression quantitative trait loci (eQTLs) and Epigenomics (DICE)	Schmiedel et al.[144]	https://dice-database.org
ENCyclopedia Of DNA Elements (ENCODE)	ENCODE Project Consortium[145]	https://www.encodeproject.org/
Tabula Sapiens	Tabula Sapiens Consortium[146]	https://tabula-sapiens.sf.czbiohub.org/
CORUM protein complex database	Ruepp et al.[147]	https://mips.helmholtz-muenchen.de/corum/
STRING database	Szklarczyk et al.[148]	https://string-db.org/
KEGG pathway database	Kanehisa and Goto[149]	https://www.genome.jp/kegg/
Reactome pathway database	Milacic et al.[150]	https://reactome.org/
Gene Ontology (GO Biological Process 2025)	Ashburner et al.[151]	https://geneontology.org/
Human Protein Atlas, RNA expression consensus (v25.0, Ensembl v109)	Uhlen et al.[152]	https://www.proteinatlas.org/about/download
OpenTargets Platform (v4)	Buniello et al.[87]	https://platform.opentargets.org/

EXPERIMENTAL MODEL AND STUDY PARTICIPANT DETAILS

Isolation and culture of naive human CD4+ T cells

Primary naive human CD4+ T cells were isolated from PBMC-enriched leukapheresis products (Leukopaks, StemCell Technologies, catalog no. #70500) from healthy donors (Table S1, Table S23) following institutional review board–approved informed written consent (StemCell Technologies). The leukapheresis products were washed twice with a 1X volume of EasySep buffer (DPBS, 2% FBS and 1 mM EDTA, pH 8.0) using centrifugation. The washed cells were resuspended at 5 x 10^7 cells/ml in EasySep buffer and isolated with the EasySep Human Naive CD4+ T cell Isolation Kit (catalog no. #19555, StemCell Technologies), according to the manufacturer's protocol. CD4+ T cells were cultured in complete X-VIVO 15 (cXVIVO) consisting of X-VIVO 15 (Lonza Bioscience, 04–418Q) supplemented with 5% heat-inactivated fetal bovine serum, Premium Select (R&D Systems, catalog no. S11550).

METHOD DETAILS

Genome-scale gRNA library design and library cloning

We compiled a list of genes to target by taking the union of all expressed genes in human CD4+ T cells and all transcription factors annotated in Lambert et al. (2018).[146] To find expressed genes in human CD4+ T cells across contexts and subsets, we used public gene expression datasets DICE (https://dice-database.org), ENCODE (https://www.encodeproject.org/) and Tabula Sapiens.[153] For each dataset, we selected a set of genes that accounts for >99% of total expression, then took the union of genes from three datasets and transcription factors from Lambert et al.,[146] targeting 12,779 genes in total. We then selected two gRNAs per gene cross-referencing two widely-used genome-wide CRISPRi guide RNA databases, hCRISPRiv2 and Dolcetto,[154,155] as well as hits from CRISPRi screening studies.[6,156–158] Specifically, for each gene, we selected gRNAs with the following criteria in descending priorities until two gRNAs are found: (1) gRNAs that are hits from existing CRISPRi screening studies in T cells[6] and other cell types[9,156–158]; (2) gRNAs that appear in both hCRISPRiv2 and Dolcetto; (3) gRNAs that are in Dolcetto dataset. We also included 5% of non-targeting gRNAs from the Dolcetto dataset in the library as controls. In total, our genome-scale gRNA library consists of 26,504 gRNAs (Table S3).

Plasmids

ZIM3KRAB-dCas9-BlastR (pZR316, Addgene #252529) plasmid is a kind gift from Zachary Steinhart (Addgene #252529). lentiGuide-Puro-BlpI (PJY390, Addgene #251159) was cloned by Gibson assembly with lentiGuide-Puro plasmid (Addgene #52963) as the backbone. Backbones for single gRNA expression for arrayed experiments were designed by switching puromycin resistance genes with GFP (pRZ109, Addgene #261828) or mCherry (pRZ111, Addgene #261832) and were cloned by GenScript. All gRNAs for validation experiments were cloned into pRZ109 or pRZ111 by GenScript. Sequences for all backbones used in this study and individual gRNA sequences used in validation experiments (for Figure 2) can be found in Table S2.

Please cite this article in press as: Zhu et al., Genome-scale perturb-seq in primary human CD4+ T cells maps context-specific regulators of T cell programs and human immune traits, Cell (2026), https://doi.org/10.1016/j.cell.2026.08.002

Our genome-scale CRISPRi library (htCRISPRi-Puro, Addgene #254479) was cloned into PJY390 by Golden Gate Cloning as described previously.[155] The oligonucleotide pool was obtained from Agilent and amplified with KAPA HiFi HotStart (Roche 07958935001). The PCR product was purified by MinElute PCR Purification Kit (Qiagen 28004) and ligated into lentiGuide-Puro-BlpI (PJY390) with the New England Biolabs NEB Golden Gate Assembly Kit (BsmBI-HF v2) (New England Biolabs, E1602L) per the manufacturer's instructions. The ligation product was transformed into Endura electrocompetent cells (LGC, 60242-2) per the manufacturer's instructions. Cells were expanded at 30 C for 22 h and plasmid was extracted using ZymoPURE II Plasmid Maxiprep Kit (Zymo, D4203). For library quality control, the guide RNA distribution was confirmed by NGS sequencing at coverage of >1,000×. The plasmid pool was then used for lentivirus production as described under 'Lentivirus production'.

Lentivirus production

Lentiviral particles were produced as previously described.[6] In brief, Lenti-X HEK293T cells (Takara Bio, catalog no. 632180) were maintained in DMEM, high glucose, GlutaMAX™ Supplement, HEPES (Gibco, catalog no. 10564029), supplemented with 10% heat-inactivated Fetal Bovine Serum, 100 U/ml of penicillin/streptomycin (Gibco, catalog no. 15140122), 1 mM Sodium Pyruvate (Gibco, catalog no. 11360070), and MEM Non-Essential Amino Acids Solution (Gibco, catalog no. 11140050). Cells were passaged every 2 days using TrypLE Express (Gibco, catalog no. 12604013) for dissociation and maintained at <60% confluency. One day before transfection, for a T225 flask, 3.6×10^7 Lenti-X HEK 293T cells were seeded in 45 ml complete Opti-MEM (cOPTI-MEM) consisting of Opti-MEM™ I Reduced Serum Medium, GlutaMAX™ Supplement (Thermo Fisher Scientific, catalog no. 51985034) supplemented with 5% heat-inactivated Fetal Bovine Serum, Premium Select, 1 mM Sodium Pyruvate, and MEM Non-Essential Amino Acids Solution. The next morning, cells were transfected with 38 μg transfer plasmid, 28 μg psPAX2 (Addgene #12260) and 14 μg pMD2.G (Addgene #12259) with 167 μl p3000 and 181 μl Lipofectamine 3000 (Invitrogen, L3000075). Six hours after transfection, medium was replaced with fresh cOPTI-MEM supplemented with 1x viral boost (Alstem, VB100). Another 18 hours later, virus containing supernatant was collected and spun down at 500g for 5 minutes at 4 °C to pellet cell debris. Lentivirus-containing medium was moved to a new vessel and subsequently concentrated 100-fold using Lenti-X Concentrator (Takara Bio, 631232) per the manufacturer's instructions. Viral particles were stored at −80 °C until further use.

Functional titering of lentivirus

To functionally titer ZIM3KRAB-dCas9-BlastR (pZR316) lentivirus, primary naive human CD4+ T cells were isolated and seeded at 1 x 10^6 cells/mL in cXVIVO supplemented with 200 IU/mL IL-2 and activated with 25 μL/mL ImmunoCult human CD3/CD28/CD2 T cell activator, aliquoted at 150 μL/well in 96-well flat-bottom plates. The next morning (day 1), ZIM3KRAB-dCas9-BlastR lentivirus was added at 0% (no virus), 1%, 2%, 3% and 4% volume to volume (v/v, corresponding to 0, 1.5, 3, 4.5 and 6 μL/well). In the afternoon of day 1, 3 μL of a CD45-targeting gRNA lentivirus (pRZ103-CD45KD, expressing a gRNA against CD45 in a GFP-marked backbone) was added to each well. On day 3, 5, 7, the culture was split into cXVIVO with 200 IU/mL IL-2 with or without 10 μg/mL Blasticidin (Gibco, catalog no. A1113903) to ∼5 x 10^5 cells/mL. On day 9, cells were stained with Ghost Dye™ Red 780 viability dye (Cytek Biosciences, catalog no. 13-0865-T500) and PE-conjugated anti-CD45 antibody (Biolegend, catalog no. 304008) and analyzed by flow cytometry. Functional titer was determined as the v/v dose yielding the desired fraction of GFP+ and CD45-knockdown cells while maintaining blasticidin-dependent selection relative to the no-antibiotic control (Figure S1).

To titer genome-scale gRNA library lentivirus functionally, primary naive human CD4+ T cells were isolated and seeded at 1 x 10^6 cells/mL in cXVIVO supplemented with 200 IU/mL IL-2 and activated with 25 μL/mL ImmunoCult human CD3/CD28/CD2 T cell activator, aliquoted at 150 μL/well in 96-well flat-bottom plates. The next morning (day 1), ZIM3KRAB-dCas9-BlastR lentivirus was added at 2% v/v. In the afternoon of day 1, genome-scale gRNA library lentivirus was added at 0%, 1/32%, 1/16%, 1/8%, 1/4%, 1/2%, 1%, 2% v/v. On day 3, the culture was split into cXVIVO with 200 IU/mL IL-2, 10 μg/mL Blasticidin and with or without 2 μg/mL Puromycin to ∼5 x 10^5 cells/mL. On day 5, cells were stained with GhostDye 780 viability dye and analyzed by flow cytometry. Functional titer was determined as the v/v dose yielding the desired fraction of cells (∼0.2-0.3) surviving puromycin selection.

Genome-scale perturb-seq

After isolation (day 0), 30 million naive human CD4+ T cells were seeded at 1 x 10^6 cells/ml cXVIVO supplemented with 200 IU/ml of recombinant human IL-2 (Amerisource Bergen, catalog no. 10101641). Cells were activated using ImmunoCult human CD3/CD28/CD2 T cell activator (10990, STEMCELL Technologies) at 25 μl/ml. The next morning, cells were transduced with 2% v/v concentrated ZIM3KRAB-dCas9-BlastR lentivirus. In the afternoon, cells were transduced with 0.1% v/v (multiplicity of infection ∼ 0.2) genome-scale gRNA library lentivirus. At day 3, cells were centrifuged and resuspended with above medium supplemented with 200 IU/mL IL-2. Blasticidin and puromycin were added to 10 μg/mL and 2 μg/mL final concentrations, respectively. At day 5, cells were counted and diluted to 5 x 10^5 cells/mL with cXVIVO supplemented with 200 IU/mL IL-2 and 10 μg/mL blasticidin. Recombinant human IL-7 (R&D Systems, catalog no. 207-IL) was also added to a final concentration of 5 ng/mL. At day 7, cells were counted and diluted to 7.5 x 10^5 cells/mL with cXVIVO supplemented with 200 IU/mL IL-2, 5 ng/mL IL-7 and 10 μg/mL blasticidin. At day 8, cells were centrifuged and resuspended at 1 x 10^6 cells/mL with cXVIVO supplemented with 200 IU/mL IL-2 and 5 ng/mL IL-7. At day 10, cells were centrifuged and resuspended at 5 x 10^5 cells/mL and 1 x 10^6 cells/mL with cXVIVO supplemented with 200 IU/mL IL-2 and 5 ng/mL IL-7. At day 12 morning, cells were centrifuged and resuspended at 1 x 10^6 cells/ml with cXVIVO supplemented with

Please cite this article in press as: Zhu et al., Genome-scale perturb-seq in primary human CD4+ T cells maps context-specific regulators of T cell programs and human immune traits, Cell (2026), https://doi.org/10.1016/j.cell.2026.08.002

200 IU/mL IL-2 and split into three populations. The first population (Rest) was kept at a rested state without restimulation and harvested in the afternoon after 8 hours. The second population (Stim8hr) was restimulated by adding 12.5 μL/ml ImmunoCult human CD3/CD28/CD2 T cell activator and harvested in the afternoon after 8 hours. The third population (Stim48hr) was restimulated by adding 12.5 μL/ml ImmunoCult human CD3/CD28/CD2 T cell activator and harvested after 48 hours. Cells were harvested, fixed and stored using GEM-X Flex Sample Preparation v2 Kit (10x genomics, catalog no. 1000781) per the manufacturer's instructions.

Single-cell library construction

Stored cells were processed to scRNA-seq and gRNA sequencing libraries using GEM-X Flex Gene Expression Human n-plex kit (10x genomics, catalog no. 1000829) for 16-plex probes and GEM-X gel beads and GEM-X Flex Gene Expression Human kits (catalog no. 1000792) for additional GEM-X gel beads, following the manufacturer's protocol. Protocols were modified to enable CRISPR gRNA detection according to 10x's technical note "CG000814, CRISPR Screening with GEM-X Flex Gene Expression". Spike-in probes to detect gRNA expression were ordered from IDT as oPool. To assess the off-target gRNA detection by off-target probe binding, we also ordered 768 gRNA probes that detect gRNA that are not in our genome-scale library. Less than 0.2% of cells had an assignment of "guides" corresponding to one of out-of-library gRNA probes, demonstrating the low off-target detection of gRNA by probe-based methods. Probes to detect puromycin resistant (PuroR) gene expression were also ordered from IDT and were spiked in following 10x's technical note "CG000621, Custom Probe Design for Visium Spatial Gene Expression and Chromium Single Cell Gene Expression Flex". Briefly, 12 samples were processed in three batches.

Batch 1: Rest - D1, Rest - D2, Stim8hr - D1, Stim8hr - D2.
Batch 2: Rest - D3, Rest - D4, Stim8hr - D3, Stim8hr - D4.
Batch 3: Stim48hr - D1, Stim48hr - D2, Stim48hr - D3, Stim48hr - D4.

Of the three batches, the second batch and the third batch were processed on the same days (see Table S1). For each batch, we thawed, counted and put 8 million cells from each of the four biological samples into the hybridization step (32 million cells in total). The 8 million cells from each biological sample (e.g. Rest - D1) were resuspended with 640μL Hyb Mix and evenly distributed into 4 hybridization reaction tubes. Then we added WTA probes for gene expression, spike-in probes for gRNA expression and PuroR expression. In summary, we had 16 hybridization reaction tubes, with 4 hybridization reaction tubes per biological sample. Each hybridization reaction tube consisted of 2 million cells, 160μL Hyb Mix, 40μL WTA probes, 20nM CRISPR LHS probe, 2nM/probe CRISPR RHS probes, 2nM/probe PuroR LHS probes, 2nM/probe PuroR RHS probes with total volume slightly more than 200μL. We further split each ~200μL hybridization reaction into 4 aliquots, with each aliquot tube having ~50μL hybridization reaction before putting into thermocycler for ~19 hours overnight incubation (including a ~1.5hr 60C-42C ramp-down phase specific for CRISPR). The next day, we performed the post-hybridization wash protocol. Then we loaded:

Batch 1: 1.161M cells per lane for 23 lanes (~2.5x overloading)
Batch 2: 0.926M cells per lane for 24 lanes (~2x overloading)
Batch 3: 0.8M cells per lane for 24 lanes (~1.7x overloading)

We proceeded with library construction according to the manufacturer's protocol (10x Genomics).

Sequencing

The final 10x libraries were converted into Ultima compatible libraries in 7 PCR cycles using conversion primers provided by Ultima Genomics. Converted libraries were purified with SPRISelect beads (Beckman Coulter) and quantified using Qubit 1X dsDNA High Sensitivity Assay kit (Thermo Fisher). Converted libraries were sent to Psomagen to sequence on Ultima sequencers. Each 10x lane was sequenced on one Ultima wafer with ~10B sequencing reads.

Arrayed validation of *IL10/IL21* regulation

At day 0, primary naive human CD4+ T cells were seeded at 1 x 10^6 cells/ml in cXVIVO and 200 IU/ml IL-2 at 150μL/well in 96-well flat bottom plates. Cells were activated using 25 μl/ml ImmunoCult human CD3/CD28/CD2 T cell activator. The next morning, cells were transduced with 2% v/v concentrated ZIM3KRAB-dCas9-BlastR lentivirus. In the afternoon, cells in each well were transduced with a distinct, individual single gRNA expressing lentivirus (Table S2) at 2% v/v. On day 3, cells were split to ~5 x 10^5 cells/mL and Blasticidin was added at 10 μg/mL final concentration. At day 5, cells were centrifuged and resuspended with cXVIVO supplemented with 200 IU/mL IL-2, 5 ng/mL IL-7 and 10 μg/mL blasticidin at ~5 x 10^5 cells/mL. At day 7, cells were counted and diluted to 1 x 10^6 cells/mL with cXVIVO supplemented with 200 IU/mL IL-2, 5 ng/mL IL-7 and 10 μg/mL blasticidin. At day 8, cells were centrifuged and resuspended at 1 x 10^6 cells/mL with cXVIVO supplemented with 200 IU/mL IL-2 and 5 ng/mL IL-7. On day 10 morning, cells were split into two pools. In one pool, cells were centrifuged and resuspended at 2 x 10^6 cells/ml with cXVIVO supplemented with 200 IU/mL IL-2 and 1 μL/mL Activation Cocktail with Brefeldin A (BioLegend). After 6 hours, cells were stained for IL-10 (Brilliant Violet 421 anti-human IL-10 Antibody, catalogue number 501422, Biolegend) and IL-21 (PerCP/Cyanine5.5 anti-human IL-21 Antibody, catalogue number 513012, Biolegend) protein expression following the BD Cytofix/Cytoperm kit instructions (BD Biosciences, catalog no. 554714). In another pool, cells were centrifuged and resuspended at 2 x 10^6 cells/ml with cXVIVO supplemented with

200 IU/mL IL-2 and 12.5 μL/mL ImmunoCult human CD3/CD28/CD2 T cell activator. After 8 hours, cells were centrifuged and resuspended in DNA/RNA Shield (Zymo Research) and sent for bulk RNAseq by Plasmidsaurus.

For each of the 9 selected regulator genes, we chose two different gRNAs to target them. The first gRNA was chosen from one of the two gRNAs used in perturb-seq. The second gRNA was chosen outside of our perturb-seq library from hCRISPRiv2. The non-targeting control samples of this experiment were intentionally designed to be transduced with a mixture of two non-targeting control gRNAs (NTC425 and NTC720, Table S2). This is to avoid systematic perturbation effect biases from small chance of using a non-targeting control gRNA that induces off-target effects.

Arrayed validation of TCR functional clusters

At day 0, primary naive human CD4+ T cells were seeded at 1 x 10^6 cells/ml in cXVIVO and 200 IU/ml IL-2 at 150μL/well in 96-well flat bottom plates. Cells were activated using 25 μl/ml ImmunoCult human CD3/CD28/CD2 T cell activator. The next morning, cells were transduced with 2% v/v concentrated ZIM3KRAB-dCas9-BlastR lentivirus. In the afternoon, cells in each well were transduced with a distinct, individual single gRNA expressing lentivirus (Table S2) at 2% v/v. On day 3, cells were split to ~5 x 10^5 cells/mL and Blasticidin was added at 10 μg/mL final concentration. At day 5, cells were centrifuged and resuspended with cXVIVO supplemented with 200 IU/mL IL-2, 5 ng/mL IL-7 and 10 μg/mL blasticidin at ~5 x 10^5 cells/mL. At day 7, cells were counted and diluted to 1 x 10^6 cells/mL with cXVIVO supplemented with 200 IU/mL IL-2, 5 ng/mL IL-7 and 10 μg/mL blasticidin. At day 8 and day 10, cells were centrifuged and resuspended at 1 x 10^6 cells/mL with cXVIVO supplemented with 200 IU/mL IL-2 and 5 ng/mL IL-7. On day 12 morning, cells were centrifuged and resuspended at 2 x 10^6 cells/ml with cXVIVO supplemented with 200 IU/mL IL-2 and split into two pools. In the first pool (Stim8hr), cells were restimulated by adding 12.5 μL/ml ImmunoCult human CD3/CD28/CD2 T cell activator and harvested in the afternoon after 8 hours. In another pool (Stim48hr), cells were restimulated by adding 12.5 μL/ml ImmunoCult human CD3/CD28/CD2 T cell activator and harvested after 48 hours. During harvest, cells were centrifuged and resuspended in DNA/RNA Shield and sent for bulk RNAseq by Plasmidsaurus.

Arrayed validation of predicted Th1/Th2 regulators

At day 0, primary naive human CD4+ T cells were seeded at 1 x 10^6 cells/ml in cXVIVO and 200 IU/ml IL-2 at 150 μL/well in 96-well flat bottom plates. Cells were activated using 25 μl/ml ImmunoCult human CD3/CD28/CD2 T cell activator. The next morning, cells were transduced with 2% v/v concentrated ZIM3KRAB-dCas9-BlastR lentivirus. In the afternoon, cells in each well were transduced with a distinct, individual single gRNA expressing lentivirus (Table S2) at 2% v/v. On day 3, cells were centrifuged and resuspended with 150 μL cXVIVO supplemented with 200 U/mL IL-2 and 10μg/mL blasticidin. For Th1 and Th2 conditions, 0.3 ng/mL IL-12 and 20 ng/mL IL-4 were added, respectively. From day 5 to day 9, cells were split every 2 days to ~5 x 10^5 cells/mL with cXVIVO supplemented with 200 U/mL IL-2, 5 ng/mL IL-7, 10 μg/mL blasticidin, with 0.3 ng/mL IL-12 added to Th1 condition wells and 20 ng/mL IL-4 added to Th2 condition wells. On day 9 and day 11, cells were centrifuged and resuspended at ~1 x 10^6 cells/mL with cXVIVO supplemented with 200 IU/mL IL-2, 5 ng/mL IL-7, with 0.3 ng/mL IL-12 added to Th1 condition wells and 20 ng/mL IL-4 added to Th2 condition wells. On day 12, cells were centrifuged and resuspended with cXVIVO at 2 x 10^6 cells/ml with cXVIVO. The next day, the cells were stimulated with 12.5 μL/mL ImmunoCult human CD3/CD28/CD2 T cell activator. After 8 hours, cells were centrifuged and resuspended in DNA/RNA Shield and sent for bulk RNAseq by Plasmidsaurus.

For Th1/Th2 protein marker phenotyping using antibody staining and flow cytometry, fraction of IL-5 (a Th2-specific marker) expressing cells was very low at day 12 (Figure S3H). Therefore cells from day 12 were restimulated at 5 x 10^5 cells/mL with 6.25 μl/ml ImmunoCult human CD3/CD28/CD2 T cell activator in cXVIVO supplemented with 200 U/mL IL-2, with 20 ng/mL IL-4 added to Th2 condition wells. Cells were split every two days to ~5 x 10^5 cells/mL with cXVIVO supplemented with 200 U/mL IL-2, with 20 ng/mL IL-4 added to Th2 condition wells. On day 21, cells were centrifuged and resuspended with cXVIVO without supplements at 2 x 10^6 cells/mL and split into two groups. In group 1, cells were restimulated with 12.5 μL/mL ImmunoCult human CD3/CD28/CD2 T cell activator the next morning. After 2 hours, Golgiplug protein transport inhibitor (BD Biosciences) was added at 1 μL/mL. After another 4 hours, cells were stained for IFN-γ (Brilliant Violet 711 anti-human IFN-γ Antibody, catalogue number 502540, Biolegend) and IL-5 (IL-5 Monoclonal Antibody (TRFK5), PE, catalogue number 12-7052-82, eBioscience) protein expression following the BD Cytofix/Cytoperm kit instructions (BD Biosciences). In group 2, cells were directly stained without restimulation for T-bet (Brilliant Violet 421 anti-T-bet Antibody, catalogue number 502540) and GATA3 (Gata-3 Monoclonal Antibody (TWAJ), PE, catalogue number 12-9966-42, eBioscience) protein expression following the True-Nuclear™ Transcription Factor Buffer Set kit instructions (Biolegend).

Amongst the top predicted Th1/Th2 regulators included in the first batch of validation experiments, we found perturbations with low robustness across guides or donors, and showed poor replication in arrayed experiments (Table S18). In subsequent batches, we applied stringent filtering on DE effect cross-guide correlation ($R > 0.25$, with significant on-target knock-down in both guides), cross-donor correlation ($R > 0.35$) and strength of perturbation (N DE genes > 30).

Perturb-seq data preprocessing and quality control

The sequencing reads were processed by Psomagen into single cell gene expression count matrices using CellRanger on 10x Cloud services with following configuration setting (chemistry,auto; no-secondary,false; create-bam,false; Filter-probes,true) and our

Please cite this article in press as: Zhu et al., Genome-scale perturb-seq in primary human CD4+ T cells maps context-specific regulators of T cell programs and human immune traits, Cell (2026), https://doi.org/10.1016/j.cell.2026.08.002

custom probe set. The custom probe set consists of Chromium Human transcriptome Probe Set v1.1.0 plus two spike-in probes targeting the puromycin resistance gene associated with gRNA expression cassette. Spike-in probes are these two lines in the custom_probe_set.csv:

CUSTOM001_PuroR,TCCGCGACCCACACCTTGCCGATGTCGAGCCCGACGCGCGTGAGGAAGAG,CUSTOM001_PuroR|PuroR|8aab555,TRUE,unspliced,PuroR

CUSTOM001_PuroR,AACCACGCGGGCTCCTTGGGCCGGTGCGGCGCCAGGAGGCCTTCCATCTG,CUSTOM001_PuroR|PuroR|8aab556,TRUE,unspliced,PuroR

After CellRanger analysis was performed, we processed in parallel mRNA and gRNA UMI count matrices for each sample and lane. We initially filtered out cells with >20% mitochondrial gene expression and < 200 detected genes.

We used the Poisson-Gaussian mixture model to assign guides to cells, following the model in Replogle et al.,[9] using the implementation in the *crispat* package[133] (https://github.com/velten-group/crispat). This models the distribution of UMIs across cells as a mixture of 2 distributions, one for background guide probe detection and one for true signal from cells where the guide is expressed. In our pilots, this approach outperformed using a fixed threshold to assign guides to cells excluding background (in terms of number of cells with multiple guides assigned and identification of guides with frequent non-specific binding). We fit a separate model for each guide in each processed sample, assuming there might be differences in mean UMI counts per guide across samples. We then identified cells with no assigned gRNA, one assigned gRNA or multiple assigned gRNAs and the UMI counts of the most abundant guide in each cell.

After guide assignment, we excluded cells with low quality transcriptomes (>5% mitochondrial reads, <500 genes), ambiguous gRNA assignments ("multi_sgRNA"), or no detectable gRNA. Summaries of quality control metrics for each sample and lane are reported in Table S4.

When reporting normalized expression values, raw counts were normalized per cell and log-transformed using default parameters implemented in *scanpy*.[134,137] To assess batch effects between lanes, we analyzed non-targeting control (NTC) cells across experimental conditions, subsampling 10 sequencing lanes per sample from all experimental batches, resulting in 395,030 cells. We performed dimensionality reduction with scVI, minimizing differences between donors with the following parameters: 30 latent dimensions, negative binomial gene likelihood, 2 hidden layers with 128 units, 0.2 dropout rate. This revealed no substantial batch effects between 10x lanes or experimental batches, with most transcriptional variance explained by culture condition and proliferation status (Figures S3A–S3E). We observed expected expression patterns for canonical T cell activation markers across stimulation timepoints, although expression levels varied between donors, especially post-stimulation (Figure S3F).

For a preliminary estimate of guide efficiency (Figure S4), we calculated the expression of the targeted gene in cells with each guide and compared it to expression in NTC cells with a one-sided T-test, using the Benjamini-Hochberg correction to control the false discovery rate. The knockdown was considered significant if FDR < 10% and t-statistic < 0. Guides for which no significant knock-down was detected in any condition (with at least 10 cells and mean log-normalized expression in NTCs > 0.01) were considered inefficient and excluded from differential expression analysis (n=869). Summary statistics on target expression per condition are reported in Table S5.

Analysis of trans effects

Differential expression analysis

To estimate the average effect of each perturbed gene in each culture condition, we aggregated data from all cells within the same biological sample (donor and condition) harboring the same guide, by summing mRNA counts. We chose to estimate variance in gene expression across donors and guides to naturally downplay inconsistent effects across replicates, which might arise from technical artifacts. We refer to each experimental unit of donor-condition-guide as a "pseudobulk" sample. We discard pseudobulks with data from less than 5 cells, and where the total mRNA count was much lower compared to other pseudobulk in the same conditions (< 0.5% percentile). Only perturbed genes represented by at least 3 pseudobulks across guides and donors were included in differential expression testing (N perturbed genes per condition: Rest = 11,289; Stim8hr = 11,417; Stim48hr = 11,333). For downstream gene selection in each condition, we first removed expression outliers (mean counts > 10,000 or < 1, and percentage of expressing pseudobulks > 99.9% or < 1%). We then retained the top 10,000 highly variable genes for differential expression analysis using the Scanpy function *scanpy.pp.highly_variable_genes* (flavor = 'seurat_v3') on pseudobulk expression profiles.

We performed differential expression (DE) analysis with the DESeq2 method,[138] using the python implementation.[139,159] Briefly, the mRNA counts of gene *j* in pseudobulk *p* were modeled by a negative-binomial generalized linear model:

$$y_{j,p} = NB\left(\mu_{j,p}, \theta_{j,p}\right),$$

The expected count value is given by the following log-linear model:

$$log\mu_{j,p} = \beta_0 + log_{10}\left(n_p\right)\beta_{j,n} + \sum_d x_{d,p}\beta_{j,d} + \sum_k x_{k,p}\beta_{j,k} + log\left(s_p\right)$$

- β_0 denotes the intercept

Please cite this article in press as: Zhu et al., Genome-scale perturb-seq in primary human CD4+ T cells maps context-specific regulators of T cell programs and human immune traits, Cell (2026), https://doi.org/10.1016/j.cell.2026.08.002

- n_p denotes the number of aggregated cells in pseudobulk p
- $x_{d,p}$ denotes the assignment of pseudobulk p to donor d
- $x_{k,p}$ denotes the assignment of pseudobulk p to perturbed gene k
- $\beta_{j,n}$, $\beta_{j,d}$ and $\beta_{j,k}$ denote the effect of number of cells, donor and perturbation, respectively, on the mean expression of gene j
- s_p denotes the library size (total UMI counts per pseudobulk)

For each perturbed gene k, we estimated the log2 fold-change in gene expression $\beta_{j,k}$ and test for differential expression using the Wald test, contrasting expression estimates for each perturbed gene against non-targeting control pseudobulks. For each culture condition, we fit DE models independently, to obtain context-specific perturbation estimates ($\beta_{j,k}^{Rest}$, $\beta_{j,k}^{Stim8hr}$, $\beta_{j,k}^{Stim48hr}$). To account for differences in noise between perturbations with different number of recovered cells across replicates, unless otherwise specified we use the z-score of the DE log-fold change ($\tilde{\beta}_{j,k}$) as normalized perturbation effect estimates, where:

$$\tilde{\beta}_{\mathrm{j,k}}^{\ \mathrm{context}} = \beta_{\mathrm{j,k}}^{\ \mathrm{context}} / \mathrm{SE}\left(\beta_{\mathrm{j,k}}^{\ \mathrm{context}}\right),$$

The standard error of the log-fold change is obtained from DESeq2 outputs. We define $\tilde{B}^{\mathrm{context}}$ as the K x J matrix of DE effect estimates in each cellular context.

To improve computational scalability across thousands of perturbed genes, we randomly partitioned perturbed genes into groups of 50 and fit one GLM for each group along with non-targeting controls (NTCs) in each condition in parallel. Pilot experiments with alternative partitioning schemes confirmed that DE estimates for individual perturbed genes were consistent regardless of which genes were included in the model, and that covariate effect estimates remained stable (data not shown). We further verified robustness by comparing mean expression estimates for each condition across partitions.

To assess the statistical calibration of the DE analysis (Figure S5B), we performed a null model validation comparing cells with NTC guides. We select amongst guides with cell counts between the 5th and 95th percentile of the NTC distribution to ensure comparable sample sizes to true targeting guides. For each of five independent random splits, we randomly assigned 2 NTC guides to a simulated target group, selecting guides with cell counts between the 5th and 95th percentile of the NTC distribution to ensure comparable coverage to that of the true targeting guides. The remaining NTC guides are used as controls. We performed DE analysis on each split across all three culture conditions (Rest, Stim8hr, Stim48hr) using the same statistical model and design formula applied to targeting perturbations (Figure S5B).

We detected significant on-target knock-down in 73% of tested condition-target pairs. Beyond low baseline expression, perturbations without detectable on-target knockdown also showed significantly fewer cells per perturbation (Kolmogorov-Smirnov test, p = 6.57e-12). To estimate off-target prevalence on proximal genes, we annotated each gRNA's distance to the nearest non-target transcription start site (TSS) and assessed DE effects on that gene (Table S3). Putative off-targets were flagged where we detected significant knock-down of the nearest TSS gene (DE z-score < -1, FDR < 10%) (Table S7).

Guide robustness and off-target effects analysis

To assess the reproducibility of perturbation effects across independent gRNAs targeting the same gene, we performed guide-level differential expression analysis. For each culture condition, we retained guides with at least 3 pseudobulk replicates passing per-sample QC ($\geq$5 cells per guide per sample). This yielded 19,822 guides in Rest, 20,654 guides in Stim8hr, and 20,295 guides in Stim48hr. Each guide was treated as an independent perturbation and tested against NTC controls using the same DESeq2-based framework as the target-level analysis, with design $\sim$ *log10_n_cells + target*, and a minimum of 10 total counts per gene. To quantify reproducibility, for each gene targeted by exactly two testable guides we computed the Pearson correlation between guide-level DE effects across two gene sets: (i) all tested genes; and (ii) genes called as hits (10% FDR) in the corresponding target-level test (e.g. estimates considering both guides). The rationale for subsetting to target-level hits is to test the robustness of DE estimates on hits that we then consider as significant regulatory relationships in the rest of our analyses.

CRISPRi repression is mediated by dCas9 binding to genomic DNA guided by PAM-proximal complementarity, and off-target binding can occur at unintended loci sharing sequence similarity with the sgRNA seed region. Early work established that the 8-12 nucleotide PAM-proximal "seed" region of the protospacer is critical for target recognition, and that mismatches outside this region are better tolerated.[160,161] More recently, Rohatgi et al. (2024)[143] systematically demonstrated that off-target effects in CRISPRi are pervasive and largely explained by complementarity between the 3′ half of the sgRNA protospacer (the seed sequence) and PAM-adjacent sites in gene promoters, with as few as 8-9 bp of seed match sufficient to cause transcriptional repression at off-target loci. Based on these findings, we adapted a recently published computational pipeline[162] to identify and flag putative off-target CRISPRi effects in our Perturb-seq dataset.

We focused on perturbations with sufficient DE signals (>10 significant DE genes with 10% FDR at the target level or >10 significant DE genes with 10% FDR for either individual guide), then filtered out perturbations with good inter-guide concordance when all these criteria are met: (1) Pearson correlation between the two guides' DE LogFC profiles > 0.1 across all measured genes; (2) Pearson correlation among union-significant (10% FDR in either DE LogFC profile) genes > 0 with P value < 0.05; (3) Both guides induce significant (10% FDR) on target knockdown. Furthermore, perturbations with >10 DE genes and with only a single guide (and thus lacking concordance information) were automatically included.

For each guide in the follow-up set, we focused on all the downstream genes that were significantly downregulated in the guide-level DE analysis (10% FDR), excluding the intended on-target gene and any gene whose transcriptional start site fell within 2kb of the

Please cite this article in press as: Zhu et al., Genome-scale perturb-seq in primary human CD4+ T cells maps context-specific regulators of T cell programs and human immune traits, Cell (2026), https://doi.org/10.1016/j.cell.2026.08.002

sgRNA's genomic alignment positions, as proximal genes are expected to be repressed through the intended CRISPRi mechanism rather than off-target binding. We then performed seed matching by searching the promoter region (±2kb from the transcriptional start site) of each remaining downregulated gene for PAM-adjacent complementarity to the 3′-end seed of the protospacer sequence, requiring a minimum seed match length of 8 bp. The resulting genes that are both significantly down-regulated and have seed matching at their promoters are candidate off-target genes.

Candidate off-target genes were then validated by Pearson correlation between the guide's genome-wide DE z-score profile and the candidate off-target gene's target-level DE z-score profile. For each candidate, we computed correlations across all genes and separately across union-significant genes (10% FDR in either profile), excluding the on-target gene and the focal candidate off-target gene from the correlation. A candidate was flagged as a putative off-target hit if all three criteria are met: (1) the genome-wide correlation exceeded 0.1; (2) the correlation among union-significant genes exceeded 0.5; (3) the associated P-value for union-significant correlation analysis was less than 0.01; (4) the number of union-significant DE genes exceeded 10. The final off-target analysis results are reported in Table S6.

Validation of trans-effects with complementary screens

To validate perturb-seq measurements, we first compared them with transcriptome-wide effects of genetic knock-outs from published arrayed KO screens with bulk RNA-seq measurements.[5,14] DESeq2 statistics (comparing expression levels in perturbed cells against non-targeting controls) were either downloaded from supplementary tables or obtained from re-analysis of count matrices, replicating the differential analysis design used by the original authors. We compared arrayed screen results for 28 perturbed genes tested in both perturb-seq and arrayed screen datasets, where the perturbation had a strong effect in the arrayed screens (at least 100 significant DE genes at FDR 10%). This analysis was performed using the results from the Rest condition in the perturb-seq screen, to match experimental conditions of the arrayed screens. We computed the Pearson correlation between DE log-fold changes estimated from perturb-seq and arrayed screen RNA-seq for the measured genes that were significantly DE in the arrayed screen (FDR 10%). As a negative control, for each perturbed gene we also computed the DE effect correlation with perturbation of a randomly picked perturbed gene in the set of 28 tested genes. For each comparison, we performed 100 bootstrap iterations, each randomly sampling 70% of shared measured genes. We estimated the theoretical maximum achievable correlation (correlation ceiling) by accounting for measurement uncertainty in the log fold change estimates of each test. For each test, we estimate the error variance (σ^2_{error}) and true variance (σ^2_{true}) of log-fold changes as:

$$\sigma^2_{\text{error}} = mean_j\left(SE(\beta_j)^2\right),$$

$$\sigma^2_{\text{true}} = var_j(\beta_j) - \sigma^2_{\text{error}}.$$

The reliability of log-fold change measurement is calculated as the proportion of observed variance that is due to true signal rather than measurement error:

$$reliability = \sigma^2_{\text{true}} \;/\; \left(\sigma^2_{\text{true}} + \sigma^2_{\text{error}}\right).$$

The correlation ceiling was then calculated as the geometric mean of reliabilities for the two guides being compared.

To validate regulator predictions for individual measured genes, we collected a set of published CRISPRi FACS-based screens.[6,13,15] For each FACS-based screen and target gene, we computed correlations between FACS log fold changes (MAGeCK statistics) and perturb-seq z-scores across shared perturbations with FDR < 0.05 in FACS. To control for expression-level confounding, we selected control genes with similar baseline expression (we ranked all genes by mean expression, and picked genes within ±20 expression ranks of the target gene). For each comparison, we performed 100 bootstrap iterations, each randomly sampling 70% of shared perturbations. We then calculated Pearson correlations between effects in FACS-based screen and perturb-seq z-scores for both matched comparisons (target gene in both assays) and mismatched comparisons (FACS target vs. expression-matched controls in perturb-seq).

Cross-donor robustness analysis

To quantify the reproducibility of perturbation effects across donors, we performed differential expression analysis on donor subsets of the pseudobulk data. This analysis was restricted to condition-target tests meeting the following criteria in the full dataset: >75 perturbed cells and >30 significantly differentially expressed genes at 10% FDR. For each target-condition pair, we conducted 6 separate DE analyses using the method described above, each time subsetting the expression data to include only two donors, representing all possible pairwise combinations of the 4 donors. We then calculated the cross-donor correlation by comparing tests performed on disjoint donor pairs (e.g., donors 1+2 vs. donors 3+4) for the same perturbed gene. For each target gene we computed the Pearson correlation between log fold changes across two gene sets: (i) all tested genes; and (ii) genes called as hits (10% FDR) in the target-level DE test on all donors.

For each target-condition pair, there are 3 possible comparisons between disjoint donor pairs. The reported mean and minimum cross-donor correlation represents the average of these 3 correlations (Figures S9A and S9B; Table S7).

Comparison with K562 genome-wide perturb-seq and targeted Jurkat perturb-seq

Gene expression count matrices and cell-level metadata for K562 genome-wide perturb-seq data[9] (K562-GW) and Jurkat perturb-seq on essential genes[19] (Jurkat-essential) were downloaded from the *scPerturb* database.[132] We pseudobulked expression profiles

for cells with the same guide in the same batch and performed differential expression analysis on the pseudobulked profiles as described above for our dataset, testing the effect of perturbation compared to non-targeting controls for perturbed genes that met two criteria: (1) Perturbed genes with significant trans-effects on at least one gene other than the target gene in at least one culture condition in CD4+ T perturb-seq; (2) perturbed genes with sufficient coverage in cell line data: at least 3 pseudobulk replicates aggregating data from at least 3 cells, with at least 10 mRNA counts per gene. This resulted in 3081 perturbed genes tested in K562-GW and 92 perturbed genes tested in Jurkat-essential.

To compare DE analysis results accounting for differences in statistical power between the datasets, we processed DE summary statistics for K562 cells and CD4+ T conditions using Multivariate Adaptive Shrinkage (MASH[140]), which fits a mixture of multivariate normal distributions to model the joint distribution of effect sizes for all tests (perturbed gene-measured gene) across all 4 cell contexts (K562, CD4+ T Rest, CD4+ T Stim8hr, CD4+ T Stim48hr). The use of MASH posterior estimates is akin to the bivariate analysis proposed by Nadig et al.,[19] although we fit a single model for all cell types on a subset of all tests, following the recommended eQTL analysis workflow (https://stephenslab.github.io/mashr/articles/eQTL_outline.html). We then considered 5% local false sign rate (LFSR) as a threshold for significant trans-effects across datasets, and consider a trans-effect "shared" between cell types if the regulator-to-gene test passed the LFSR threshold in both CD4+ T and K562 cells (Figure S11A). The same workflow was used for Jurkat-essential recall analysis (Figure S11D).

We compare effect size estimates between K562 and CD4+ T results computing the Pearson correlation between MASH posterior estimates of perturbation effects in K562 and each CD4+ T condition (Figure S11C). As a negative control, we correlate each the effect of each perturbation to the effect of 3 random perturbations in the other cell types. Results of comparisons of effect sizes are shared in Table S8.

Power analysis

We tested the robustness of perturbation effect estimates to downsampling the number of reads, cells and replicates (donors) profiled per perturbed genes. This analysis was performed in Rest condition and on effects of perturbation of 12 perturbed genes with significant downstream effects replicated by arrayed KO RNA-seq screens (see validation of trans-effects with complementary screens).

To make downsampled versions of the perturb-seq data, we split 10x lanes into disjoint groups of 5 lanes (with 3 independent splits). For each downsampling experiment, we randomly designated one group of 5 lanes as the validation set, ensuring no overlap with training data (pseudobulking by donor-guide). Then we sequentially pool data from 5, 10, 15 and 20 lanes, simulating an increase in number of cells profiled. Finally, from each group of lanes, we aggregate data from all combinations of 1, 2, 3 or 4 donors, simulating an increase in the number of replicates profiled. To downsample the number of UMIs, we use the method described in Dixit et al.[7] on pseudobulk expression profiles. For example, a vector of gene expression counts for 4 genes in a sample with values [3,0,1,6] is converted into the vector [1,1,1, 3,4,4,4,4,4,4] (i.e. from counts to individual instances of each gene), on which sampling is performed with equal probability without replacement. We downsample to 10% of UMIs to match the depth of perturbation datasets profiled with split-pool scRNA-seq protocols[99] and to 50% of UMIs to simulate the depth of perturbation datasets profiled with capture-based 10x Genomics scRNA-seq.[9] We then test for differential expression as described above for the sampled perturbed genes in subsampled pseudobulks with downsampled number of cells, reads or donors.

We evaluate the robustness to downsampling by comparing the DE effects (raw log-Fold changes) for perturbation of each target in each subsample with 2 validation datasets: (a) DE effect estimates in arrayed KO RNA-seq screens from Freimer et al.[5] (Pearson correlation of log-Fold Changes for significant genes at 10% FDR); and (b) DE effect estimates on all donors in the held-out validation set of 5 lanes (Pearson correlation of log-Fold Changes for significant genes at 10% FDR).

Analysis of arrayed validation of *IL10/IL21* regulation

Count matrices were generated by Plasmidsaurus using build GRCh38_114 as follows: quality of the fastq files was assessed using FastQC v0.12.1. Reads were then quality filtered using fastp v0.24.0 with poly-X tail trimming, 3′ quality-based tail trimming, a minimum Phred quality score of 15, and a minimum length requirement of 50 bp. Quality-filtered reads were aligned to the reference genome using STAR aligner v2.7.11 with non-canonical splice junction removal and output of unmapped reads, followed by coordinate sorting using samtools v1.22.1. PCR and optical duplicates were removed using UMI-based deduplication with UMIcollapse v1.1.0. Alignment quality metrics, strand specificity, and read distribution across genomic features were assessed using RSeQC v5.0.4 and Qualimap v2.3, with results aggregated into a comprehensive quality control report using MultiQC v1.32. Gene-level expression quantification was performed using featureCounts (subread package v2.1.1) with strand-specific counting, multi-mapping read fractional assignment, exons and three prime UTR as the feature identifiers, and grouped by gene_id.

From count matrices, we performed differential expression analysis using DESeq2 as previously described. Exploratory principal component analysis of gene expression profiles revealed that the first principal component (PC) captured technical variation between samples, correlated with experimental batches. Therefore, we tested for differential expression between each target and NTC controls, using donor identity and the first PC as confounders (DESeq2 *design:* $\sim donor + PC1 + target_gene$). Per-perturbation Pearson r values were computed both genome-wide and restricted to the union of significantly (FDR<10%) differentially expressed genes between regulators, excluding the on-target gene so the dominant self-knockdown effect did not drive the correlation. To evaluate perturbation robustness comprehensively, the two independent guides targeting each regulator were analyzed by DESeq2 both separately and together. This allowed us to assess the individual transcriptional impact of each guide relative to non-targeting

Please cite this article in press as: Zhu et al., Genome-scale perturb-seq in primary human CD4+ T cells maps context-specific regulators of T cell programs and human immune traits, Cell (2026), https://doi.org/10.1016/j.cell.2026.08.002

controls (guide-level), as well as their consensus differential expression effect when aggregated (target-level). Raw fastq and count matrices are available via GEO (see key resources table). DESeq2 results are summarized in Table S9 and Table S10.

For IL-10/IL-21 protein expression analysis, flow cytometry data were processed by FlowJo software version 10.10.1 following gating strategy in Figure S18. The percentages of IL-10+ and IL-21+ cells in each sample (donor-perturbation) are reported in Table S11. We quantify for each sample the Log2 fold change in percentage of IL-10/IL-21+ cells compared to the mean percentage across NTC samples in the same donor replicates. We tested the perturbation's Log2FCs against 0 using Welch's two-sample t-test followed by FDR correction.

To quantify effects of perturbation on cell proliferation, fold expansion was calculated by dividing final cell count at day 10 to initial cell count (150K) and reported in Table S12. We then normalized by the mean fold expansion of non-targeting control wells for each donor replicate.

Functional clustering of perturbations

Clustering workflow

To define regulator clusters, we performed clustering on the $\tilde{B}$ matrix of differential expression z-scores, representing the effects of perturbations on measured genes, where each perturbation corresponds to a perturbed gene in a cellular context (culture condition). We first filtered for high-quality perturbations (each perturbation is a perturbed gene x culture condition) with strong effects, requiring >75 differentially expressed genes and >50 cells per perturbation. This yielded 3341 perturbations across three conditions (Rest: 1088; Stim8hr: 1136; Stim48hr: 1117). We also trimmed the feature space to 10941 highly variable genes (from an initial 13959) by requiring a sum of absolute z-scores >= 1,200 (~20 percentile) across the selected perturbations. To preclude strong on-target knockdown effects from driving cluster assignment, on-target z-scores were masked to zero.

We used Leiden clustering on the first principal components of the filtered $\tilde{B}$ matrix, using the methods implemented in scanpy (*scanpy.tl.leiden*). We observed that the resulting cluster assignments showed some sensitivity to hyperparameter selection (PCA dimensions, k-neighbors, and leiden resolution). To ensure stability and robustness against hyperparameter selection and sampling bias, we implemented a consensus clustering approach. We generated a grid ensemble of 27 clustering parameters, varying PCA dimensions (50, 100, 150), k-nearest neighbors (k=15, 31, 63), and Leiden clustering resolution (r=2, 3, 4) across 400 randomly bootstrapped subsampled datasets. Specifically, for each of the 27 hyperparameter combinations, we then performed clustering with the hyperparameter grid on 200 perturbation-subsampled and 200 measured gene-subsampled datasets (70% random sampling rate), resulting in 10800 clustering outcomes. After collecting all the clustering results, we computed a pairwise co-occurrence matrix representing the frequency with which perturbations were co-clustered across all runs and converted this to a distance matrix (1 – consensus frequency). Final clusters were identified using HDBSCAN on this precomputed distance matrix (min_cluster_size=4, min_samples=1, cluster_selection_method='eom'), resulting in 111 regulator clusters.

Annotation of clusters

We annotated the possible functions of clusters by performing gene set enrichment analysis on clustered regulators on public biological complexes, pathways, and process datasets including CORUM, STRINGDB, KEGG, and Reactome. To focus on more specific complexes/pathways, we only used terms in these databases with less than 200 genes. For each database, we then performed a hypergeometric test to detect complex/pathway enrichment among unique regulator genes in each cluster compared to all regulators included in the clustering analysis (genes with >75 total DE genes and >50 cells per target). In cases where no overlap existed between the tested gene sets and complex/pathway genes, we assigned a p-value of 1. We controlled for multiple testing using the Benjamini-Hochberg method to estimate false discovery rates. Based on FDR ranking, we reported the best-matching protein complex name (CORUM), the best functional description (STRINGDB) or the top associated pathways (KEGG and Reactome), enrichment significance (hypergeometric test p-value/FDR), the fraction of cluster genes overlapping with the term, and the specific overlapping genes. We assigned annotations to clusters showing strong enrichment (FDR < 0.05). For clusters without strong enrichment in any of these datasets, we used a combination of Gene Ontology analysis (https://geneontology.org/), LLM lookup, and manual literature search.

Assessing condition specificity of clusters

To assess the condition specificity of regulator clusters (Figures 3A and 3B), we analyzed the correlation of perturbation effects between distinct regulators. For a given cluster containing a set of regulator genes G, we computed the mean pairwise correlation for each condition $c \in \{Rest, Stim8hr, Stim48hr\}$:

$$\bar{\rho}_c = \left(\frac{1}{|P|}\right) \sum_{(i,j) \in P} Corr\left(v_{i,c}, v_{j,c}\right)$$

where $v_{i,c}$ is the perturbation effect vector (z-score) for gene i in condition c, and $P = \{(i,j) \mid i,j \in G, i < j\}$ represents all unique pairs of distinct regulators. We similarly computed a "Shared" mean correlation, $\bar{\rho}_{\text{shared}}$, using pairs of perturbations drawn from different conditions.

We classified cluster specificity (e.g. used in Figures 7A and S21) using the coefficient of variation (CV) of the intra-condition means $\mathcal{M} = \{\bar{\rho}_{Rest}, \bar{\rho}_{Stim8hr}, \bar{\rho}_{Stim48hr}\}$. Clusters with $CV < 0.5$ were classified as "across_condition." Clusters with high variability ($CV < 0.5$) were further sub-classified based on condition enrichment. A condition c was considered enriched if it satisfied two criteria:

$\frac{\bar{\rho}_c}{mean(\mathcal{M})} > 1.2$ and $\bar{\rho}_c > 0.2$.

Clusters were labeled according to their enriched conditions (e.g., "Rest", "Rest_Stim8hr"). High-variability clusters meeting no enrichment criteria were retained as "across_condition".

Cluster annotations and condition-specificity statistics are provided in Table S13.

Curation, ranking and annotation of downstream genes

To characterize the downstream target genes associated with each regulator cluster, we performed a rank aggregation analysis on the perturbation effects. Because we frequently observe the same set of regulators genes in a cluster regulate distinct downstream genes in different conditions, the curation and ranking of downstream genes are stratified by conditions.

For each cluster identified by HDBSCAN, we first get the differential gene expression results of regulators on all measured genes in one of the three conditions. Then we defined the set of potential downstream genes as the union of all genes significantly differentially expressed (10% FDR) by at least one regulator within that cluster in the corresponding condition.

For each potential downstream gene, we calculated three key metrics to quantify the strength and consistency of the trans-effect:

- Upstream regulator count: the number of regulators that significantly affected the gene (10% FDR) in the corresponding condition.
- Sign Coherence: to assess the consistency of directionality, we calculated the sign coherence as the sum of the signs (+/- 1) of the z-scores for all significant regulators, normalized by the upstream regulator count. A score of 1 or -1 indicates perfect directional agreement among regulators.
- Aggregate Rank Score: to prioritize genes with the strongest aggregate response, we utilized a rank-sum approach. For each downstream gene, we first converted the perturbation z-scores into ranks within each individual regulator perturbation in the corresponding condition. We then summed these ranks across all regulator perturbations in that corresponding condition.This yielded a single cumulative rank metric for each downstream gene, where the lowest cumulative sums correspond to the strongest negative z-score regulation (i.e. regulator perturbations strongly downregulate the downstream gene) and the highest cumulative sums correspond to the strongest z-score regulation (i.e. regulator perturbations strongly upregulate the downstream gene).

These downstream genes of regulator clusters are reported in Table S14.

To annotate biological processes of top downstream genes of selected clusters (Figures 3C, 3D, and S23), we performed Gene Ontology enrichment analysis using the gseapy Python package (https://github.com/zqfang/GSEApy), using the GO Biological Process 2025 libraries. For each cluster, enrichment was performed independently for its downstream genes in one of the three conditions and stratified by regulation direction (positive or negative). To prioritize the strongest co-regulated downstream genes, we selected downstream genes based on their Aggregate Rank Score in the positive or negative direction. Because the total numbers of potential downstream genes (significantly differentially expressed by at least one regulator for that cluster) for each cluster are different, the input gene list for enrichment was defined as the top 100 genes or the top 3% genes, whichever is larger. The background gene set for statistical testing consisted of the complete pool of downstream genes identified within the specific cluster and condition being analyzed. Significant GO terms were identified using an FDR threshold of <0.05. To generate a concise and non-redundant list of biological terms, we removed terms that have more than 10% overlap with any more significant term.

Tissue-specific gene expression analysis

To characterize the tissue-specific expression patterns of genes in regulator clusters (Figure S21), we utilized bulk RNA-seq data from the Human Protein Atlas (HPA) version 25.0 (based on Ensembl version 109).[152,163] We obtained the consensus transcript expression levels dataset (https://www.proteinatlas.org/about/download, ''RNA expression consensus''), which summarizes gene expression across 51 human tissues. These consensus normalized expression (nTPM) values represent the maximum nTPM value reported for each gene between the HPA and Genotype-Tissue Expression (GTEx) datasets. For organ systems containing multiple sub-tissues (e.g., brain regions, lymphoid tissues, and intestine), the maximum nTPM value across all sub-tissues was used to represent the tissue type. For each gene, to quantify the tissue specificity of gene expression, we performed two analyses.

For overall tissue specificity of gene expression, we calculated the Tau (τ) index as described by Yanai et al.[164] The Tau index provides a scalar value ranging from 0 (broadly expressed) to 1 (highly tissue-specific). It is calculated as:

$$\tau = \frac{\sum_{i=1}^{N}\left(1-\hat{x}_i\right)}{N-1}$$

where N represents the number of tissues (51), and $\hat{x}_i$ is the expression value of the gene in tissue i, normalized by the maximal expression value across all tissues:

$$\hat{x}_i = \frac{x_i}{max(x)}$$

Prior to calculation, expression values were log1p-transformed. Genes exhibiting a Tau index greater than 0.5 were classified as having high tissue specificity.

Please cite this article in press as: Zhu et al., Genome-scale perturb-seq in primary human CD4+ T cells maps context-specific regulators of T cell programs and human immune traits, Cell (2026), https://doi.org/10.1016/j.cell.2026.08.002

To determine specific tissue enrichment for each gene, we calculated the log2 fold change of gene's expression (nTPM) in a specific tissue relative to its median expression across all 51 tissues. A gene was considered enriched in a specific tissue if the log2 fold change > 2.5.

Analysis of arrayed validation of TCR functional cluster

Count matrices were built by Plasmidsaurus as described above (see "Analysis of arrayed validation of IL10/IL21 regulators"). From count matrices, we performed differential expression analysis using DESeq2 as previously described. DE analyses were run on Stim8hr and Stim48hr samples separately. Exploratory principal component analysis of gene expression profiles revealed that the first principal component (PC) captured technical variation between samples, correlated with experimental batches. Therefore, we tested for differential expression between each target and NTC controls, using donor identity and the first PC as confounders (DESeq2 design: $\sim donor + PC1 + target_gene$). For each predicted early or late regulator, we computed the Pearson correlation between its DE effect with that from each core regulator, excluding the on-target gene so the dominant self-knockdown effect did not drive the correlation. Per-perturbation Pearson R values were computed both genome-wide and restricted to the union of significantly (FDR<10%) differentially expressed genes between regulators. Raw fastq and count matrices are available via GEO (see key resources table). DESeq2 results are summarized in Table S15.

Cell state signature analysis

Model overview

To infer the regulators of a cell state of interest in observational data, we used a regularized regression approach that integrates differential gene expression signatures with context-specific perturbation effect estimates (Figure 4A). The model takes as input (a) differential expression estimates of genes in the cell state ($\tilde{\delta}_j$ for gene j, representing the z-score of the log-Fold change in differential expression), compared to a reference cell state in the observational dataset; (b) Perturbation effect estimates for K candidate regulators across genes in the perturb-seq data ($\tilde{\beta}_{j,k}$, z-score of the log-Fold change representing the effect of regulator k on gene j). We train each model with 5-fold cross validation, holding-out from the full set of measured genes a test set to use for model evaluation.

To reduce the dimensionality of the perturbation effect matrix and mitigate multicollinearity among regulators, we applied truncated singular value decomposition (SVD) to the perturbation matrix $\tilde{B} \in \mathbb{R}^{JxK}$. The truncated SVD approximates the original matrix as:

$$\tilde{B} \approx \mathbf{U}_d \mathbf{\Sigma}_d \mathbf{V}_d^T$$

where $U_d \in \mathbb{R}^{JxD}$ contains the first D left singular vectors, $\Sigma_d \in \mathbb{R}^{DxD}$ is a diagonal matrix of the D largest singular values, and $V_d \in \mathbb{R}^{KxD}$ contains the first D right singular vectors. The matrix $\tilde{B}_d = \mathbf{U}_d \mathbf{\Sigma}_d \in \mathbb{R}^{J \times D}$represents the effect of D eigen-perturbations on J genes. This decomposition was performed using the TruncatedSVD implementation in scikit-learn.[141] Unless otherwise specified, we used $D = 60$ for applications in this study, after selection with a small grid search on reconstruction of Th2/Th1 polarization signatures.

We fit an elastic net regression model to predict the differential expression signature $\tilde{\delta}_j$ from the reduced-dimensional perturbation effects $\tilde{B}_d$. The elastic net model solves the following optimization problem:

$$\min_{\theta} \frac{1}{2n} \sum_{j=1}^{n} \left(\tilde{\delta}_j - \sum_{d=1}^{D} \tilde{\beta}_{j,d} \theta_d \right)^2 + \lambda \left(\alpha \sum_{d=1}^{D} \left| \theta_d \right| + \frac{1-\alpha}{2} \sum_{d=1}^{D} \theta_d^2 \right)$$

where $\theta = (\theta_1, ..., \theta_D)$ are the regression coefficients for the D eigen-perturbations, λ is the overall regularization strength, and α is the ratio that balances L1 and L2 penalties. Hyperparameters λ and α were optimized using 4-fold cross-validation on the training set. The model was implemented using scikit-learn's ElasticNet class.[141]

To evaluate model performance on held-out genes, we first projected the test set perturbation effects onto the eigen-perturbation space learned from the training set:

$$\tilde{\beta}'_{i,d} = \sum_{k=1}^{K} \tilde{\beta}_{i,k} v_{k,d}$$

where $\tilde{\beta}'_{i,d}$is the effect of eigen-perturbation d on test gene i, $\tilde{\beta}_{i,k}$ is the original perturbation effect of regulator k on gene i, $v_{k,d}$ is the (k, d) element of V_D, and K is the total number of regulators. We then applied the fitted elastic net model to obtain the reconstructed $\tilde{\delta}_i$ from $\tilde{\beta}'_i = \left(\tilde{\beta}'_{i,1}, ..., \tilde{\beta}'_{i,D} \right)$.

To obtain interpretable coefficients at the level of individual regulators (w_k), we back-transformed the eigen-perturbation coefficients (θ_d) through the right singular vector matrix:

$$w_k = \sum_{d=1}^{D} \theta_d \sigma_d v_{k,d}$$

Please cite this article in press as: Zhu et al., Genome-scale perturb-seq in primary human CD4+ T cells maps context-specific regulators of T cell programs and human immune traits, Cell (2026), https://doi.org/10.1016/j.cell.2026.08.002

where σ_d is the d-th singular value and $v_{k,d}$ is the (k,d) element of $\mathbf{V}_D$. These regulator-level coefficients represent the estimated contribution of each regulator's perturbation signature to the observed cell state differential expression signature. We used mean coefficients across training folds for downstream analyses (Figures 4F and 5D). The model is implemented as a stand-alone python class (https://github.com/emdann/pert2state_model).

For visualization of regulator-level coefficients (Figures 4F and 5D), we implemented a modified version of the "Long Island City plots" introduced by Grabski et al.,[110] where in each plot, the x-axis consists of the set of K regulators included in the model fit, ordered by hierarchical clustering of the DE effects of regulators on significantly DE genes in the cell state of interest.

We consider signature genes as "controlled by a set of m regulators" if they meet the following conditions: (a) significant DE from knock-down of least one of the regulators (10% FDR) and (b) the sign of mean DE z-score across all regulators in the set needs to be consistent with the sign of predicted regulator effect (w_k) and of the cell state signature (δ_i):

If $w_k > 0$: a gene upregulated by the regulators (mean $(z_j) > 0$) should be upregulated in the target cell state ($\delta_i > 0$)
If $w_k < 0$: a gene upregulated by the regulators (mean $(z_j) > 0$) should be downregulated in the target cell state ($\delta_i < 0$)

Th1/Th2 polarization bulk RNA-seq data processing and analysis

Bulk RNA-seq counts for Th1 and Th2 sorted cells were downloaded from the NBDC Human Database for the Discovery cohort (NDBC: E-GEAD-397)[40] and from GEO for the Replication cohort (GEO: GSE149090).[41]

For each cohort, differential expression analysis was performed using DESeq2[138] as previously described. We fit a negative binomial generalized linear model where the expected mRNA count was modeled as a function of T cell subset (Th1 or Th2), the first principal components capturing technical variation and donor identity (where replication was present). The model designs were: $\sim$ cell_subset + PC1 + PC2 for the discovery cohort and $\sim$ cell_subset + donor + PC1 for the replication cohort. We estimated log2 fold-changes in gene expression and tested for differential expression between Th2 and Th1 samples using the Wald test. FDR < 1% after Benjamini-Hochberg correction was used as threshold for significance. Full DESeq2 results are provided in Table S16. The z-score of the differential expression log-fold change was used as the input signature for the model ($\tilde{\delta}_i$). As a negative control, we used a TCR activation signature derived from DESeq2 results comparing stimulated and resting Teff cells from Arce et al.[13] (Figure S24D).

To identify regulators of Th2 and Th1 polarization from perturb-seq effects, we considered regulators with significant differential expression effects on at least 10 measured genes in any condition. We fitted the differential expression signature reconstruction model (as described above) to reconstruct the effect of Th2/Th1 polarization, using 5-fold cross-validation on 8947 measured genes with 3 independent splits, evaluating model fit on a validation set of held-out genes in each of the 15 splits. The knock-down effect of each perturbed gene on itself was masked before training. To evaluate model fit, we computed the Pearson correlation between the reconstructed Th2/Th1 signature and the true input signature for both training set and test set genes in the Discovery cohort (samples used for training) and Replication cohort (samples not used during training). For comparisons with scrambled controls (Figures 4E and S24C), we scrambled the differential expression z-scores for each gene across regulators, preserving the mean z-score for each measured gene. This approach accounts for the tendency of highly expressed genes to show larger z-score effects. For comparison with perturbation effects in K562 cells (Figures 4 and S24C), we used differential expression estimates obtained as described above (see section Comparison with K562 genome-wide perturb-seq and targeted Jurkat perturb-seq) and fitted the regression model using only K = 2190 common perturbed genes with sufficient power in both the Stim8hr CD4+ T cell and K562 datasets. Regulator-level regression coefficients (w_k) for models fitted on CD4+ T cell conditions to reconstruct Th2/Th1 and activation signatures are provided in Table S17.

To estimate expression of Th2 and Th1 signature genes in single cells from perturb-seq data (Figures 4G and S28), we used a modified version of the *sc.tl.score_genes* function implemented in scanpy[134] to account for donor-specific differences in expression profiles. Briefly, we obtained normalized single-cell expression profiles for cells with guides targeting the regulators of interest and a subset of non-targeting control guides. We defined signature genes as those differentially expressed at 1% FDR in both the Discovery and Replication dataset, selecting the bottom 50 genes (Th1 signature) and top 50 genes (Th2 signature) ranked by z-score of differential expression log-fold change. For each gene set (Th1 and Th2 signatures), we retained genes expressed in the dataset (mean log-normalized expression > 0.1) and standardized expression values using the mean and standard deviation calculated from NTC cells matched by donor and condition. We computed the mean standardized expression across all genes in each signature as the final score.

Aging scRNA-seq data processing and analysis

Single-cell RNA-seq data from the OneK1K cohort were downloaded from the CellxGene collections (collection ID: dde06e0f-ab3b-46be-96a2-a8082383c4a1).[59] Quality control filtering was applied to remove low-quality cells based on the following criteria: cells with >8% mitochondrial reads, or cells with values ±3 median absolute deviations (MADs) from the median percentage of mitochondrial reads, or ±5 MADs from the median for total counts, number of detected genes, or percentage of counts in the top 20 genes. We subsequently subset the dataset to retain only cells annotated by the original authors as CD4+ T cells, including the subset labels "CD4 Naive", "CD4 EM", and "CD4 CM" (Figure 5A).

For differential expression analysis, we retained genes that were measured across all experimental batches (pools) and selected the top 10,000 highly variable genes using the scanpy function *sc.pp.highly_variable_genes* (parameters: *min_mean=0.1*,

max_mean=10, *n_top_genes=10000*). Gene expression data were aggregated to the pseudo-bulk level by summing mRNA counts from all cells belonging to the same donor and cell subset annotation.

We partitioned the dataset into discovery (n = 782 donors) and replication (n = 199 donors) cohorts, by splitting donors while stratifying by age bins (<40, 40-60, 60-70, 70-80, >80 years). Principal component analysis of pseudo-bulked gene expression profiles revealed that the first principal components captured technical variation between experimental batches (each donor was processed in a single batch) and donor outliers in cell type composition. Consequently, we included the first 5 principal components computed on the "CD4 Naive" subset as covariates in the differential expression model to account for these confounding factors. For each cohort, differential expression analysis was performed using DESeq2[138] as previously described. We fit a negative binomial generalized linear model where the expected mRNA count was modeled as a function of CD4+ T cell subset (Naive, EM, CM), the first 5 principal components capturing technical variation, the number of aggregated cells, donor sex, and age bin. We estimated log2 fold-changes in gene expression and tested for differential expression across age using the Wald test, with the age bin modelled as a continuous covariate. This model design was chosen to identify genes that exhibit age-associated expression changes across all CD4+ T cell subsets, while controlling for expression differences between subsets that might reflect age-related shifts in the composition of the T cell compartment (Figure S30A). FDR < 1% after Benjamini-Hochberg correction was used as threshold for significance. Full DESeq2 results are provided in Table S20. We evaluated the robustness of the resulting differential expression estimates by comparing results between the discovery and replication cohorts, and by benchmarking against published estimates from independent cohorts that tested for age-associated differential expression in CD4+ T cells[63,64] (Figure S30B). Outlier genes with inconsistent differential expression effects across cohorts were predominantly red blood cell genes, including those related to hemoglobin metabolism (e.g. HBB), likely reflecting contamination from ambient RNA during single-cell RNA-seq processing. The scaled z-score of the differential expression log-fold change with age was used as the input signature for the model. We applied centering to account for a slight bias in DE estimates, leading to logFCs being skewed towards positive values (mean logFC = 0.02), likely due to imbalance in sample numbers between age bins.

To identify regulators of the CD4+ T aging signature from perturbation effects, we considered regulators with significant differential expression effects on at least 10 measured genes in the condition of interest. We fitted the differential expression signature reconstruction model (as described above) to reconstruct the signature of CD4+ T cell aging, using 5-fold cross-validation on 6014 measured genes. The knock-down effect of each perturbed gene on itself was masked before training. To evaluate model fit, we computed the Pearson correlation between the reconstructed aging signature and the true input signature for both training set and test set genes in the Discovery cohort (samples used for training) and Replication cohort (samples not used during training). Regulator-level regression coefficients (w_k) for models fitted on CD4+ T cell conditions to reconstruct aging signatures are provided in Table S21.

Analysis of arrayed validation of predicted Th1/Th2 regulators

Count matrices were built by Plasmidsaurus as described above (see "Analysis of arrayed validation of IL10/IL21 regulators"). One sample flagged for quality issues (low RNA content) was excluded. From count matrices, we performed differential expression analysis using DESeq2 as previously described. Exploratory principal component analysis of gene expression profiles revealed that the first principal component (PC) captured technical variation between samples, correlated with experimental batches. Therefore, we tested for differential expression between each target and NTC controls, using donor identity and the first PCa as confounders (DESeq2 design: $\sim donor + PC1 + target_gene$). For each perturbed gene, we computed the Pearson correlation between bulk RNA-seq and perturb-seq z-scores, excluding the on-target gene so the dominant self-knockdown effect did not drive the correlation. Per-perturbation Pearson R values were computed both genome-wide and restricted to the Th1/Th2 reference signature genes, defined as above (Figures S26A and S26B). Raw fastq and count matrices are available via GEO. DESeq2 results are summarized in Table S19.

For protein expression analysis, flow cytometry data were processed by FlowJo software version 10.10.1 following gating strategy in Figures S27A and S27B, and were reported in Table S18. For IFN-γ/IL-5, we quantify for each sample (donor-perturbation) the Log2 fold change in percentage of protein expressing cells compared to the mean percentage across NTC samples in the same experimental batch. For T-bet/GATA3, we quantify for each sample (donor-perturbation) the Log2 fold change in median fluorescence intensity (MFI) compared to the mean MFI across NTC samples in the same experimental batch. We tested the perturbation's Log2FCs against 0 using Welch's two-sample t-test followed by FDR correction.

Integration with human population loss-of-function (LoF) burden data

We used LoF burden test summary statistics from the UKB with 454,787 participants, as previously reported.[3] Gene effect sizes were de-noised using GeneBayes[165] as previously described.[3] Replicating the analysis in Ota et al.,[3] to identify putative core genes that directly influence lymphocyte counts, we ran, for each core gene candidate j, a linear regression to test the association between knockdown effects of K regulators on the gene (log-Fold Change, $\beta_{j,k}$) and the LoF burden on lymphocyte counts (γ_k). To avoid the confounding effects of selective constraint due to the large correlation between LoF burden test effect sizes and gene-level effects on fitness (s_{het}),[166] we fit the following regression model:

$$\gamma_k \sim \beta_{j,k} + s_{\text{het},k},$$

where s_{het} is included as a covariate. We masked the effects of knock-down gene *j* on itself, as it does not reflect a trans-regulatory effect. We obtained regulator-burden correlations using perturbation effects estimated from all three CD4+ T cell culture conditions in our genome-wide perturb-seq, as well as cell lines K562[9] and Jurkat[19] (using DE estimates from Ota et al.[3]). For Stim8hr and Stim48hr conditions, we evaluated the putative core genes positively associated with lymphocyte counts using Gene Ontology enrichment analysis. We obtained genes with top 50 regulator-burden correlations by $-\log_{10} P$, and ran gene set enrichment analysis using the *gseapy* Python package (https://github.com/zqfang/GSEApy), using all tested genes in each condition as background.

Analysis of effects of autoimmunity GWAS genes

We queried the OpenTargets Platform API (v4) to retrieve genes with genetic association with autoimmune diseases (rheumatoid arthritis, systemic lupus erythematosus, inflammatory bowel disease, multiple sclerosis, type 1 diabetes, psoriasis, ankylosing spondylitis, asthma, Hashimoto's thyroiditis, celiac disease, and atopic eczema) and non-autoimmune control diseases (coronary artery disease, macular degeneration, and chronic kidney disease). We included genes with a minimum genetic evidence score of 0.1 (https://platform-docs.opentargets.org/evidence) derived from GWAS associations, gene burden studies, and somatic mutation data, which includes evidence from ClinVar (Figure S34A).

To test for enrichment of disease-associated genes among the regulators in each cluster and/or their downstream targets, we excluded clusters containing fewer than five unique regulators, keeping 77 out of 111 clusters for testing. We then performed Fisher's exact tests to assess enrichment of disease-associated genes in two gene sets for each condition: (a) cluster regulators and (b) condition-specific downstream target genes. For regulator enrichment, we tested whether disease-associated genes were over-represented among the regulators in each cluster compared to all regulators included in the clustering analysis (genes with >75 total DE genes and >50 cells per target). For downstream gene enrichment, we first selected the top 50 genes with the lowest z-score rank for positive regulation and the top 50 genes with the lowest z-score rank for negative regulation within each cluster and condition (see section "Curation, ranking and annotation of downstream genes"). We then tested whether disease-associated genes were overrepresented among the downstream targets of each cluster compared to all selected downstream genes across all clusters in that condition. Downstream genes were only considered in conditions where regulators exhibited coordinated effects. In cases where no overlap existed between the tested gene sets and disease-associated genes, we assigned a *p*-value of 1. We controlled for multiple testing using the Benjamini-Hochberg method to estimate false discovery rates. The complete results and tested gene sets are provided in Table S22.

Use of AI coding assistants

Parts of the analysis code used in this study were implemented with the assistance of AI coding agents. Claude Code (Anthropic), using the models Claude Opus 4.8 (claude-opus-4-8) and Claude Sonnet 4.6 (claude-sonnet-4-6), was used for the following tasks: implementing analysis specifications written by the authors into Python code; generating plotting code; refactoring existing code for scalability; writing documentation; and debugging. Prompts were written by the authors and specified the intended statistical procedure in each case. The choice of method, parameters and thresholds was made by the authors and not by the AI agents.

All AI-generated code was read, tested and edited by the authors before use, and all outputs reported in this paper were verified by the authors, who take full responsibility for the analyses and conclusions. The complete code base, in the form in which it was executed, is deposited at https://github.com/emdann/GWT_perturbseq_analysis_2025.

QUANTIFICATION AND STATISTICAL ANALYSIS

The statistical tests performed are indicated in the figure legends or STAR Methods. Throughout the analyses, multiple test correction was performed with Benjamini-Hochberg procedure, unless otherwise indicated.

ADDITIONAL RESOURCES

As listed in key resources table, cell-level count matrices, pseudobulk-level count matrices and differential expression estimates are available at https://virtualcellmodels.cziscience.com/dataset/genome-scale-tcell-perturb-seq. Raw sequencing data and cellranger outputs are available through SRA/GEO (accession: SRP643211 / GSE314342). Supplementary tables and additional metadata are available via our code repository (https://github.com/emdann/GWT_perturbseq_analysis_2025). All processing and analysis code is available at https://github.com/emdann/GWT_perturbseq_analysis_2025.

The model to predict regulators of observed cell states is implemented as a stand-alone python class (https://github.com/emdann/pert2state_model).